NASA/TM–2013-217992
NESC-RP-11-00753

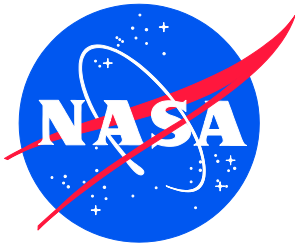

Relative Navigation Light Detection and Ranging (LIDAR) Sensor Development Test Objective (DTO) Performance Verification

Cornelius J. Dennehy/NESC
Langley Research Center, Hampton, Virginia

May 2013

NASA STI Program . . . in Profile

Since its founding, NASA has been dedicated to the advancement of aeronautics and space science. The NASA scientific and technical information (STI) program plays a key part in helping NASA maintain this important role.

The NASA STI program operates under the auspices of the Agency Chief Information Officer. It collects, organizes, provides for archiving, and disseminates NASA's STI. The NASA STI program provides access to the NASA Aeronautics and Space Database and its public interface, the NASA Technical Report Server, thus providing one of the largest collections of aeronautical and space science STI in the world. Results are published in both non-NASA channels and by NASA in the NASA STI Report Series, which includes the following report types:

- TECHNICAL PUBLICATION. Reports of completed research or a major significant phase of research that present the results of NASA Programs and include extensive data or theoretical analysis. Includes compilations of significant scientific and technical data and information deemed to be of continuing reference value. NASA counterpart of peer-reviewed formal professional papers, but having less stringent limitations on manuscript length and extent of graphic presentations.

- TECHNICAL MEMORANDUM. Scientific and technical findings that are preliminary or of specialized interest, e.g., quick release reports, working papers, and bibliographies that contain minimal annotation. Does not contain extensive analysis.

- CONTRACTOR REPORT. Scientific and technical findings by NASA-sponsored contractors and grantees.

- CONFERENCE PUBLICATION. Collected papers from scientific and technical conferences, symposia, seminars, or other meetings sponsored or co-sponsored by NASA.

- SPECIAL PUBLICATION. Scientific, technical, or historical information from NASA programs, projects, and missions, often concerned with subjects having substantial public interest.

- TECHNICAL TRANSLATION. English-language translations of foreign scientific and technical material pertinent to NASA's mission.

Specialized services also include organizing and publishing research results, distributing specialized research announcements and feeds, providing information desk and personal search support, and enabling data exchange services.

For more information about the NASA STI program, see the following:

- Access the NASA STI program home page at *http://www.sti.nasa.gov*

- E-mail your question to help@sti.nasa.gov

- Fax your question to the NASA STI Information Desk at 443-757-5803

- Phone the NASA STI Information Desk at 443-757-5802

- Write to:
  STI Information Desk
  NASA Center for AeroSpace Information
  7115 Standard Drive
  Hanover, MD 21076-1320

NASA/TM–2013-217992
NESC-RP-11-00753

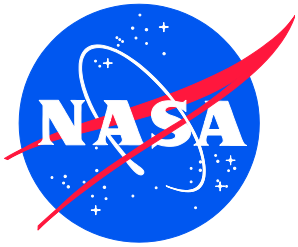

Relative Navigation Light Detection and Ranging (LIDAR) Sensor Development Test Objective (DTO) Performance Verification

Cornelius J. Dennehy/NESC
Langley Research Center, Hampton, Virginia

National Aeronautics and
Space Administration

Langley Research Center
Hampton, Virginia 23681-2199

May 2013

Available from:

NASA Center for AeroSpace Information
7115 Standard Drive
Hanover, MD 21076-1320
443-757-5802

Relative Navigation Light Detection and Ranging (LIDAR) Sensor Development Test Objective (DTO) Performance Verification

April 11, 2013

Report Approval and Revision History

NOTE: This document was approved at the April 11, 2013, NRB. This document was submitted to the NESC Director on April 19, 2013, for configuration control.

Approved:	*Original Signature on File*	4/30/13
	NESC Director	Date

Version	Description of Revision	Office of Primary Responsibility	Effective Date
1.0	Initial Release	Mr. Neil Dennehy, NASA Technical Fellow for Guidance, Navigation, and Control, GSFC	4/11/2013

Table of Contents

Appendices (Stand Alone Volume)

List of Figures

List of Tables

Technical Assessment Report

1.0 Notification and Authorization

The NASA Engineering and Safety Center (NESC) received a request from the NASA Associate Administrator (AA) for Human Exploration and Operations Mission Directorate (HEOMD), to quantitatively evaluate the individual performance of three light detection and ranging (LIDAR) rendezvous sensors flown as orbiter's development test objective (DTO) on Space Transportation System (STS)-127, STS-133, STS-134, and STS-135.

The Assessment Plan was approved by the NESC Review Board (NRB) on March 8, 2012. The preliminary stakeholder summary was approved by the NRB on January 31, 2013. Mr. Neil Dennehy, NASA Technical Fellow for Guidance, Navigation, and Control (GN&C) at the Goddard Space Flight Center (GSFC), was selected to lead this assessment.

The primary stakeholders for this assessment were Mr. William Gerstenmaier, AA for HEOMD, Orion Multi-Purpose Crew Vehicle (MPCV) Project Manager; Ms. Kathy Lueders, International Space Station Visiting Vehicle Office; and Mr. Steve Labbe, Chief of NASA's Applied Aerospace and Flight Mechanics Division.

The secondary stakeholders for this assessment were Mr. Frank Cepollini, Spacecraft Servicing Program Office; Mr. Rich Mrozinski, Automated Rendezvous and Docking Community of Practice; and Dr. Ken Lebsock, GN&C Technical Discipline Team.

2.0 Signature Page

Submitted by:
Team Signature Page on File – 5-1-13

Mr. Cornelius J. Dennehy Date

Significant Contributors:

Dr. Peter A. Parker Date

Mr. Scott P. Cryan Date

Mr. Fred D. Clark Date

Ms. Jennifer Valdez Date

Mr. Andrew F. Heaton Date

Mr. Mogi G. Patangan Date

Dr. John A. Christian Date

Mr. Gary D. Spiers Date

Mr. Matthew J. Strube Date

Mr. Douglas Brown Date

Signatories declare the findings, observations, and NESC recommendations compiled in the report are factually based from data extracted from program/project documents, contractor reports, and open literature, and/or generated from independently conducted tests, analyses, and inspections.

3.0 Team List

Name	Discipline	Organization
Core Team		
Neil Dennehy	NESC Lead	GSFC
Peter Parker	NESC Deputy Lead	LaRC
Scott Cryan	Deputy Lead	JSC
Patricia Pahlavani	MTSO Program Analyst	LaRC
Douglas Brown	Statistical Analysis	BAH
John Christian	LIDAR Sensor Algorithm SME	JSC (now with WVU)
Fred Clark	BET Development and Statistical Analysis	Draper Laboratory (Houston)
Andy Heaton	LIDAR Sensor SME	MSFC
Heather Hinkel	STORRM Sensor SME	JSC
Ricky Howard	LIDAR Sensor SME	MSFC
Mogi Patangan	Sensor Data Mapping/Error Analysis	Jacobs
Gary Spiers	Dragon Eye Sensor SME	JPL
Ryan Stillwater	Sensor Data Evaluation Support	DFRC
Matthew Strube	TriDAR Sensor SME	GSFC
Jenny Valdez	TriDAR Sensor SME	GSFC
Administrative Support		
Linda Burgess	Planning and Control Analyst	LaRC/AMA
Diane Sarrazin	Project Coordinator	LaRC/AMA
Christina Williams	Technical Writer	LaRC/AMA

4.0 Executive Summary

Light detection and ranging (LIDAR) sensors perform critical rendezvous relative navigation (RelNav) sensing from initial long-range acquisition at several kilometers (km) and tracking of the target spacecraft/body through terminal range/bearing measurements for proximity operations necessary for docking/berthing/capture. This assessment quantitatively evaluated the performance of three LIDAR rendezvous sensors: the Sensor Test for Orion RelNav Risk Mitigation (STORRM) Vision Navigation Sensor (VNS), DragonEye, and Triangulation and LIDAR (TriDAR). These sensors were flown as orbiter development test objective (DTO's) on Space Transportation System (STS)-127, STS-133, STS-134, and STS-135 from 2009-2011. All three systems were developmental units and not qualified flight systems.

The assessment team performed an independent, statistically-based analysis of LIDAR sensor data sets generated from the DTOs. Each LIDAR sensor's DTO performance is summarized relative to their individual DTO performance specifications, when provided, in range and bearing and areas of anomalous/unexplained data are identified. The assessment does not address future mission and vehicle specific objectives and specifications. In addition, detailed investigations of instrument and flight anomalies were out of scope for this assessment.

For performance analysis, each sensor's estimated range and bearing was compared to the best estimated trajectory (BET) computed from the trajectory control sensor (TCS) measurements through the Rendezvous and Proximity Operations Program (RPOP). The residual difference between the sensor and BET was statistically summarized, incorporating modeling of systematic biases and accounting for time series correlated data structure, as required.

The STORRM DTO met its objectives and provided operational and performance data to continue maturing the system design. All data processing and centroiding were performed post-flight, rather than on-board. Range performance was out of specification for a single range bin (162-324 meters). A 2-meter bias was discovered in ground testing and confirmed from comparison to the BET and pose-based estimates of range. The team found that the noise analysis method of second-differencing provided in the STORRM report [ref. 9] led to underestimates of noise performance in some cases when autocorrelation was present in the data. It is recommended that the STORRM VNS processing development be conducted to mature the algorithms that will be implemented within the sensor and navigation system to provide in-flight, on-board range, and bearing.

The DragonEye DTO met its qualitative objectives. However, performance specifications for the DTO were not established. The DragonEye bearing measurements did not meet the Dragon vehicle specifications during tracking of a single reflector. The team found that intensity peak determination impacts range measurement and pixel saturation impacts ability to identify the actual peak. Saturation impacts centroiding and feature identification. The DragonEye performance is adversely affected by host vehicle rotation with respect to the local vertical, local horizontal (LVLH) reference frame and when the host vehicle undergoes translational

maneuvers. There are significant differences in the maturity of the systems flown on STS-127 and STS-133, and the team focused its analysis on STS-133. It is recommended to consider adjusting the camera design to achieve the specifications, and/or the DragonEye specifications should be changed to reflect flight requirements.

The TriDAR DTO met its qualitative objectives. However, performance specifications for the DTO were not established. TriDAR data processing was performed on-board, real-time during the DTO. The team found a 1-meter bias in the range measurements from 200-meters to dock. In long-range blob mode, TriDAR erroneously identified a single solar array instead of the International Space Station (ISS), which resulted in range errors of 20 meters and bearing errors of 12 degrees. Several data processing and recording anomalies were found in the data including asynchronous output of pose parameters, time-based stale measurement data that were flagged as valid. It is recommended that the root cause of the bias be determined, which may involve reconciliation of computer-aided drawing (CAD) geometry, reference coordinate systems, and/or more extensive ground testing that could help determine the range error. It is recommended that the flight software should include an algorithm to determine if the scan is incomplete based on *a priori* target vehicle knowledge.

Across all three sensors, obtaining the DTO data sets required approximately 3 months of a formal agreement between NASA and the Canadian Space Agency (CSA). It is recommended that the Autonomous Rendezvous and Docking (AR&D) Community of Practice (CoP) establish data-sharing requirements and agreements prior to conducting joint DTOs. The team found that when processing raw sequence or intensity and range data from flash LIDAR sensors, data exclusion of obvious erroneous range data due to spurious reflections is critical to measurement performance, particularly for real-time flight applications. Furthermore, numerous spurious reflections from parts of the ISS, not LIDAR reflectors, occurred for the DragonEye and STORRM VNS. By contrast, the TCS, which was a scanning LIDAR used during the Space Shuttle Program (SSP) for proximity operations and docking provided few spurious reflections throughout its lifetime. These spurious reflections make reflector identification and navigation difficult. Overall, it is recommended algorithm development and testing be performed to enable robust and reliable preprocessing of flash LIDAR imagery data. Finally, it is recommended continued investments be made to the AR&D CoP into algorithm maturity for real-time flight applications of LIDAR sensors.

Ultimately, this assessment improved NASA's familiarization with and understanding of each LIDAR sensors' hardware, software, and algorithm functionality. By providing insight on design and performance of this existing family of LIDARs and their raw data processing RelNav algorithms, NASA gained an improved definition of LIDAR sensor performance/functional requirements for future sensor procurement specifications. Overall, this assessment improved NASA's smart buyer posture for future LIDAR RelNav sensor procurements.

5.0 Assessment Plan

This assessment quantitatively evaluated the individual performance of three LIDAR rendezvous sensors, (i.e., TriDAR, DragonEye, and STORRM VNS), flown as orbiter DTOs on STS-127, STS -133, STS-134, and STS-135. The evaluation was based on the specifications and objectives defined by each DTO's Principal Investigator (PI).

The primary objectives, as defined by the stakeholders, were:

1. Perform an independent, detailed, and statistically-based analysis of LIDAR sensor data sets (i.e., raw and processed data) generated from the SSP DTOs.
2. Summarize each LIDAR sensor's DTO performance relative to their individual DTO performance specifications.
3. Identify specific areas of anomalous/unexplained LIDAR DTO data (for subsequent discussion with LIDAR providers).

Future mission and vehicle-specific objectives and specifications were outside the scope of this assessment. Detailed investigations of instrument and flight anomalies were not performed. Anomalies, including missing data, were noted, but not investigated. A root cause investigation of instrument performance relative to the DTO specification and operational flight anomalies were outside the scope of this assessment. However, these anomalies were documented for future investigations.

Overall, this assessment provided insight and guidance to improve NASA's posture as a smart buyer for future LIDAR RelNav sensor procurements. Furthermore, it improved NASA's familiarization with an understanding of each LIDAR sensors' hardware and software (algorithm) functionality. By providing insight on design and performance of this existing family of LIDARs and their raw data processing RelNav algorithms, NASA gained an improved definition of LIDAR sensor performance/functional requirements for future sensor procurement specifications.

LIDAR sensors are baselined for several of NASA's, and its industry partners, future missions. LIDAR sensors perform the critical rendezvous RelNav sensing from initial long-range (several km) acquisition and tracking of the target spacecraft/body through terminal range/bearing measurements for proximity operations and for final alignment for docking/berthing/capture. LIDAR RelNav sensors will be used on the Orion Multi-Purpose Crew Vehicle (MPCV), expected to be used on the new generation of commercial crew and cargo vehicles being developed by industry. A LIDAR sensor was baselined for the guidance, navigation, and control (GN&C) subsystem on NASA's Origins, Spectral Interpretation, Resource Identification, and Security Regolith Explorer Asteroid Sample Return Mission under development. Similarly, LIDAR sensors will be employed for RelNav sensing for future spacecraft servicing missions. Consequently, given this reliance on LIDAR sensors for future missions and the need to mitigate the technical risk of their use, NASA engineers and mission designers must better understand the

intrinsic functionality and performance characteristics of flash and scanning LIDAR sensors. This assessment of the LIDAR sensor data sets (obtained from multiple SSP DTO flight tests) will increase NASA's understanding and knowledge of LIDAR sensor technology. The result of this assessment improves NASA's familiarization with an understanding of the current generation of LIDAR sensor hardware and associated software-based data processing RelNav algorithms.

Six SSP missions have supported DTOs in which on-orbit flight testing of three different LIDAR rendezvous sensors have been performed. From these six, four were assessed (two DTOs from STS-128 and STS-131 were considered to be of low value since they utilized older versions of the TriDAR sensor and therefore are not included in this assessment). Each DTO data set was analyzed by the sensor supplier or the organization that supported the DTO. However, a comprehensive, quantitative analysis of the individual performance of each sensor versus their individual DTO performance specifications had not been performed for all DTOs. The specifications and objectives for each DTO were defined by their respective PI. Table 5.0-1 provides the mission summary for each DTO, sensor system, and key personnel.

Table 5.0-1. LIDAR Sensor and DTO Summary

Rel Nav LIDAR Sensor	STS DTO	Mission App	DTO Principal Investigator	NASA DTO Sponsor
DragonEye (ASC)	127 (2009)	SpaceX Dragon S/C	Paul Wooster (SpaceX)	Mike Horkachuck and Warren Reummele (COTS)
DragonEye (ASC)	133 (2011)	SpaceX Dragon S/C	Paul Wooster (SpaceX)	Mike Horkachuck and Warren Reummele (COTS)
STORRM VNS (Ball)	134 (2010)	Orion MPCV S/C	Heather Hinkel (JSC/EG)	Howard Hu (Orion)
TriDAR (Neptec)	135 (2011)	Orbital Cygnus S/C	Stephane Ruel (Neptec)	Larry Schmidt (JSC/MV)

6.0 Background

This section provides a high-level overview of the team's approach and activities described in subsequent sections. At the beginning of the assessment, the team reached a consensus on analyzing the range and two components of bearing as compared to the BET for the performance metrics for all of the LIDAR sensors. The BET is not measured without error; therefore uncertainty in the BET was recognized and considered in the comparison analyses contained in this report. The DTO data sets were obtained from a draft release of reference 9; SpaceX-supplied data from the DragonEye DTO, and TriDAR data through a NASA/CSA formal agreement. The BETs (discussed in detail in a subsequent section) were generated for each DTO, only STS-134 BET existed, and was used as the benchmark for comparison. A pre-processing step was performed to identify the targets and align the LIDAR sensor with the BET. A statistical comparison methodology was developed to compare LIDAR sensor-derived estimates of range and bearing with the BET. The analyses of the three sensors were conducted in a modular analysis utilizing multiple subteams to perform independent confirmatory analyses for each DTO. Figure 6.0-1 is a view into the orbiter payload bay that illustrates the location of the LIDAR sensors relative to the TCS. The BET is computed from TCS measurements through the RPOP Kalman filter, and the BET is used as the reference for comparison. Figure 6.0-2 is a view looking at the ISS docking ring and highlights some of the typical locations of reflective targets discussed throughout the report.

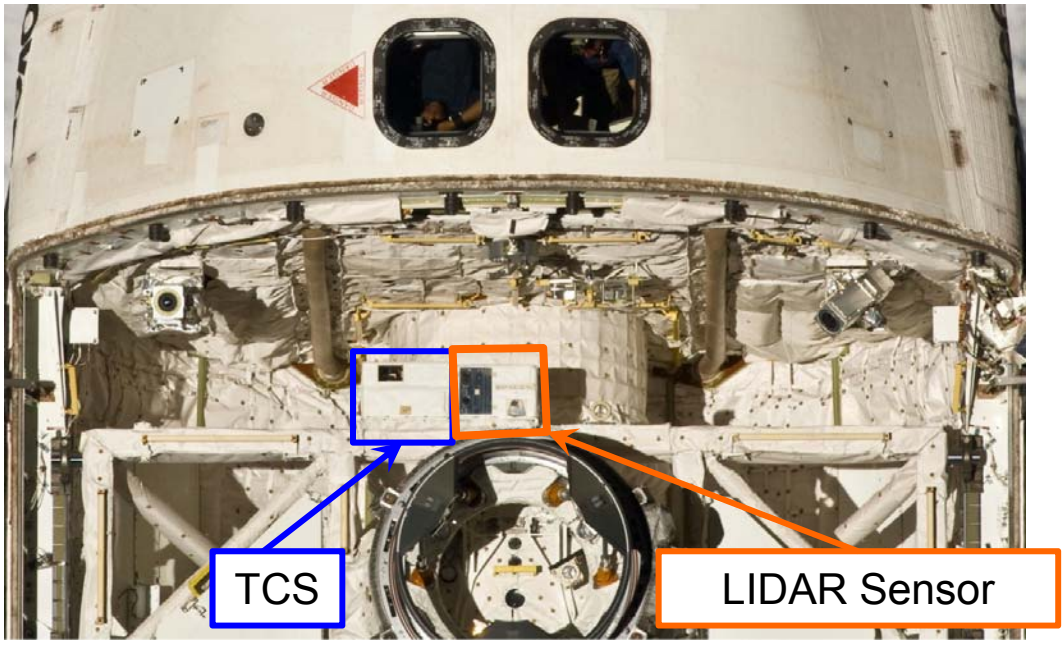

Figure 6.0-1. View into Orbiter Bay Illustrating LIDAR Sensor Location

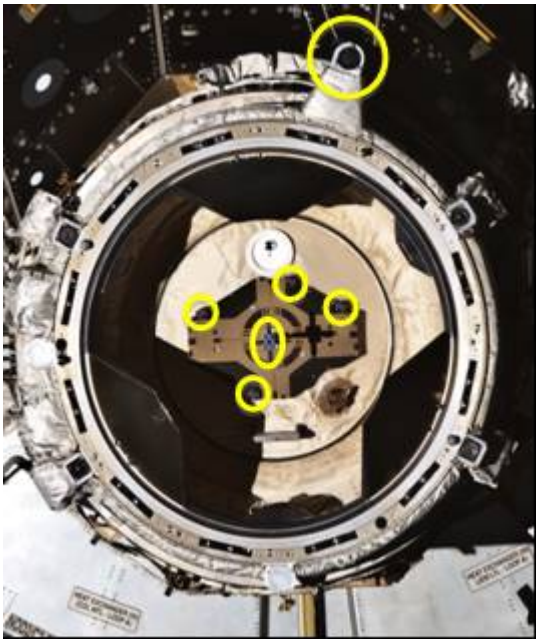

Figure 6.0-2. View into the ISS Docking Ring Illustrating Reflective Target Locations

Figure 6.0-3 shows the ranges of each sensor and the sensors' range bins that were analyzed during the assessment. The range bins were defined by the sensor developers to optimize sensor parameter settings by range.

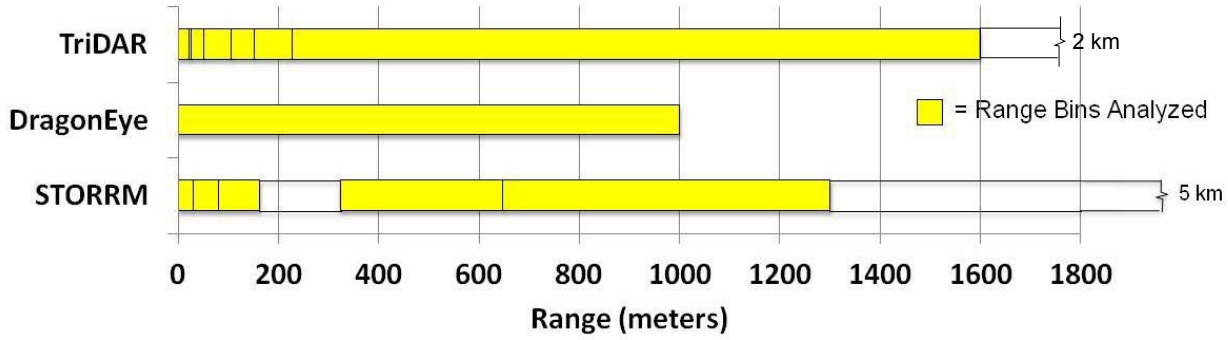

Figure 6.0-3. Overlay of NESC Assessment Ranges Analyzed (5 km extension of STORRM with yellow denoting as analyzed by the NESC)

In the following sections, details of the analysis process are described followed by the results for the three LIDAR sensors.

6.1 BET Generation

The BET is derived post-flight from multiple sources and is used as a benchmark for comparison to LIDAR sensor-derived range and bearing. An overview of the BET is provided in this section, see Appendix D, E, F, and G for additional details. The BET is used as the reference for comparison, and the development process is outlined in Figure 6.1-1, **Φ** denotes the state transition matrix, **P** denotes the state covariance matrix, and **x** denotes the [6 × 1] state vector. The equations of the smoother are given below [ref. 1].

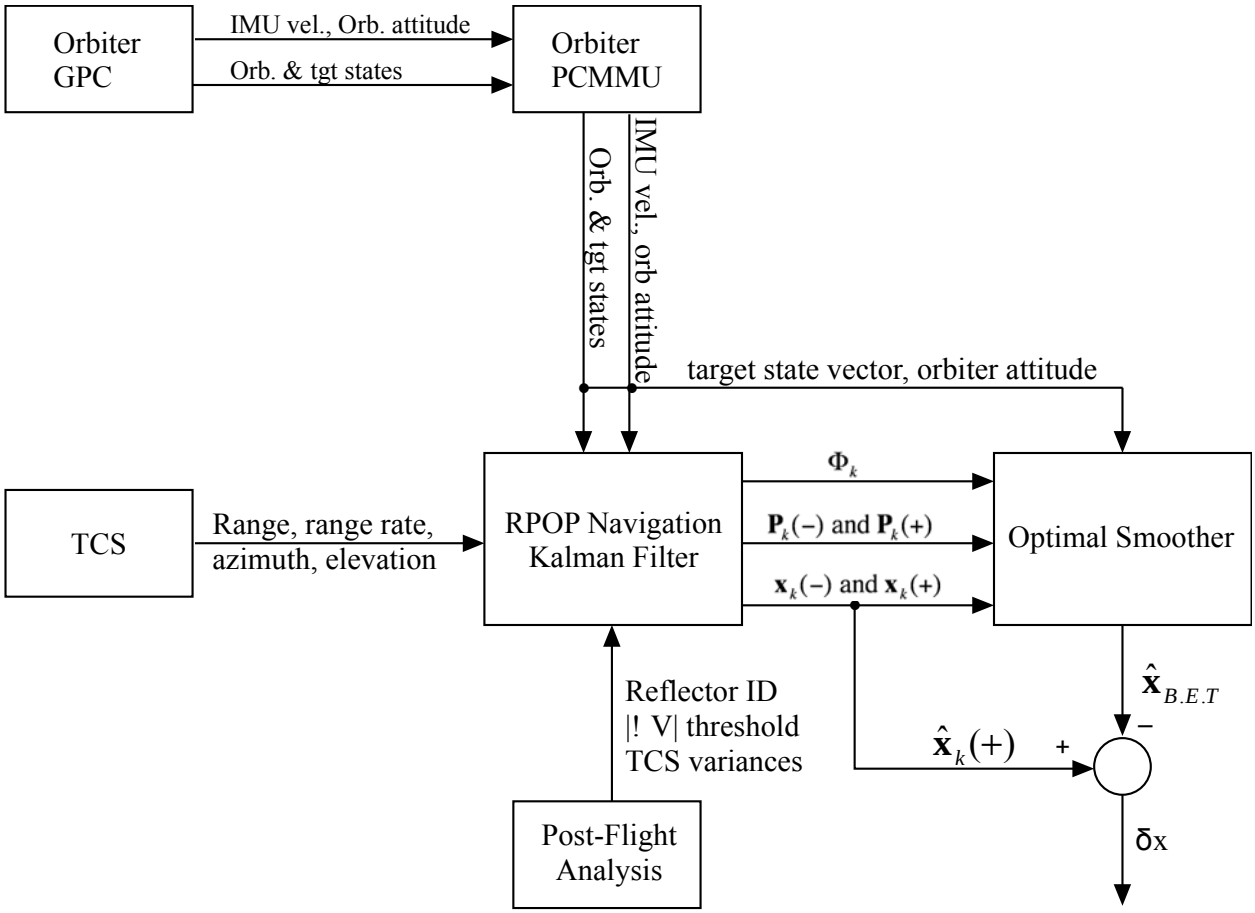

Figure 6.1-1. BET Development Process

Let the final step be denoted by the subscript *N*. The smoothing algorithm begins at the last state and moves backward in time. The smoothed state vector at step *k* is estimated from:

$$\hat{\mathbf{x}}_{k|N} = \hat{\mathbf{x}}_k(+) + \mathbf{A}_k[\hat{\mathbf{x}}_{k+1|N} - \hat{\mathbf{x}}_{k+1}(-)]$$

where $\mathbf{A}_k = \mathbf{P}_k(+)\Phi_k^T\mathbf{P}_{k+1}^{-1}(-)$ and $\hat{\mathbf{x}}_{N|N} = \hat{\mathbf{x}}_N(+)$ for $k = N - 1$

The smoothed covariance matrix is computed from:

$$\mathbf{P}_{k|N} = \mathbf{P}_k(+) + \mathbf{A}_k[\mathbf{P}_{k+1|N} - \mathbf{P}_{k+1}(-)]\mathbf{A}_k^T$$

where $\mathbf{P}_{N|N} = \mathbf{P}_N(+)$ for $k = N - 1$

Flights to the ISS since STS-114 included an R-bar pitch maneuver (RPM). During this maneuver, the orbiter rotated 360 degrees in pitch at 0.75 degree/second (deg/sec). There are no TCS measurements available to the RPOP Kalman filter throughout the rotational maneuver. The output of RPOP is input to the optimal smoother. Without measurements during this time interval, the optimal smoother is unable to maintain an accurate trajectory. Therefore, after TCS reacquisition following the RPM there is a discontinuity in the trajectory.

For each flight that a BET is constructed, there is analysis required to determine the reflectors tracked by the TCS during the approach. RPOP has automatic reflector identification as a built-in feature, but does not reliably work at long range.

After identifying the reflectors TCS tracked, the appropriate RPOP output file is adjusted and RPOP is run in "replay" mode. In replay mode, the data were input to RPOP during flight are processed by RPOP after the flight. In addition, during replay mode, the state transition matrix and the state covariance matrix are output, whereas in flight they were not output to save data storage space on the hard drive.

RPOP assumes the ISS is fixed in LVLH attitude during the approach. To obtain a more accurate BET, the estimated ISS attitude from the ISS on-board software is used. The data sets were retrieved from the orbiter data reduction complex (ODRC).

In addition to setting the playback data with appropriate reflectors that TCS tracked, the team varied some of the RPOP navigation initialization loads (I-loads) to obtain optimal performance. The RPOP I-loads were developed to allow the filter to work for a variety of realized performance from the TCS. Therefore, the variances of the measurements were chosen to be larger than the anticipated performance. When chosen in this way, if the TCS had modestly degraded performance on a particular flight, the filter would have been able to operate nominally.

In developing the BET, estimates of the noise were generated because the TCS flight data were analyzed after most flights [ref. 2]. The team does not need to run the Kalman filter with the conservative I-loads developed for flight, but may tune the I-loads to account for the flight performance for which a BET is developed.

The quantization of the orbiter's inertial measurement unit (IMU)-sensed velocity was 0.01049 m/sec in each axis [ref. 3]. To guarantee an IMU bias, within its specification, is not used in RPOP state propagation, the IMU-sensed delta-velocity (ΔV) is used only when its magnitude exceeds 0.01829 m/sec. The Space Shuttle On-Orbit/Rendezvous Navigation Principal Function software used the same threshold [ref. 4].

Previous experience has shown that lowering the ΔV threshold to 0.01219 m/sec improves performance in constructing a BET, which was done for each of the flights analyzed during this study.

In addition to the changes in TCS-related parameters and the ΔV threshold, the team used Kalman filter underweighting when the square root of the sum of the first three diagonal elements of the covariance matrix exceeds 10. During this time, the HPH^T term in the calculation of the Kalman gain was increased by 20 percent [ref.4].[1]

Finally, in executing RPOP in playback mode, the orbiter body-to-TCS coordinate transformation matrix was redefined. The TCS is mounted to the orbiter docking system (ODS). ODS pressurization results in deflecting the TCS about 0.9 degrees toward the forward orbiter bulkhead. The effect of this was the orbiter body-to-TCS frames were related by a rotation of only 89.1 degrees, rather than the nominal value of 90 degrees. This effect is accounted for in constructing each BET for this assessment, but the nominal value (90 degrees) was used in the flight RPOP versions.

6.2 ISS Retro-reflector Location

The ISS has several retro-reflector assemblies located on various modules to aid incoming vehicles in their relative navigation determination through the use of LIDAR units. In support of the orbiter TCS, the reflectors were cataloged for quicker processing and identification within RPOP. Figure 6.2-1 shows the general location of the reflector assemblies and their corresponding field of regard (FOR). The color-coded traces highlight the FOR of each reflector. Table 6.2-1 lists the same reflectors and matches their TCS identification number to their location and pointing direction. This information is utilized throughout this report when discussing various reflectors investigated. ISS modules and appendages cause blockage to some of the reflectors, thus reducing their effective FOR. The blockage is seen in the Figure 6.2-1 by the segmented and/or shortened arcs.

[1] Here, **H** denotes the partial derivative of the measurement with respect to the relative state vector and **P** denotes the state covariance matrix.

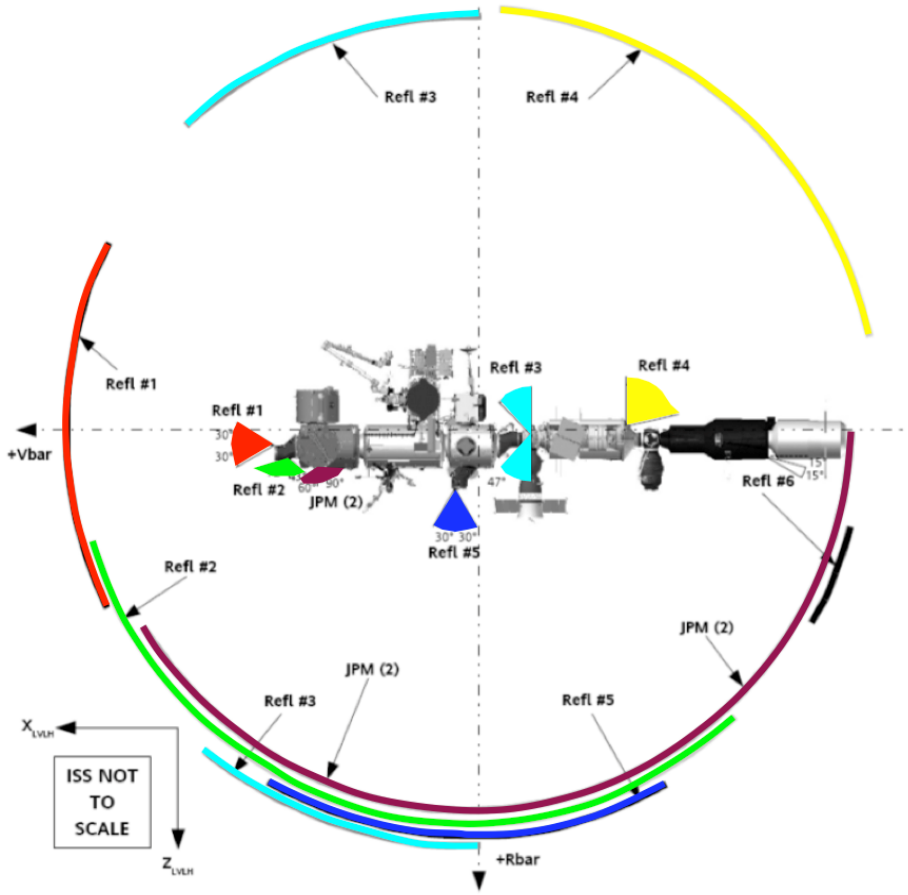

Figure 6.2-1. ISS Retro-reflector Locations and FOR

Table 6.2-1. ISS Retro-reflector Information

TCS #	Component Name	Pointing Direction *	FOR ** (degree)	Reflector Type
1	PMA2 Node2 FWD, Planar	+X	30	Single Planar
2	PMA2 Node2 FWD, Hemi	+Z	90	Hemispherical
3	FGB FWD, Hemi	+X	20	Hemispherical
4	FGB AFT, Hemi	-X	40	Hemispherical
5	PMA3 / PMM Node 1 Nadir	+Z	30	Single Planar
6	SM AFT	-X	30	Multiple Planars
7	JEM A {JPM (2) in figure}	+Z	90	Hemispherical
8	JEM B {JPM (2) in figure}	+Z	90	Hemispherical

* Pointing direction with respect to the ISS LVLH reference frame (as per Figure 6.2-1)
** FOR, half-angle in degrees

6.3 LIDAR Sensor Attitude Alignment

The vehicle state inputs from the BET for each DTO flight could account for misalignments between the predicted and actual reflector centroids. The ISS attitude was held fixed in the LVLH reference frame. The second factor was the alignment of the detector behind the sensor optics. For the STORRM VNS and TriDAR, the translational alignments were mapped to the detectors but the rotational alignments were unknown. For the DragonEye, the detector translational and rotational alignments to the sensor optics were unknown. A sensor-to-BET attitude alignment analysis may provide some of the missing information. The last factor emphasizes the importance of precise knowledge of the sensor location with respect to the orbiter structure. For the DragonEye flights, the sensor location was not surveyed and may have contributed errors to the predicted reflector centroids.

To correct for some of the identified misalignments and to employ the predicted reflector centroid data for easier BET comparison, two auxiliary features were included with the reflector visibility tool: the sensor to BET attitude misalignment correction and centroid matching for reflector identification and sorting.

The sensor to BET attitude misalignment was computed to achieve maximum agreement between the predicted data and actual sensor measurements. A single angular misalignment matrix was computed for the entirety of the data collected on each DTO mission (STS-127, STS-133, and STS-134) using the Davenport q-method solution to Wahba's problem. A shortcoming of this method is when the translational misalignment is unknown, which is the case for the DragonEye data. Additionally, performing this alignment correction on smaller sections of the trajectory data produce better agreement between the predicted and actual centroids.

6.4 Reflector Visibility Identification

The reflector visibility tool was used to generate the predicted reflector locations with respect to the sensor frame for the STORRM VNS on STS-134 and DragonEye on STS-127 and STS-133. A detailed description of this tool developed for STORRM is provided in Appendix I. Through a series of coordinate frame transformations, the tool used the ISS and orbiter relative position and attitude as obtained from RPOP, reflector locations with respect to the ISS structure frame, and sensor location with respect to the orbiter body frame (OBF) to check for line of sight visibility between reflectors and the sensor. The locations of STORRM reflective elements were obtained through a photogrammetric survey performed on STS-134. The tool accounted for reflector obscuration from ISS structure. However, the tool did not account for reflector return signal strength and signal interference.

Reflector visibility was contingent on the sensor being in the reflector's unobscured FOR which is target specific and the reflector being in the sensor's field-of-view (FOV). For the STORRM VNS, a third requirement for visibility was the reflector must be illuminated by the VNS laser since the laser field of illumination was commanded between 12- and 20-degrees. Once these checks were satisfied, the reflector was projected on the sensor image plane. Figure 6.4-1 shows

a screenshot of reflector visibility tool graphical user interface (GUI). The output panel includes the predicted reflectors in the intensity image, the relative motion plot of the orbiter with respect to the ISS center of gravity (CG) in a LVLH reference frame, time tags, calculated and raw TCS and state vector derived range, vehicle position and attitude inputs, and a table of visible reflectors and their predicted pixel locations.

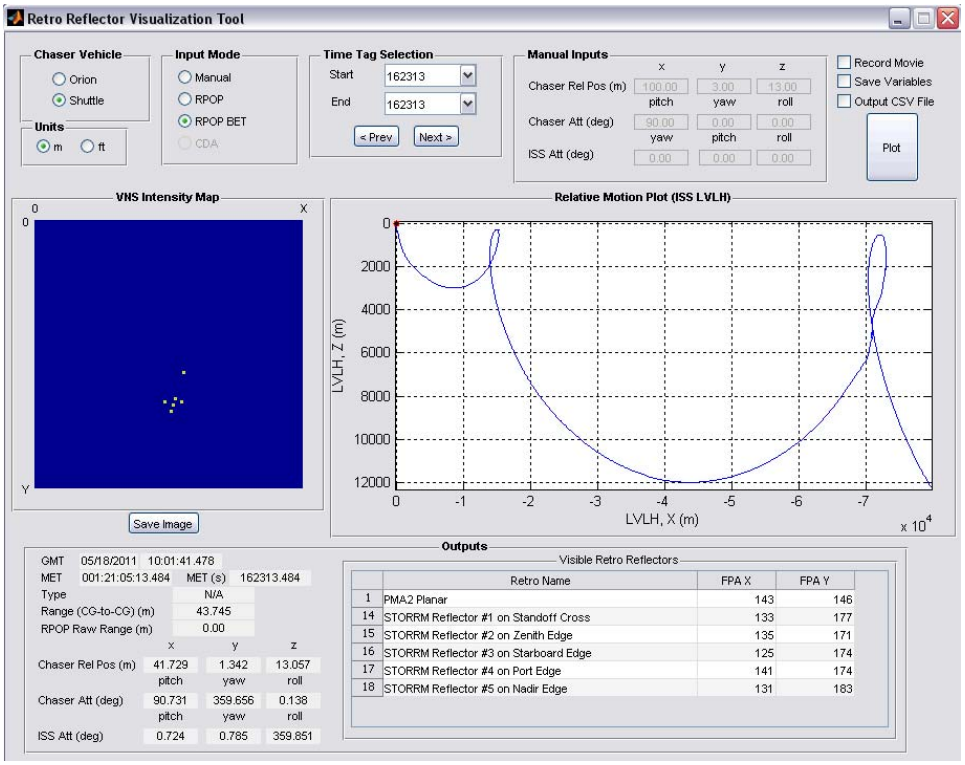

Figure 6.4-1. Reflector Visibility Tool GUI

The tool's accuracy in predicting exact reflector pixel location was dependent on the following factors:

1. Vehicle state inputs and misalignments.
2. Detector alignment to sensor optics.
3. Knowledge of sensor location with respect to the OBF.

After correcting for attitude misalignment, the predicted centroid data was used to match sensor centroids with ISS reflectors. The closest flight measurement to the predicted centroid was identified as that particular reflector. Through this process, the sets of centroids were sorted per reflector, which streamlined the process of comparing sensor to BET measurements.

Coordinate Frame Definitions

Reference 21 details the orbiter vehicle and body frames, the STORRM VNS camera frame, and the VNS image plane. The ISS document in reference 22 describes the ISS LVLH frame and the Space Station Analysis Coordinate System (SSACS). This section discusses the pertinent coordinate frames used in the tool that are not described in the aforementioned reference documents. These coordinate frames are the VNS transmit optics frame and the local reflector frame.

STORRM VNS Transmit Optics Frame

The STORRM VNS transmit optics frame is parallel to the VNS camera frame. The frame origin is a variable input in the run configuration and its values are with respect to the VNS camera frame. The intent of this frame was to improve simulation fidelity of the VNS receive and transmit optics. The specular nature of the corner cube reflector return causes issues with the bi-static configuration of the VNS receive and transmit optics. However, this phenomenon was not fully modeled and implemented in the tool since it is sufficient to rely on line of sight for STORRM.

Local Reflector Frame

The local reflector frame is fixed to the reflector's front plane with the positive x-axis along the boresight and the y- and z-axes lying on the reflector's front plane to complete a right-handed Cartesian coordinate frame (Figure 6.4-2).

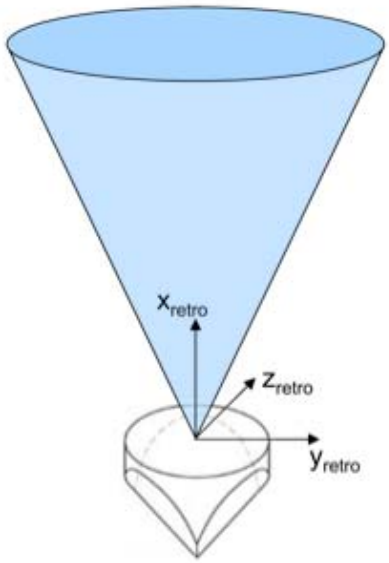

Figure 6.4-2. Local Reflector Frame

STORRM VNS and Reflector Line of Sight Vectors

Given the known values from the run configuration and input data, the goal is to obtain the line of sight vectors between the reflectors and the STORRM VNS to determine visibility. Figure 6.4-3 shows the process of computing the line of sight vectors from the known vectors.

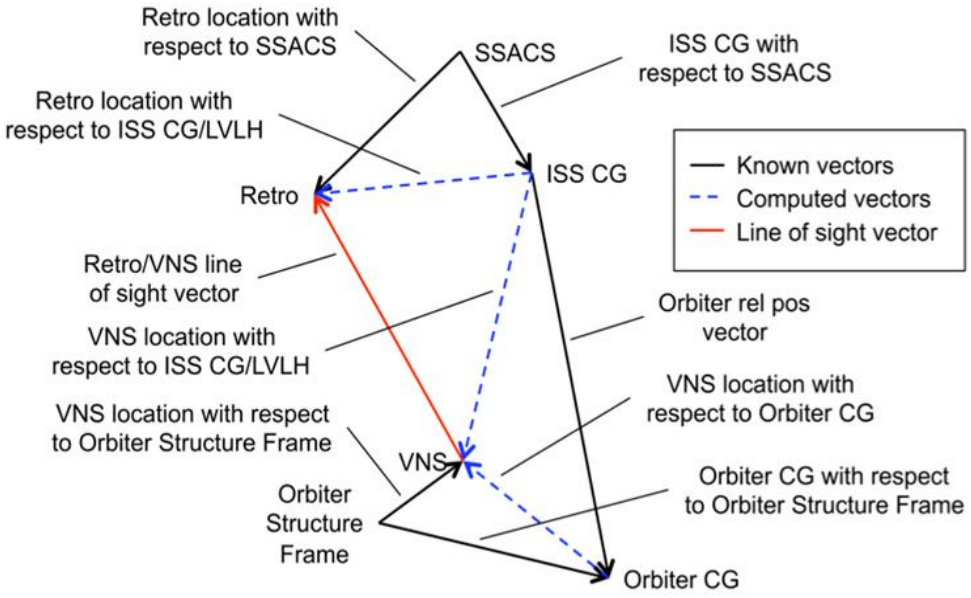

Figure 6.4-3. Frame Transformation Sequence

Transformation from one frame to another was obtained using:

$$\overline{\mathbf{X}}_B = \mathbf{M}_B^A \overline{\mathbf{X}}_A \quad \rightarrow \quad \begin{bmatrix} x \\ y \\ z \\ 1 \end{bmatrix}_B = \begin{bmatrix} \mathbf{T}_B^A & \mathbf{t}_{A/B} \\ \mathbf{0}_{1x3} & 1 \end{bmatrix} \begin{bmatrix} x \\ y \\ z \\ 1 \end{bmatrix}_A$$

where $\overline{\mathbf{X}}_A$ is the location of the object in frame *A* and $\overline{\mathbf{X}}_B$ is the location of the object in frame *B*. $\mathbf{T}_B^A$ is the transformation matrix from frame *A* to frame *B*, and $\mathbf{t}_{A/B}$ is the location of the origin of frame *A* with respect to frame *B* [1].

Reflector Obscuration Model

The reflector obscuration model requires the line of sight vector from the reflector to the STORRM VNS. Given how the obscuration data is structured, the line of sight vector is rounded to the nearest 10-degree increment in the reflector y-z plane. The corresponding minimum and maximum FOR angles are then used to determine visibility or obscuration. Figure 6.4-4 shows the coordinate frame convention for the reflector obscuration data. The y-z plane of the reflector

is divided into 10-degree increments with the 0-degree lying on the y-axis and the 90-degree mark lying on the z-axis. The reflector FOR angle is measured with zero degrees at the reflector's boresight (x_{retro}) and increasing towards the y-z plane (90 degrees on the y-z plane).

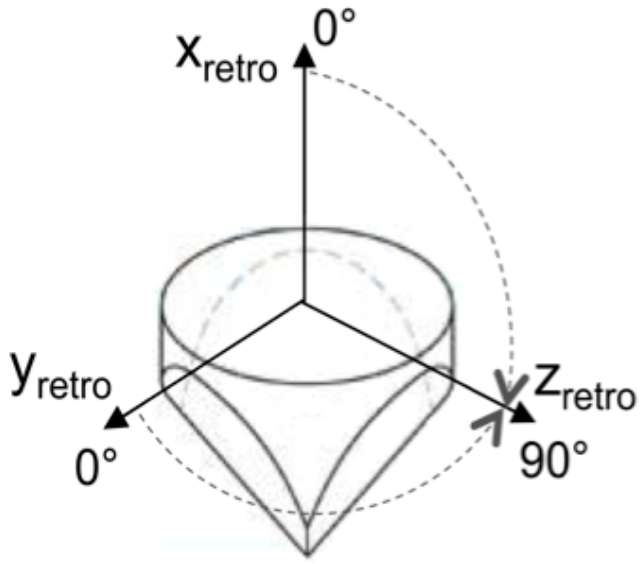

Figure 6.4-4. Reflector Obscuration Data Coordinate Frame Convention

Transformation to STORRM VNS Image Frame

Once the STORRM VNS to reflector line of sight is obtained and the obscuration checked, the reflector location can then be transformed into the VNS image frame using:

$$\bar{\mathbf{u}}_{IP} = \mathbf{K}_{IP}\bar{\mathbf{x}}_{IP} \quad \rightarrow \quad \begin{bmatrix} u \\ v \\ 1 \end{bmatrix}_{IP} = \begin{bmatrix} -s_x & 0 & u_p \\ 0 & -s_y & v_p \\ 0 & 0 & 1 \end{bmatrix} \begin{bmatrix} x \\ y \\ 1 \end{bmatrix}_{IP}$$

where $\boldsymbol{s_x}$ and $\boldsymbol{s_y}$ are the x-axis and y-axis scale factors in units of pixel/length, and $\boldsymbol{u_p}$ and $\boldsymbol{v_p}$ is the location of the VNS boresight with respect to the VNS image [u, v] coordinate system [1].

6.5 Statistical Analysis Methodology

Sensor performance is based on a comparison to the BET. In this assessment, the BET is given as a CG-to-CG state vector of relative position and velocity. From the CG-to-CG position vector, the sensor-to-reflector position vector through coordinate transformation may be computed. The BET-estimated range, horizontal, and vertical measurements are functions of the BET-based sensor-to-reflector vector. Figure 6.5-1 shows the computation of the sensor-to-reflector position vector.

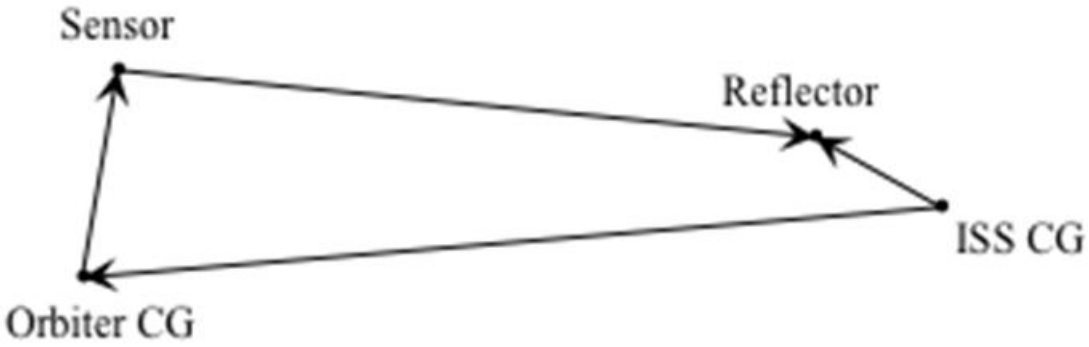

Figure 6.5-1. Measurement Geometry

The BET is expressed in LVLH coordinates based on Figure 6.5-1:

$$\mathbf{r}^{(LVLH)}_{sensor\,to\,reflector} = \mathbf{r}^{(LVLH)}_{ISS\,CG\,to\,Orbiter\,CG} + \mathbf{T}^{LVLH}_{Orbiter\,body}\,\mathbf{r}^{(Orbiter\,Body)}_{Orbiter\,CG\,to\,sensor} - \mathbf{T}^{LVLH}_{ISS\,body}\,\mathbf{r}^{(ISS\,body)}_{ISS\,CG\,to\,reflector}$$

The vector $\mathbf{r}^{(LVLH)}_{sensor\,to\,reflector}$ is transformed to sensor coordinates. The BET-estimated measurements are computed from the definition of the measurement in terms of $\mathbf{r}^{(sensor)}_{sensor\,to\,reflector}$. These definitions vary from sensor to sensor.

The estimated measurement errors are the sensor-derived measurement minus the BET-derived measurement.

Before computing estimated errors, the measurements must be sorted so each measurement is of the same reflector. Because the BET and sensor had different data rates, interpolation is necessary to synchronize the measurements. As an example, for STORRM the BET is given in approximately 4-second intervals, and the sensor data is given in 0.2-second intervals. Linear interpolation is used in this analysis. It has been shown that the error introduced by interpolation is small (see Appendices A, B, and C).

During each rendezvous of the orbiter with the ISS from STS-114 through STS-135, the orbiter executed the R-bar pitch maneuver at about 183 meter on the positive R-bar. During most of this time, the orbiter's TCS and DTO sensors were not pointed at the ISS and thus no measurements were produced. At the beginning and end of the RPM, the TCS was able to track a reflector on the ISS, but the accuracy of the BET is compromised during these intervals. Therefore, measurements by the DTO sensor at the beginning and end of the RPM are not included in this analysis because the estimated errors during these times are not reliable.

Any bias in the BET potentially adds to the estimated bias. Unless corrected for the bias, the estimated bias may be an underestimate. As explained in references 5 and 6, the TCS mounting

and misalignment biases are unknown, but estimated to be no worse than 1 degree. Because of this, although the team reports deviations between the BET-estimated horizontal and vertical measurements and the DTO sensor measurements, the team did not attempt to separate these deviations into bias components attributable to the DTO sensor and the BET.

For range measurements, the team estimated biases of the sensor measurements. The team computed the estimated bias by a two-step procedure. First, the team fit a polynomial ordinary least squares (OLS) regression to the estimated range errors. Next, the team computed the autocorrelation at lag 1 in the residuals from the OLS regression and then refit using generalized least squares (GLS) regression, accounting for the autocorrelation[2] [refs. 7, 8].

The DTOs tested scanning and flash LIDARs. The scanning LIDARs employ at least one set of gimbaled mirrors coupled with a narrow light source (typically an infrared (IR) laser operating in a pulse or continuous waveform manner). The two mirrors operate concurrently to produce a predefined scan pattern, providing mirror azimuth and elevation measurements. The scan pattern can be variable and adjusted based on moding and light energy returns. The TriDAR is a scanning LIDAR. Flash LIDARs employ a multi-pixel detector array and a light source (typically an IR laser). The laser emits a short pulse, which transmits through space and reflects off the target vehicle and returns. The laser energy returns and strikes the detector through a set of optics that steer/focus the light onto the detector. Each pixel measures the time of flight and laser energy intensity. The DragonEye and STORRM VNS are two variants of flash LIDARs.

7.0 Data Analysis

7.1 STORRM

7.1.1 Overview of STORRM DTO

The STORRM DTO flew aboard the Endeavour on STS-134 in May-June 2011. STORRM was designed to characterize the performance of the VNS flash LIDAR and docking camera (DC) being developed for the Orion MPCV Program. In addition, STORRM was designed to collect data from these sensors to mitigate the loss-of-mission risk in Orion test flights and to increase the sensor technology readiness level (TRL). Because the present report is concerned only with LIDARs, only the VNS will be reviewed. Information on the DC may be found in other STORRM-specific documentation [ref. 9].

The STORRM VNS will be the primary navigation instrument used by the Orion vehicle during RPOD starting at 5 km from the target vehicle. To assess sensor performance during the DTO, the VNS and DC were placed in the STORRM sensor enclosure assembly (SEA). The SEA was

[2] Autocorrelation is a measure of randomness ascertained by computing the correlation, or systematic relationship, between data values at varying time lags. If random, such autocorrelations should be near zero for any and all time-lag separations.

then mounted in the orbiter payload bay directly next to the TCS, a scanning LIDAR system used during proximity operations. A BET utilizing TCS measurements served as the benchmark for VNS post-flight analysis. The VNS data collection opportunities occurred on flight day 3 (FD3) during rendezvous and docking to the ISS and flight day 15 (FD15) during undock, fly-around, re-rendezvous and final separation. The re-rendezvous, designed to mimic the planned Orion rendezvous profile, differed from the nominal Shuttle trajectory. Throughout all of these mission phases, VNS data were produced and recorded at a rate of 30 Hz. These data were then combined during post-flight analysis to produce reflector range and bearing measurements at a rate of 1 or 5 Hz. More specifically, the range and bearings at each measurement time were generated through a NASA-developed centroiding algorithm [ref. 10] designed to deal directly with reflectors in f lash LIDAR imagery.

The prototype VNS tested during the STORRM DTO had eight different range bins. Using the phonetic alphabet, these are referred to as range bins Alpha through Hotel. Each range bin corresponded to a different set of sensor settings (e.g., gain, sensor internal timing, etc.) to improve its performance over a specific range. Therefore, the VNS results presented performance statistics and observations as a function of range bin.

In general, STORRM VNS performance during rendezvous, docking, undocking, fly-around, and re-rendezvous was as expected. Minor issues were encountered during rendezvous, but timely response from the STORRM team put on-board contingency procedures in motion resulting in minimal disruption to STORRM activities. STORRM collected 380 GBytes of VNS data while on-orbit. The STORRM team was able to observe through periodic data snapshots that the VNS performed as expected in terms of sensor moding (detector gain settings) and laser firing. The VNS performed well in imaging the ISS and exceeded expectations for its long-range ISS acquisition.

The overall STORRM VNS mission objectives were to test the on-orbit performance on three different trajectories:

1. A nominal orbiter RPOD trajectory to the ISS.
2. A nominal orbiter undocking trajectory from the ISS.
3. An Orion-like flight rendezvous/proximity operations trajectory to the ISS.

To meet the third objective, the space shuttle separated from the ISS and then performed an unprecedented re-rendezvous with the ISS with an approach of approximately 291 meters (956 feet).

Because the results discussed in this report deal only with the rendezvous and not the undock or re-rendezvous, focus in the subsequent sections will only be on the rendezvous performed on STS-134 FD3. Re-rendevous analyses are included in reference 9. The team decided to exclude it from this assessment since the approach was representative of performance. A graphical depiction of the STORRM rendezvous is shown in Figure 7.1-1. A summary of the VNS-related mission objectives are provided in Table 7.1-1.

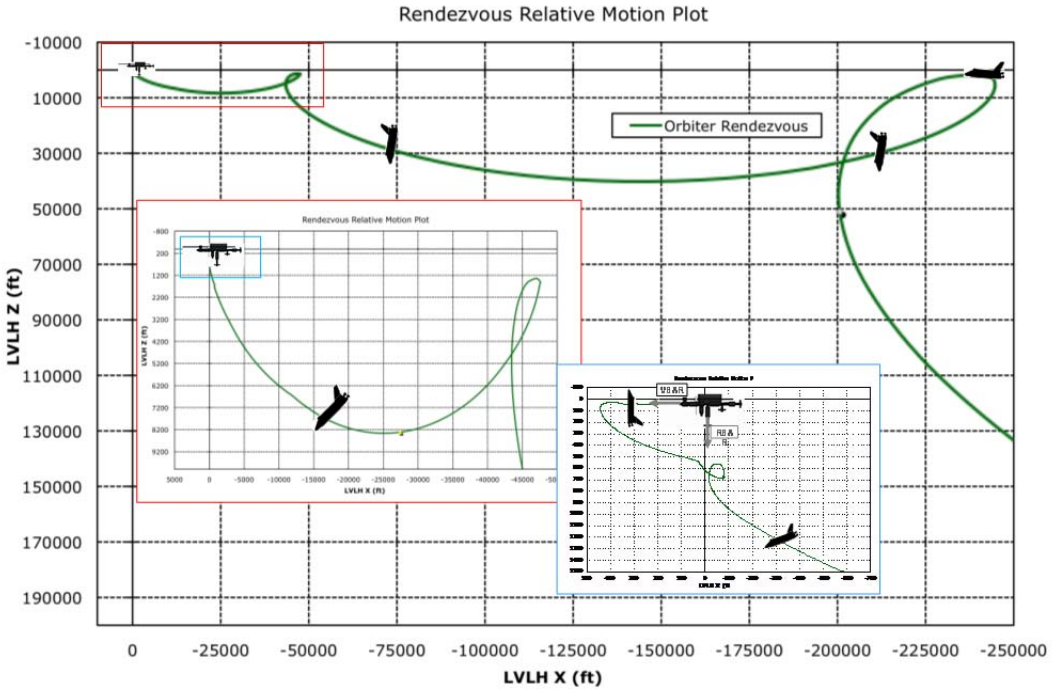

Figure 7.1-1. Relative Motion Profile for Nominal Orbiter Rendezvous and Docking

Table 7.1-1. STORRM VNS-related Mission Objectives

Flight Phase	#	VNS Objective
Rendezvous / Prox Ops (6 km – 3 km)	V01P	Characterize the ISS in the VNS wavelength (hot spots, obscuration, reflectance map)
	V02P	Determine initial acquisition range
	V03P	Prove operation with large relative velocities
Prox Ops (3 km – 50 m)	V04P	Characterize the ISS in the VNS wavelength (hot spots, obscuration, reflectance map)
	V05P	Collect data through known break track and reacquire conditions
	V06P	Prove tracking through accelerations while maneuvering
	V07P	Demonstrate transition between 3-degree-of-freedom (DoF) and pose modes
Final Approach (50 m – dock)	V08P	Allow for overlap with ground testing facilities
	V09P	Collect data to support pose calculation
	V10P	Characterize the ISS pressurized mating adaptor 2 (PMA2) augmented docking target
All Flight Phases	V11P	Perform calculations on raw data (R and I measurements) to determine geometric centroids to reflective elements
	V12P	Perform calculations on raw data to determine range and horizontal/vertical angles to target
	V14P	Characterize noise and bias

The range bin for STORRM are detailed in Table 7.1-2, the green highlighted boxes were assessed by the team.

Table 7.1-2. STORRM Range Bins

STORRM Bin	Range Bounds (m)
Hotel	0 - 30
Golf	30 - 81
Foxtrot	81 - 162
Echo	162 - 324
Delta	324 - 648
Charlie	648 - 1300
Bravo	1300 - 2590
Alpha	2590 - 5760

Summary of the STORRM VNS Performance from Reference 9

To obtain information useful for assessing the STORRM VNS's performance as a navigation sensor, a number of post-processing steps were performed on the raw data stored on the STORRM data recording units (DRUs). First, a range calibration algorithm supplied by Ball Aerospace Technologies Corporation was applied to the raw VNS images, which resulted in the "range corrected" images. Then, centroiding and reflector identification algorithms were used to identify candidate reflectors within the VNS imagery. For the bulk of the rendezvous, this algorithm combined six consecutive VNS images (collected at 30 Hz) to produce centroid measurements to candidate reflectors at a rate of 5 Hz. These candidate reflectors were compared to what the VNS was expected to see based on the BET. Using this comparison information, each candidate reflector could then be matched to a known reflector or be identified as a spurious reflection. Finally, after each candidate reflector in each VNS image was identified, a statistical analysis was performed to summarize the performance relative to the reference trajectory derived from the BET on the range and bearing of each reflector. A comparison with the BET, an enlargement of range bin Hotel (the closest range bin) is shown in Figures 7.1-2 and 7.1-3.

The range performance was noted to be out of specification in range bin Echo (162-324 meters). This anomaly is described in reference 9 and was attributed to VNS settings for that particular range bin. However, the nature of the problem was not fully resolved. Therefore, the team did not perform any further analysis on this range bin.

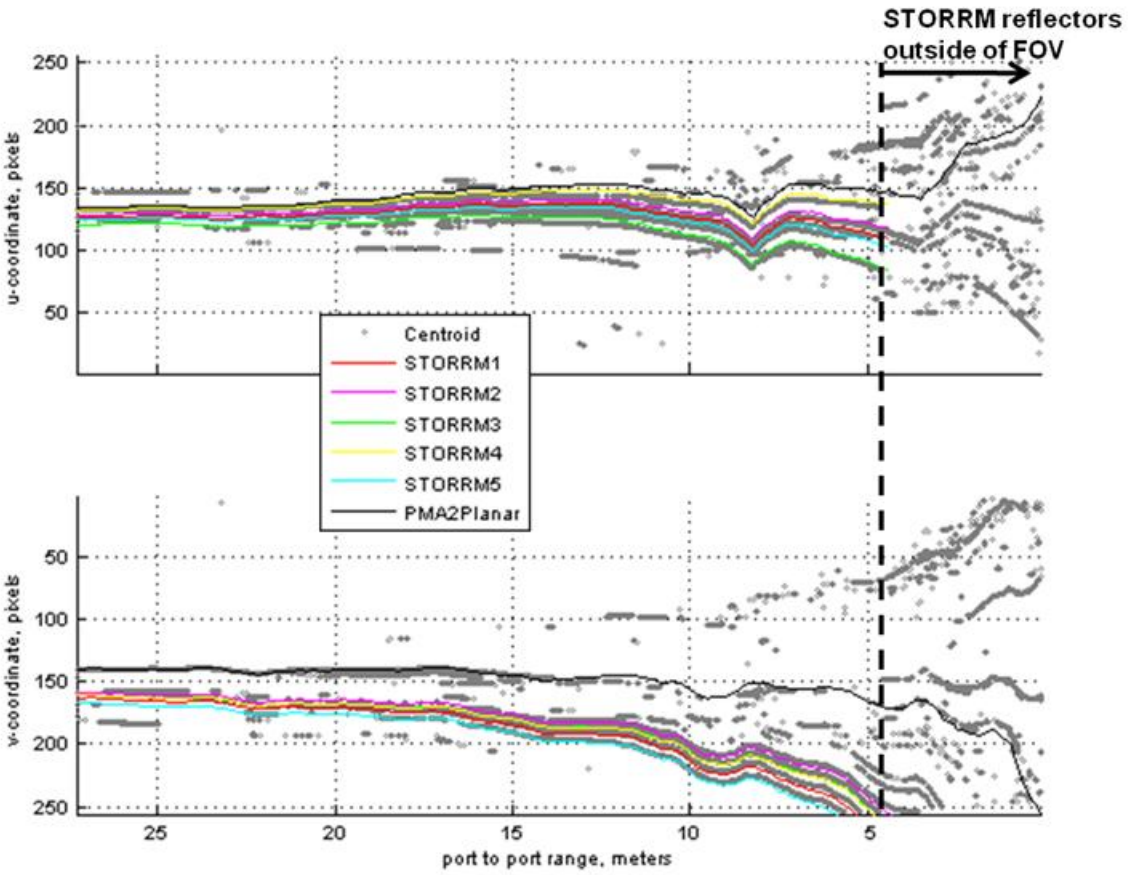

Figure 7.1-2. Time History of Centroid [u,v] Coordinates from STS-134 Docking: Range Bin Hotel

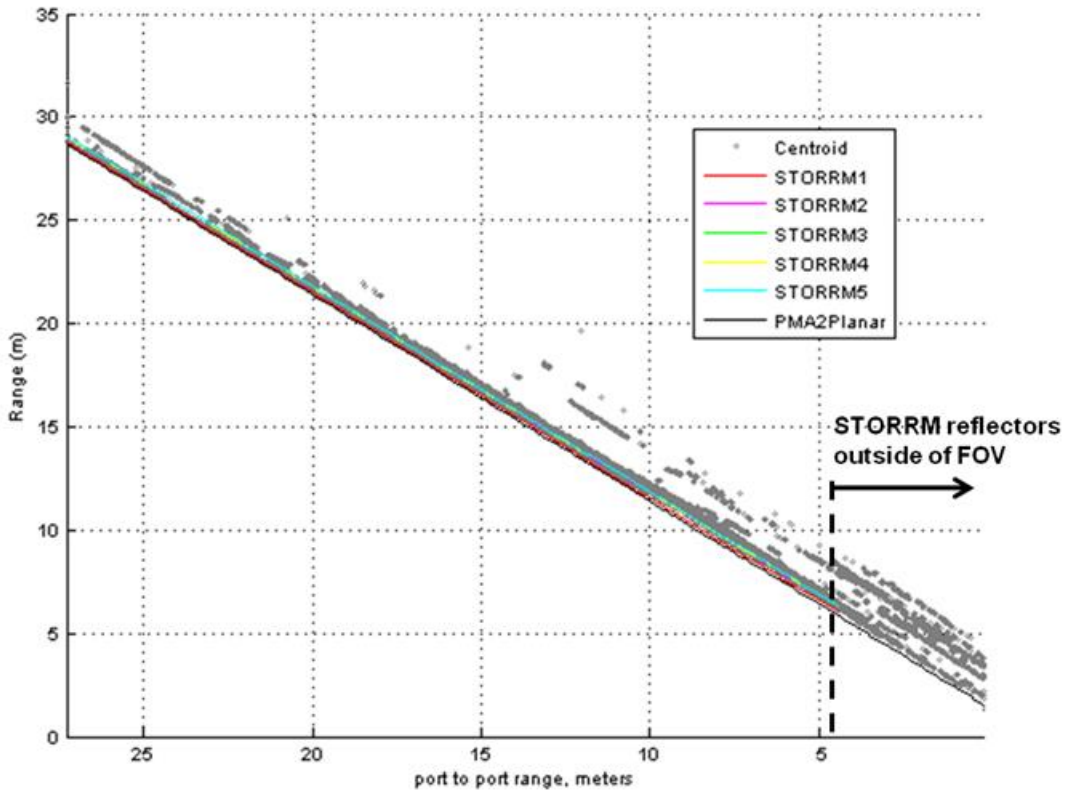

Figure 7.1-3. Time History of Centroid Ranges from STS-134 docking: Range Bin Hotel

Reference 9 captures an exhaustive analysis of the noise statistics for each range bin in all phases of flight.

In the following subsections, the VNS range performance will be analyzed, in order of range bin (Charlie, Delta, and Hotel), and following that will be descriptions of the bearing performance analysis.

7.1.2 STORRM VNS Range Measurement Performance Analysis

Based on the statistical methodology described in Section 6.5, this section presents the performance analysis of the STORRM VNS by comparing it to the BET. The analysis is presented by range bin starting with the farthest distance from the ISS rendezvous. Range comparisons are presented first, followed by bearing comparisons.

Figure 7.1-4 shows the range measurements to TCS reflector 2 co-plotted with the corresponding sensor-to-reflector range computed from the BET for range bin Charlie. There are two extreme range errors seen in Figure 7.1-4.

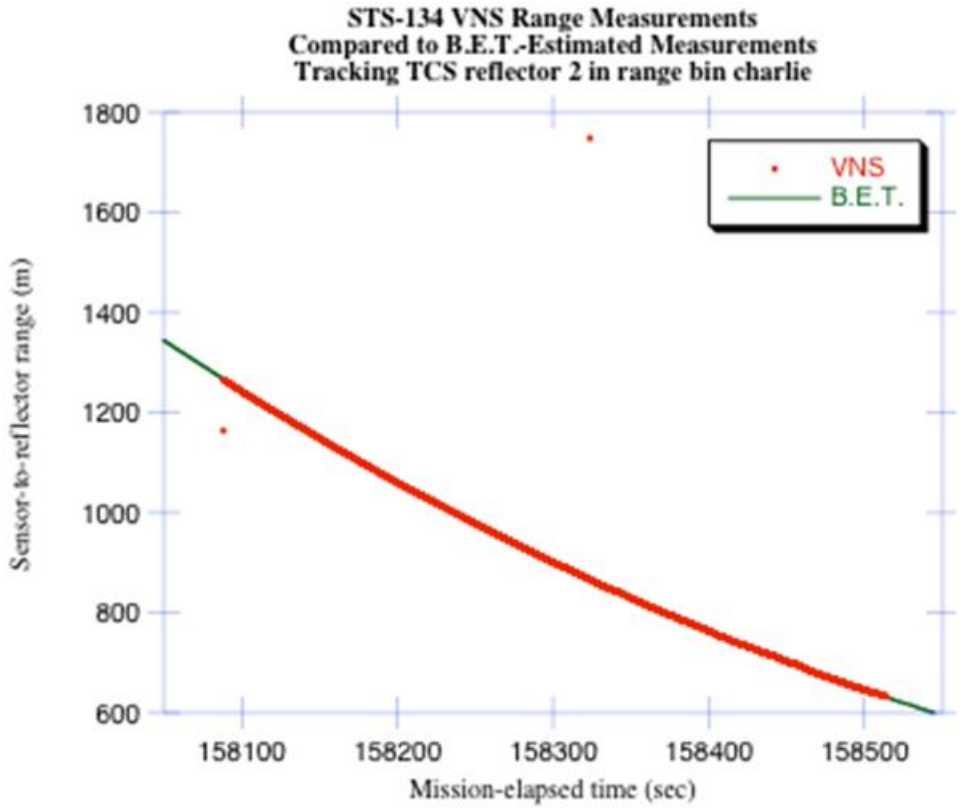

Figure 7.1-4. STS-134 STORRM VNS Range Measurements of Reflector 2 with BET-estimated Range

Figure 7.1-5 shows the estimated range errors in range bin Charlie with two outliers omitted. The errors are designated as "estimated" because the BET does not precisely match the true range. From Figure 7.1-5, the estimated range error does not behave as white noise. The green line shows the estimated bias in the STORRM VNS range measurements in range bin Charlie. The orange bands above and below the estimated bias are 90 percent confidence bands.

These bands are the sum of the Working-Hotelling bands obtained by generalized least-squares regression and the confidence bands in the BET. Working-Hotelling confidence bands that provide a confidence limit for the entire regression line, in contrast to the confidence interval for a single predicted value, were considered by the team to provide a conservative estimate of uncertainty. At any range the orange bands exclude zero, the corresponding estimated bias is statistically significant at significance level 0.10. The reason why the data lies outside the

confidence bands is because the bands apply to the estimated bias, not to the overall scatter in the estimated errors.

Figure 7.1-5 shows the estimated range bias in range bin Charlie was relatively small, being at most about 2.5 meter at a range of nearly 1300 meters.

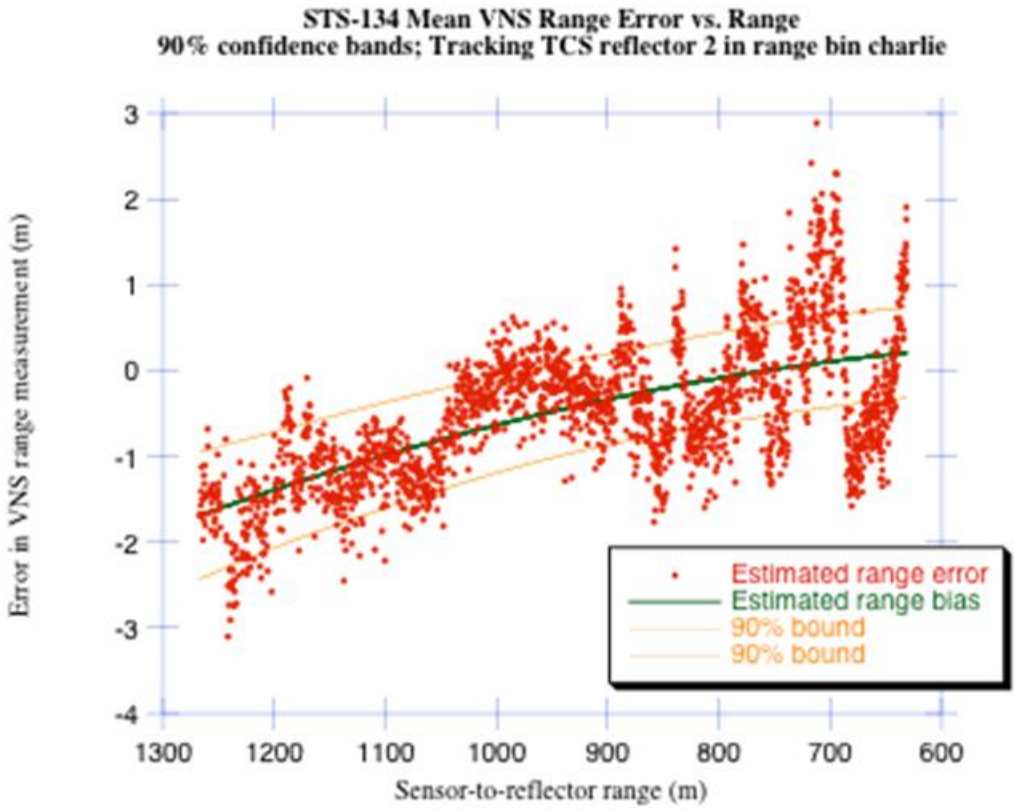

Figure 7.1-5. STS-134 STORRM VNS Bias with 95 percent Working-Hotelling and 90 percent Composite Bands

The estimated standard deviation of the STORRM VNS range measurement noise is given in Table 7.1-3 by multiple methods. The most accurate estimate of the noise is the GLS regression of second degree with two outliers omitted. In that case, the standard deviation is 0.643 meters. A 90 percent confidence interval on the standard deviation (again omitting the two outliers) is (0.626, 0.661) meter. This interval is short because the sample size is large (n = 2063). The data are not normally distributed. Therefore, the interval is computed by a bootstrap method [refs. 11, 12].

Table 7.1-3. Estimated Standard Deviations of STORRM VNS Range Measurement Noise; Tracking TCS Reflector 2 in Bin Charlie; N = 2063 + Two Outliers

Method	Estimated standard deviation (m)
Degree 2 OLS regression of diff. from BET; with 2 outliers	19.859
Second-difference method including the 2 outliers	19.497
Degree 2 OLS regression of difference from BET	0.643
Degree 2 GLS regression of difference from BET	0.643
Quadratic OLS regression of range measurement versus time	0.979
Loess of range versus time with smoothing parameter 0.20	0.602
Second-difference method (assumes white noise)	0.305
Second-difference method (assumes auto-regressive (AR) (1) process)	0.303

The team found the variance of the error is nearly constant as a function of range.

STS-134 STORRM VNS Range Measurement Performance in Range bin Delta

Figure 7.1-6 shows the STORRM VNS range measurements to TCS reflector 2 in range bin Delta, co-plotted with the corresponding sensor-to-reflector range computed from the BET. Numerous extreme errors can be seen in Figure 7.1-6.

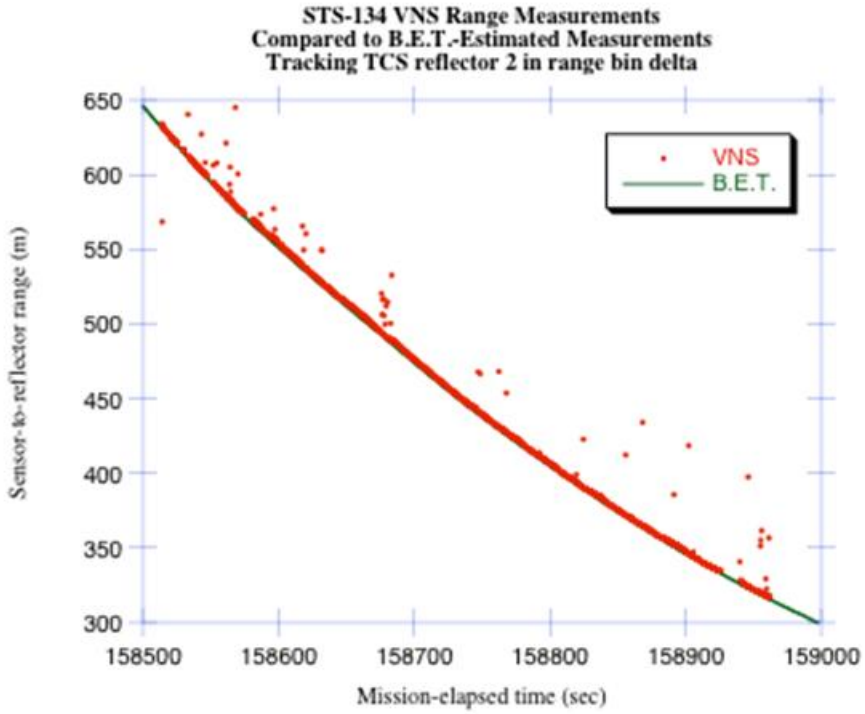

Figure 7.1-6. STS-134 STORRM VNS Range Measurements to Reflector 2 with BET-estimated Range

Figure 7.1-7 shows the estimated STORRM VNS range errors in range bin Delta with the 48 largest extremes omitted, and the estimated bias with the extremes omitted and the corresponding 90 percent confidence bands. The bias is statistically significantly different from zero (at level 0.10) at all ranges. Details of the statistical analysis are provided in Appendix A.

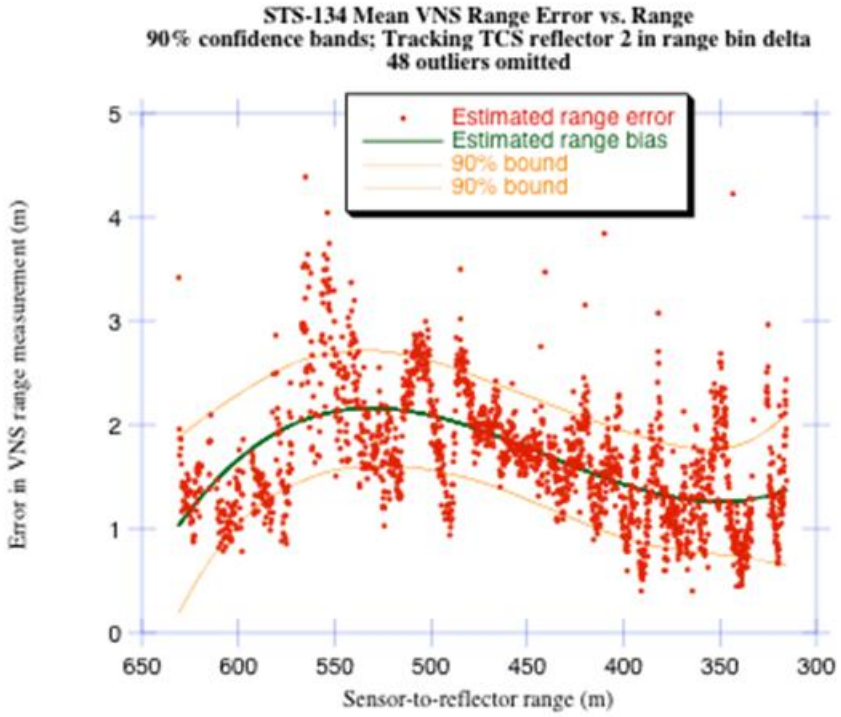

Figure 7.1-7. STS-134 STORRM VNS bias with 95 Percent Working-Hotelling and 90 Percent Composite Bands

Only one extreme estimated error was negative (i.e., –62.56 meters). All the other extreme errors were positive. The remaining 47 extremes were not normally distributed. It was hypothesized the extremes were distributed as a lognormal. Applying the Anderson-Darling goodness-of-fit test [ref. 13], the hypothesis is accepted at significance level 0.05.

The noise, calculated using the standard deviation of the residuals was characterized. The estimates calculated using multiple methods are shown in Table 7.1-4. Note the large difference in standard deviation with and without inclusion of the 48 extreme values.

Table 7.1-4. Estimated Standard Deviations of STORRM VNS Range Measurement Noise; Tracking TCS Reflector 2 in Range Bin DELTA; N = 1956

Method	Estimated standard deviation (m)
Direct calculation of standard deviation from 1956 range errors	4.988
Degree 3 OLS regression fit omits 48 outliers, but residuals include outliers	4.970
Second-difference method without omitting extremes (n = 1913)	4.706
Degree 3 OLS regression of difference from BET; omit 48 outliers	0.479
Degree 3 GLS regression of difference from BET; omit 48 outliers	0.473
Second-difference method omitting 162 extremes (n = 1751)	0.145

A two-sided 90 percent confidence interval on the standard deviation of the noise including the outliers was 4.118 and 6.066 meters. A 90 percent confidence interval on the standard deviation of the noise with the outliers excluded is (0.442, 0.531) meter. The variance changes modestly as a function of range, but not enough to be of practical significance.

STS-134 STORRM VNS Range Measurement Performance Tracking TCS Reflector 1 in Range Bin Hotel

Figure 7.1-8 shows the STORRM VNS range measurements to TCS reflector 1 in range bin Hotel, co-plotted with the corresponding sensor-to-reflector range computed from the BET.

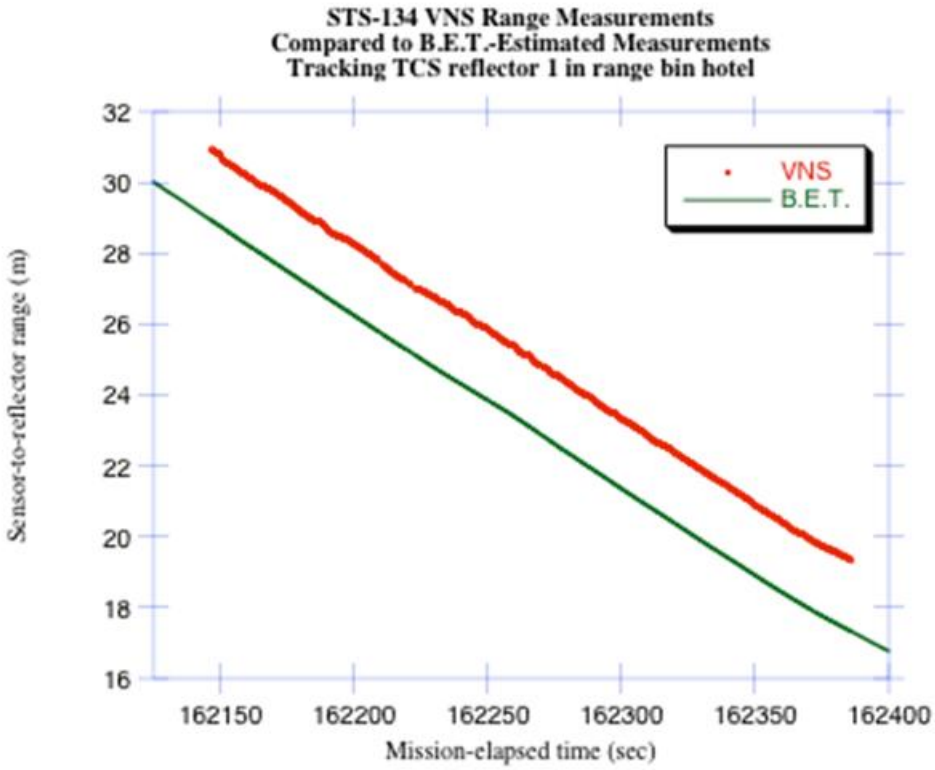

Figure 7.1-8. STS-134 STORRM VNS Range Measurements to Reflector 1 with BET-estimated Range

Figure 7.1-9 shows the estimated range measurement errors when STORRM VNS tracked reflector 1 with the estimated bias and its 90 percent confidence bounds. The range bias is statistically significantly different from zero at all ranges (at level 0.10). Reference 9 notes a 1.918-meter bias was observed in ground testing in range bin Hotel. The estimated bias seen in Figure 7.1-9 is close to this number though the bias varied with range.

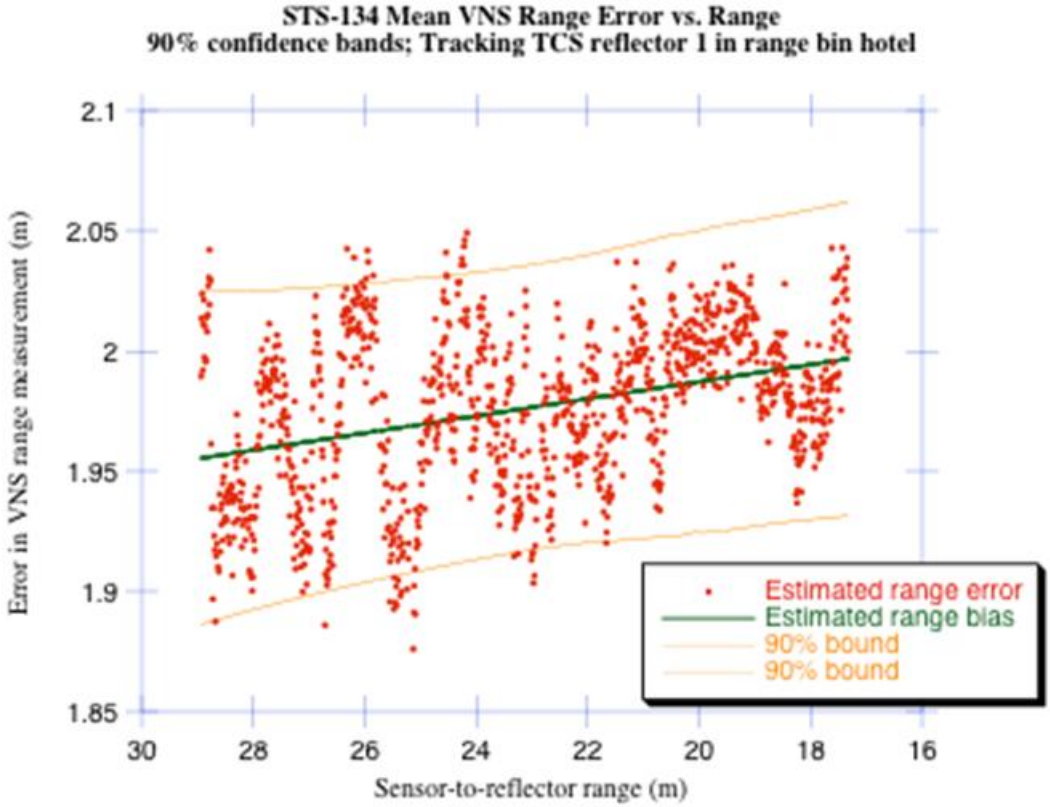

Figure 7.1-9. STS-134 STORRM VNS Bias with 95 percent Working-Hotelling and 90 percent Composite Bands

The residuals may be well-modeled by a normal distribution. Application of an Anderson-Darling goodness-of-fit test [ref. 13] results in accepting the hypothesis of normality at significance level 0.05.

The standard deviation of the residuals was characterized and the estimates are shown in Table 7.1-5. Note the estimates obtained from the second-difference method were lower than those obtained by the regression methods. This is consistent with TCS experience [ref. 2]. In either case, the estimated standard deviation of range noise was small.

Table 7.1-5. Estimated Standard Deviation of the STORRM VNS Range Measurement Noise; Tracking TCS Reflector 1 in Bin Hotel; N = 1138

Method	Estimated standard deviation (m)
Degree 1 OLS regression of difference from BET	0.031
Degree 1 GLS regression of difference from BET	0.031
Second-difference method (n = 1130); assume white	0.012
Second-difference method (n = 1128); assume AR(1)	0.014

A two-sided confidence interval on the standard deviation of the noise while the STORRM VNS tracked reflector 1 is (0.030, 0.032). This is based in the residuals from a GLS regression. The standard deviation of the noise is nearly constant as a function of range in range bin Hotel.

STS-134 STORRM VNS Bearing Measurement Performance in Range bin Charlie

There is a bias in the vertical measurements relative to the BET. As mentioned in references 5 and 6, the TCS bearing and misalignment biases are unknown. They may be as large as 1 degree, though that is probably a worst case. A rotation matrix was computed to attempt to align the BET and the STORRM VNS measurements [ref. 14]. It is not possible to separate the bias in the BET from the bias in the VNS bearing. The magnitude of the deviation between VNS and the BET was reported, but it was not ascribed to the VNS bias.

Noise estimates are made with and without having applied the alignment, though plots of the estimated errors are shown only for the case that the transformation is used. Transformation to the bearing measurements was applied to reflector 2 in range bin Charlie. The result for the horizontal measurements are shown in Figure 7.1-10 and the corresponding estimated errors are shown in Figure 7.1-11.

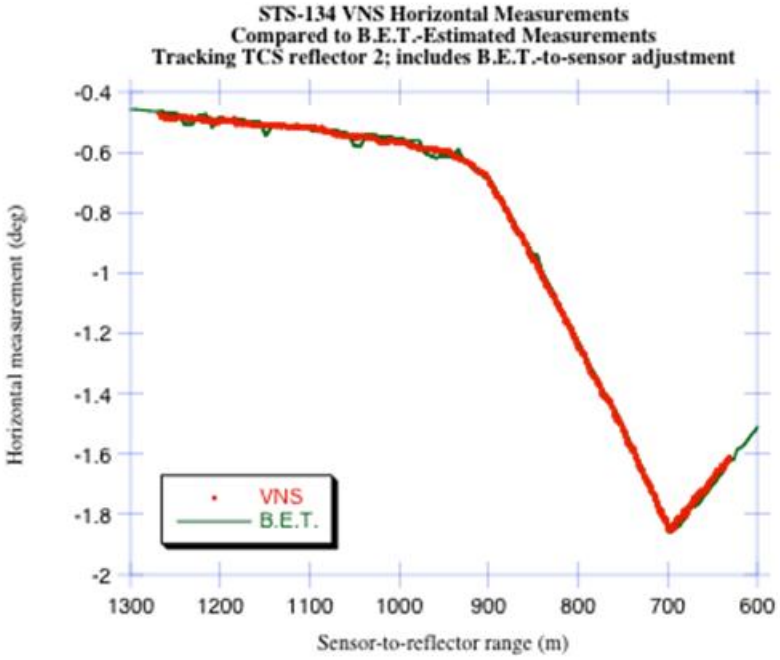

Figure 7.1-10. STORRM VNS Horizontal Measurements Compared to Altered BET Estimates

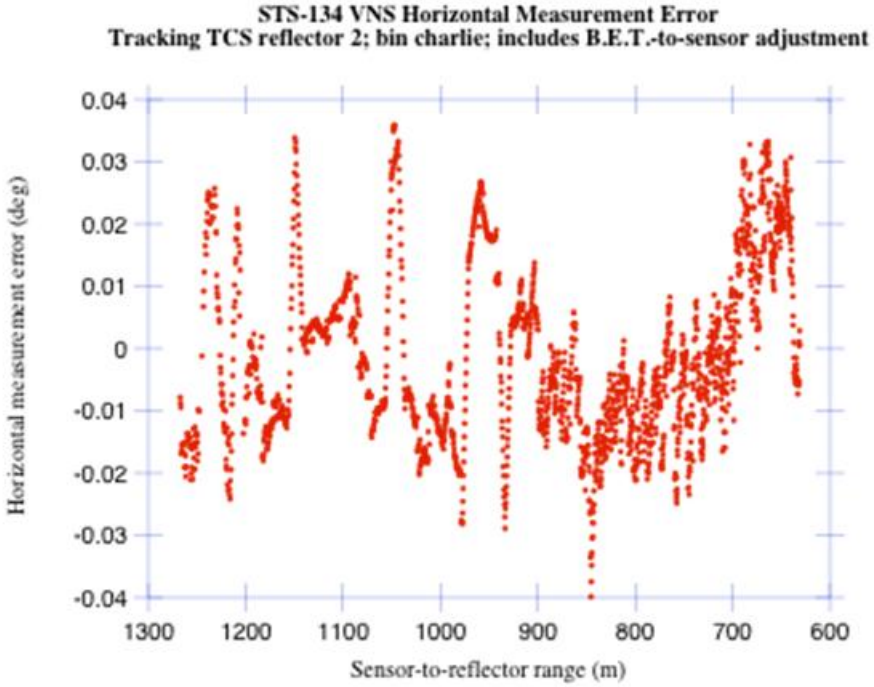

Figure 7.1-11. Estimated STORRM VNS Horizontal Measurement Error; Tracking TCS Reflector 2

A co-plot of STORRM VNS vertical measurements and the BET-estimated measurements are shown in Figure 7.1-12. The estimated errors are shown in Figure 7.1-13.

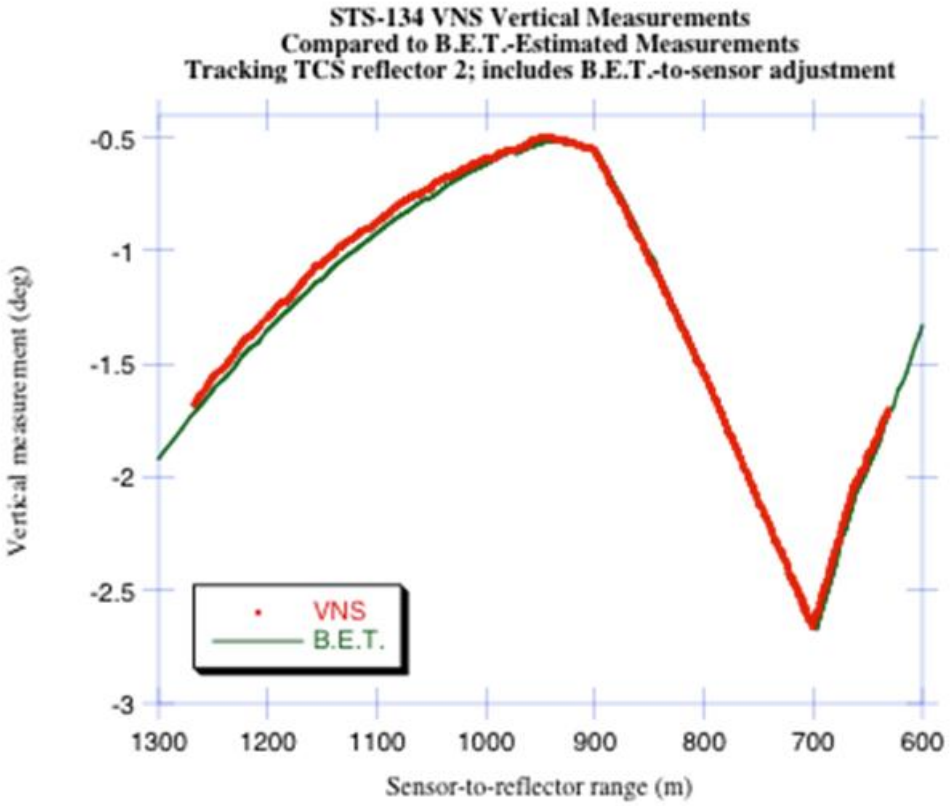

Figure 7.1-12. STORRM VNS Vertical Measurements Compared to Altered BET Estimates

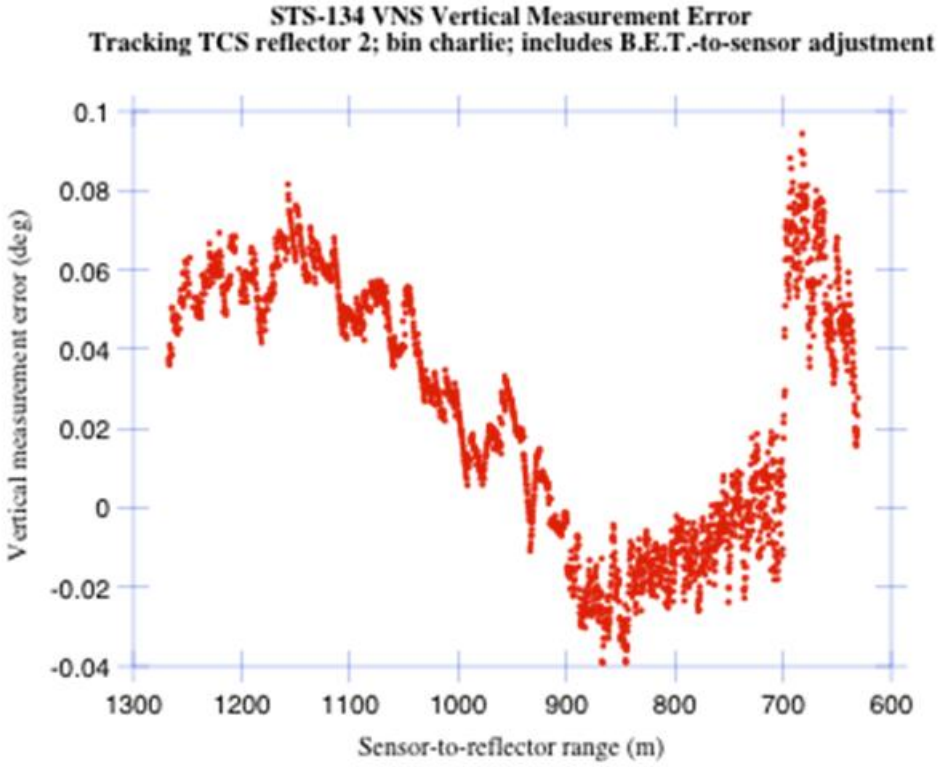

Figure 7.1-13. Estimated STORRM VNS Figure 7.1-9 Vertical Measurement Error; Tracking TCS Reflector 2

Table 7.1-6 gives estimates of the mean differences and standard deviations of the bearing errors with and without the alignment of the BET to the data.

Table 7.1-6. Mean Differences and Standard Deviations of Bearing Errors; STORRM VNS Tracking TCS Reflector 2 in Range Bin Charlie (N = 2065)

	Mean diff. (deg)	Std. Dev. (deg)
Horizontal, not aligned	0.001	0.015
Horizontal, aligned	–0.001	0.014
Vertical, not aligned	0.277	0.032
Vertical, aligned	0.023	0.032

Ninety-percent confidence intervals on the standard deviations computed from the aligned values are given (0.0136, 0.0142) degree for the horizontal measurements, and (0.0316, 0.0325) degree for the vertical measurements.

The autocorrelation coefficients at lag 1 for the horizontal and vertical measurement residuals are 0.9739 and 0.9880, respectively.[3] These coefficients were computed without accounting for missing data.

STS-134 STORRM VNS Bearing Measurement Performance while Tracking TCS Reflector 2 in Range bin Delta

Figure 7.1-14 shows the horizontal angle measurements from the STORRM VNS to TCS reflector 2 in range bin Delta, co-plotted with the corresponding estimates computed from the BET. Figure 7.1-15 shows the estimated errors in the horizontal angle measurements. A co-plot of the vertical measurements and the vertical measurements computed from the BET is shown in Figure 7.1-16. The estimated vertical angle errors are shown in Figure 7.1-17.

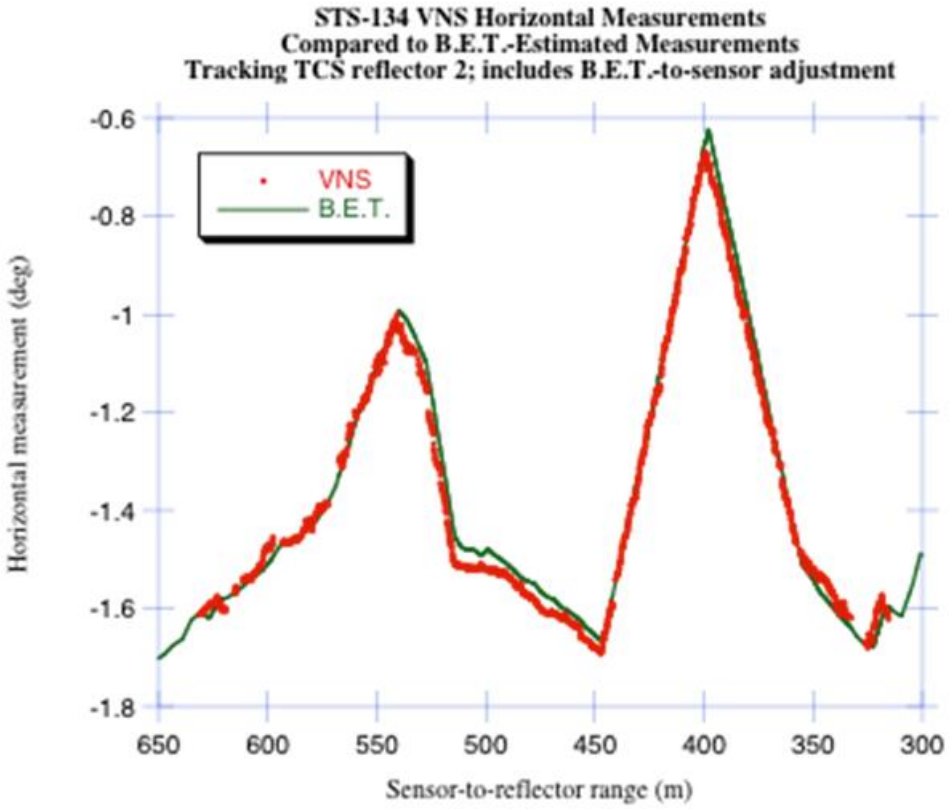

Figure 7.1-14. STORRM VNS Horizontal Measurements Compared to Altered BET Estimates

[3] The computation of a sample autocorrelation coefficient assumes the data are equally spaced in time with no missing data. The VNS data include numerous instances for which this is violated. No attempt was made to account for the missing data in calculation of the sample autocorrelation coefficient.

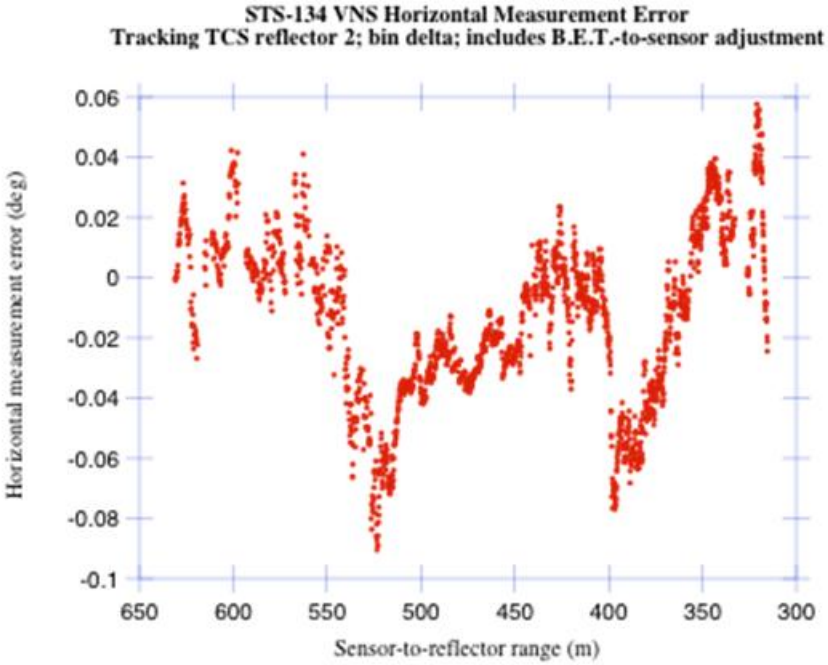

Figure 7.1-15. Estimated STORRM VNS Horizontal Measurement Error; Tracking TCS Reflector 2

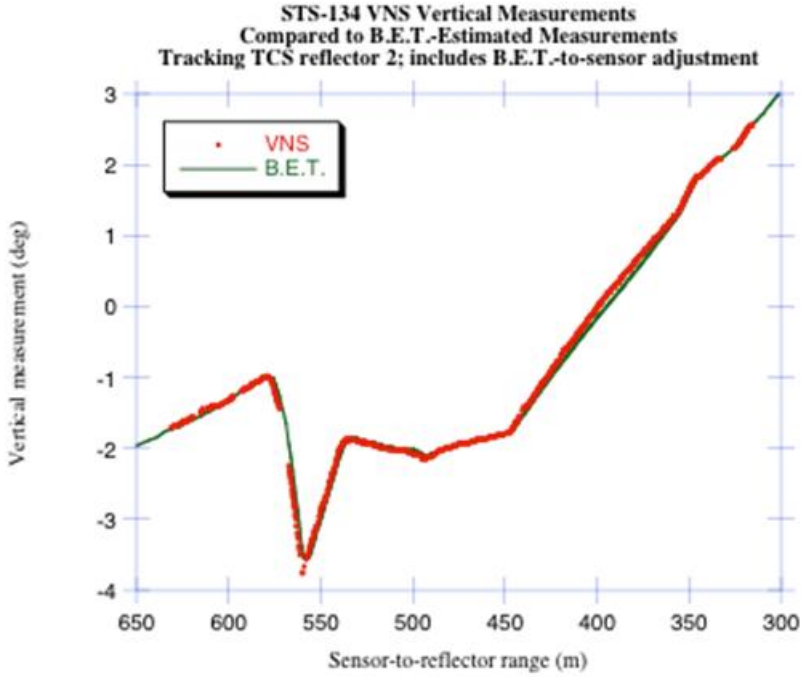

Figure 7.1-16. STORRM VNS Vertical Measurements Compared to Altered BET Estimates

The interval of range over which the fourth midcourse maneuver (MC4) executed by the orbiter occurs is indicated in Figure 7.1-17. Translational acceleration has been known to result in increases in errors in bearing. In this case, larger changes in vertical measurement error occur subsequent to the MC4 maneuver.

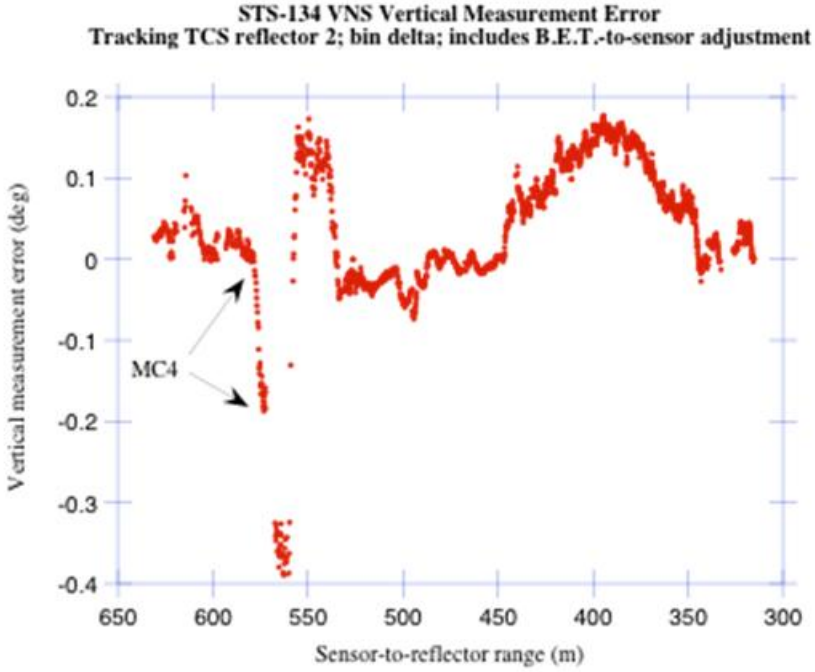

Figure 7.1-17. Estimated STORRM VNS Vertical Measurement Error; Tracking TCS Reflector 2

Table 7.1-7 gives estimates of the mean differences and standard deviations of the bearing errors with and without the alignment of the BET to the data.

Table 7.1-7. Mean Differences and Standard Deviations of Bearing Errors; STORRM VNS Tracking TCS Reflector 2 in Range Bin Delta; N = 1956

	Mean diff. (deg)	Std. Dev. (deg)
Horizontal, not aligned	0.003	0.030
Horizontal, aligned	–0.014	0.028
Vertical, not aligned	0.293	0.086
Vertical, aligned	0.039	0.087

Ninety-percent bootstrap confidence intervals (see reference 12 for more details on the method) on the standard deviations of the bearing measurement noise, computed from the aligned values, are (0.027, 0.029) degree and (0.082, 0.092) degree for the horizontal and vertical measurements, respectively.

The sample autocorrelation coefficients at lag 1 for the estimated horizontal and vertical measurement errors are 0.9852 and 0.9945, respectively.

The standard deviation of the vertical noise was greater than the horizontal noise. There appears to be a time-varying bias with the noise relatively small based on examining Figure 7.1-17. The standard deviation of the residuals is 0.011 based on fitting the vertical measurement error at ranges less than 533 meter with a fourth-degree OLS regression.

Alternatively, the team may treat the vertical errors when the range is less than 533 meter as an AR(1) process. From this point of view, the errors may be modeled with an exponentially correlated random variable of standard deviation 0.066 degree and time constant 62 second.

STS-134 STORRM VNS Bearing Measurement Performance while Tracking TCS Reflector 1 in Range bin Hotel

Figure 7.1-18 shows the horizontal angle measurements from STORRM VNS to TCS reflector 1 in range bin Hotel, co-plotted with the corresponding estimates computed from the BET. The estimated horizontal measurement errors are shown in Figure 7.1-19.

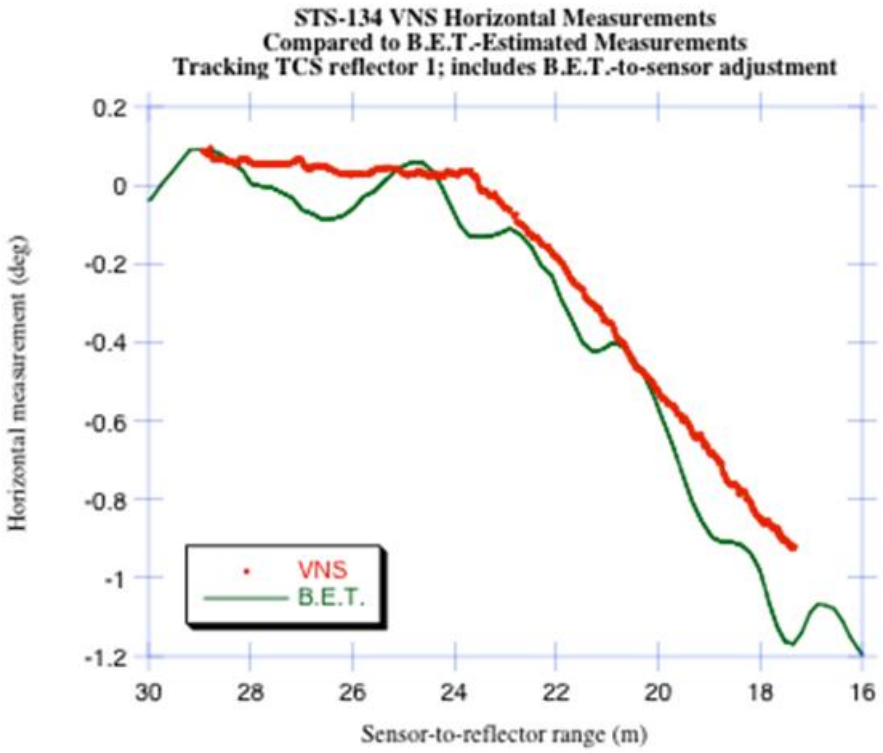

Figure 7.1-18. STORRM VNS Horizontal Measurements Compared to Altered BET Estimates

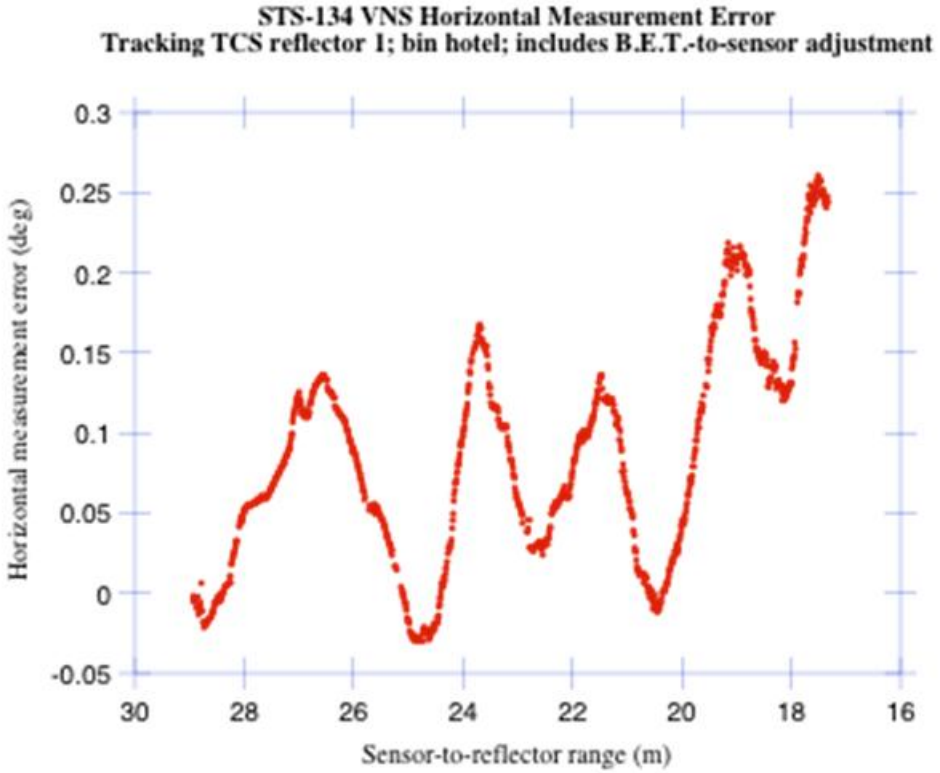

Figure 7.1-19. Estimated STORRM VNS Horizontal Measurement Error; Tracking TCS Reflector 1

Figure 7.1-20 shows the vertical angle measurements from STORRM VNS to TCS reflector 1 in range bin Hotel, co-plotted with the corresponding estimates computed from the BET. The estimated vertical measurement errors are shown in Figure 7.1-21.

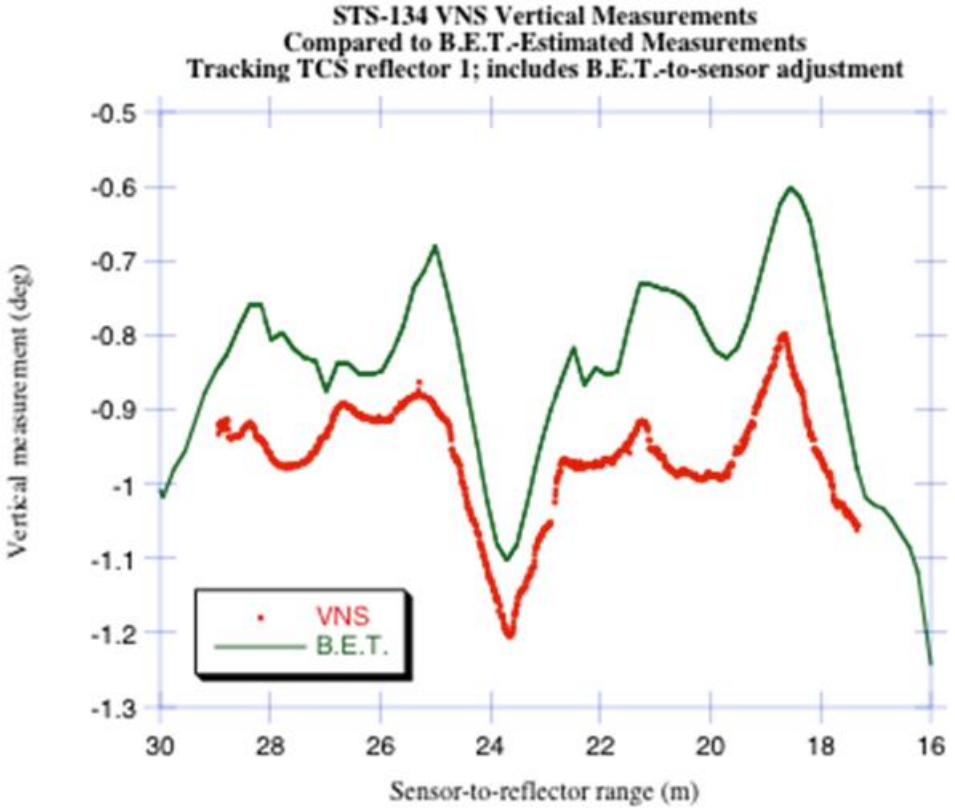

Figure 7.1-20. STORRM VNS Vertical Measurements Compared to Altered BET Estimates

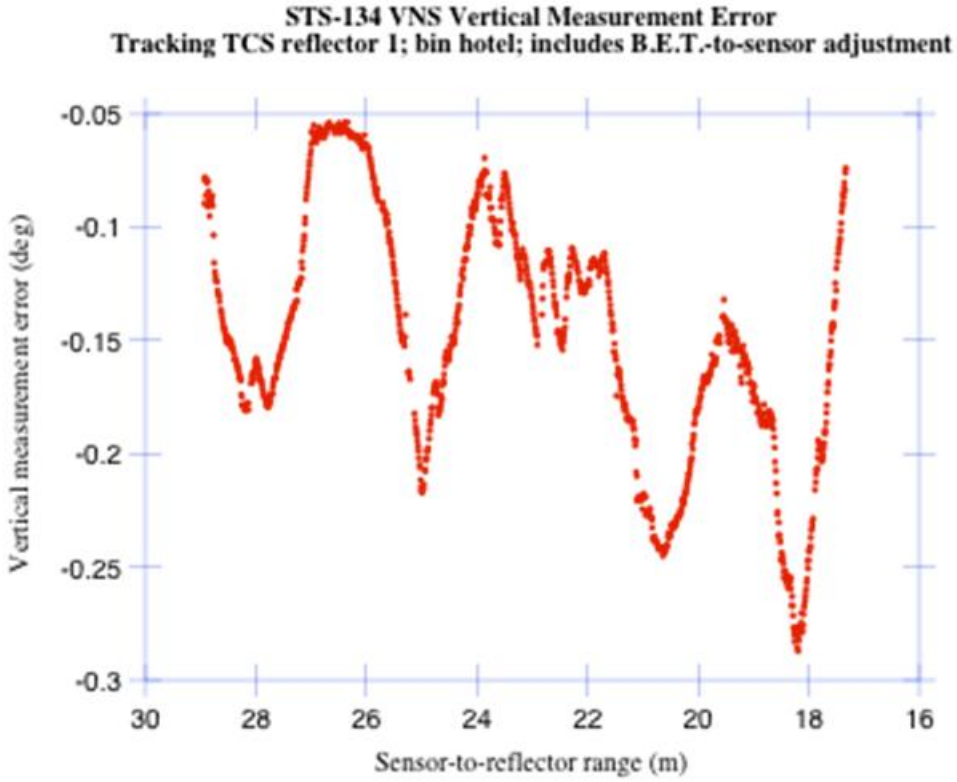

Figure 7.1-21. Estimated STORRM VNS Vertical Measurement Error; Tracking TCS Reflector 1

Table 7.1-8 gives estimates of the mean differences and standard deviations of the bearing errors with and without the alignment of the BET to the data.

Table 7.1-8 also provides estimates from the second-difference method. The estimates were obtained under the assumption the data are white noise [ref. 9]. The estimates under the assumption the data follow an AR(1) process that are computed by the method discussed in reference 15. Comparison between these two kinds of second-difference estimates shows the assumption that white noise yields underestimates, but the degree of underestimation is small compared to the difference between the BET-derived estimates and the corresponding estimates computed by second differences. The estimated errors shown in Figures 7.1-19 and 7.1-21 suggest that residuals from a bias correction are closer to the small estimates of noise obtained by the second-difference method than the standard deviations given in Table 7.1-7. The horizontal and vertical measurements were fit as a function of time using loess with smoothing parameter (α) of 0.05 [ref. 16]. The estimated standard deviations of the noise from the loess residuals are given in Table 7.1-7. The estimated standard deviations obtained from loess residuals are closer to those obtained by the second-difference method than those derived from comparison to the

BET. This shows the second-difference method estimates the high-frequency noise well, but tends to eliminate the effect of slowly varying biases.

The method chosen to estimate biases in the bearing data is less sophisticated than the range data. The bias is estimated as the mean of the differences between the BET-estimated measurements and the sensor measurements. When the bearing errors have a slowly time-varying bias, the bias corrupts the estimate of the standard deviation, making it larger. As explained previously, the team did not attempt to separate the error in the sensor from the error in the BET. This may increase the estimated error quoted.

Interestingly, for Kalman filtering and optimal smoothing purposes, reference 9 recommended assuming the STORRM VNS bearing errors are uniformly distributed over a single pixel. Since each pixel corresponds to 0.0787 degree, the standard deviation of the bearing noise under this assumption is $0.0787/\sqrt{12} = 0.0227$ degree. The data in Table 7.1-8 show this value was closer to the estimates obtained by the BET-based method than the second-difference method that was used in the STORRM analysis contained in reference 9.

Table 7.1-8. Mean Differences and Standard Deviations of Bearing Errors; STORRM VNS Tracking TCS Reflector 1 in Range Bin Hotel; N = 1138

	Mean diff. (deg)	Std. Dev. (deg)
Horizontal, not aligned	0.644	0.138
Horizontal, aligned	0.087	0.070
Horizontal, second difference (white)		0.0019
Horizontal, second difference, AR(1)		0.0024
Horizontal, from loess, $\alpha = .05$		0.0039
Vertical, not aligned	0.105	0.055
Vertical, aligned	–0.149	0.055
Vertical, second difference (white)		0.0018
Vertical, second difference, AR(1)		0.0021
Vertical, from loess, $\alpha = .05$		0.0047

Ninety-percent bootstrap confidence intervals on the standard deviations of the horizontal and vertical angle measurement noise, computed from the aligned values, are (0.067, 0.072) degree and (0.054, 0.057) degree, respectively.

The sample autocorrelation coefficients at lag 1 for the estimated horizontal and vertical measurement errors are 0.9958 and 0.9970, respectively.

7.1.3 STORRM Performance Summary

Table 7.1-9 is a summary of the STORRM performance based on the analysis performed by the NESC team.

Table 7.1-9. Summary of STORRM Performance

STORRM Bin	Range Bounds (m)	Est. Range Bias (m)	Stdev of Range Error (m)	Stdev of Horiz. Bearing Error (deg)	Stdev of Vert. Bearing Error (deg)
Hotel	0 - 30	1.95 - 2.00 (refl 1) 2.01 - 2.20 (refl 14)	0.031 (refl 1) 0.044 (refl 14)	0.070 (refl 1) 0.077 (refl 14)	0.055 (refl 1) 0.056 (refl 14)
Golf	30 - 81	11.68	11.676 (0.130 omit 1)	0.030	0.043
Foxtrot	81 - 162	2.15 - 2.34	4.813 (0.169, omit 8)	0.014	0.178
Echo	162 - 324	-----	-----	-----	-----
Delta	324 - 648	1.03 - 2.16	4.988 (0.48, omit 48)	0.028	0.087
Charlie	648 - 1300	-1.69 - 0.21	0.643 (omit 2)	0.014	0.032
Bravo	1300 - 2590	-----	------	-----	-----
Alpha	2590 - 5760	-----	-----	-----	-----

7.1.4 STORRM Pose-Based Range Estimates

A review was conducted independent of the STORRM team to provide comments on the report, and to perform limited quantitative comparison of performance by comparing the VNS time of flight (TOF) range estimate to a pose-based range estimate for the portions of the trajectory where three retro-reflectors were available simultaneously. The pose-based estimates were compared to the VNS TOF range and the BET.

Comments on Reference 9

The review of reference 9 did not lead to any significant observations. This reference is comprehensive, therefore a detailed examination of each section was not within the scope of this assessment. However, the sections that presented details of the VNS coordinate frames, centroid detection algorithms, and range data results were reviewed in detail. Since the report identifies the range estimates from the VNS in range bin Echo were of poor quality, it was not analyzed for the independent pose-based range estimates.

Pose Estimate

The second part of the review consisted of calculating a pose estimate for the STORRM VNS whenever three reflectors could be identified. The range estimate from the pose solution was compared to the VNS TOF solution. The range estimate from the pose solution is independent of the TOF solution, but in the same coordinate frame, which eliminates noise induced into the solution from coordinate frame transformations. With the published 1.918 meter bias of the VNS applied, the VNS data was in the range of 45 centimeters (cm) specified for the STORRM flight experiment. The exception to this is range bin Echo, which as noted in reference 9, had issues with the accuracy of the range estimate. The cause of this anomaly remains under investigation.

A pose estimate works by comparing the geometry of at least three known locations on the target to the measurements by the sensor. If the Cartesian locations of at least three targets in the body frame are known, then three sides of a triangle can be constructed, as shown in Figure 7.1-22.

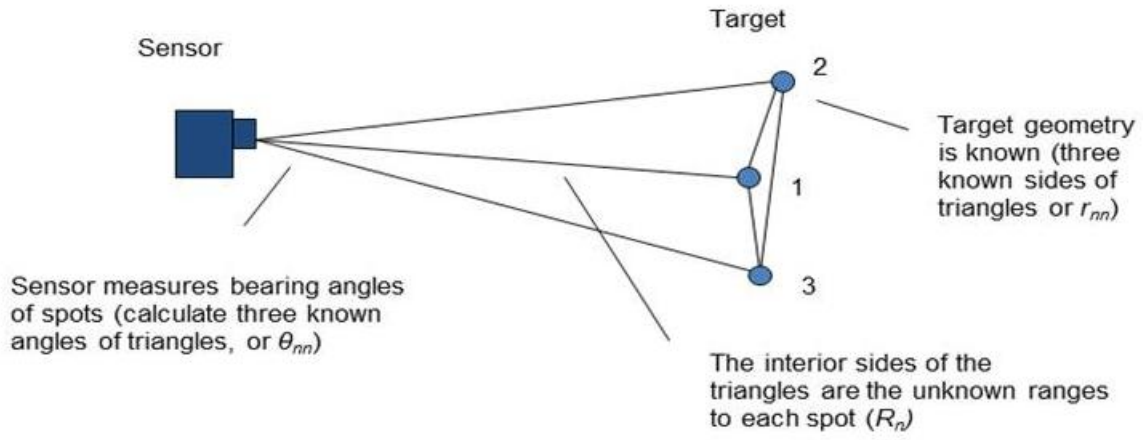

Figure 7.1-22. Sensor to Target Geometry

Additionally, the azimuth and elevation of each target spot measured by the sensor can be converted to three known angles. The three sides and three angles can be combined into three

equations with three unknowns by using the Law of Cosines. These equations can then be solved with a polynomial or iteratively to determine the individual ranges to each spot.

$$R_1^2 + R_2^2 - 2 R_1 R_2 \cos(\theta_{12}) - r_{12}^2 = 0$$

The procedure previously described for calculating a pose estimate of range to three targets was applied to Delta, Echo, Foxtrot, and Hotel range bins. As previously noted, the VNS data did not compare well in range bin Echo due to known problems with the STORRM VNS TOF range estimate in that bin. In all the other bins, the VNS met its experiment requirement of 45 cm when compared to the pose estimate.

Comparison of the Pose Estimate to the STORRM VNS TOF Range and BET Range Estimates

Figures 7.1-23 through 7.1-28 are plots of the pose estimate versus STORRM VNS TOF range and BET results from range bin Hotel. For this assessment, the three reflectors selected for the pose estimate were from the STORRM target assembly on the ISS. There are two figures per reflector. One shows the comparison of the pose range estimate to the raw (not corrected for bias) VNS TOF range estimate and the BET range estimate. The plots show the pose estimate is noisier at longer ranges in range bin Hotel. As the angles between the target reflectors decreased, the noise from the spot azimuth and elevations reduce. The gaps in the plots are because the pose estimate was not always possible since, in some cases, three target reflectors were not available.

The BET data came from the reflector visibility tool, see Appendix I. This file contained the STORRM target assembly reflector centroids and the ranges for each ISS reflector as translated into the VNS sensor coordinate frame from the BET coordinate frame, which was published as the range between the orbiter and ISS respective CGs. In the process of translating the data from the orbiter-to-ISS coordinate from the VNS frame, additional noise may have been introduced into the BET.

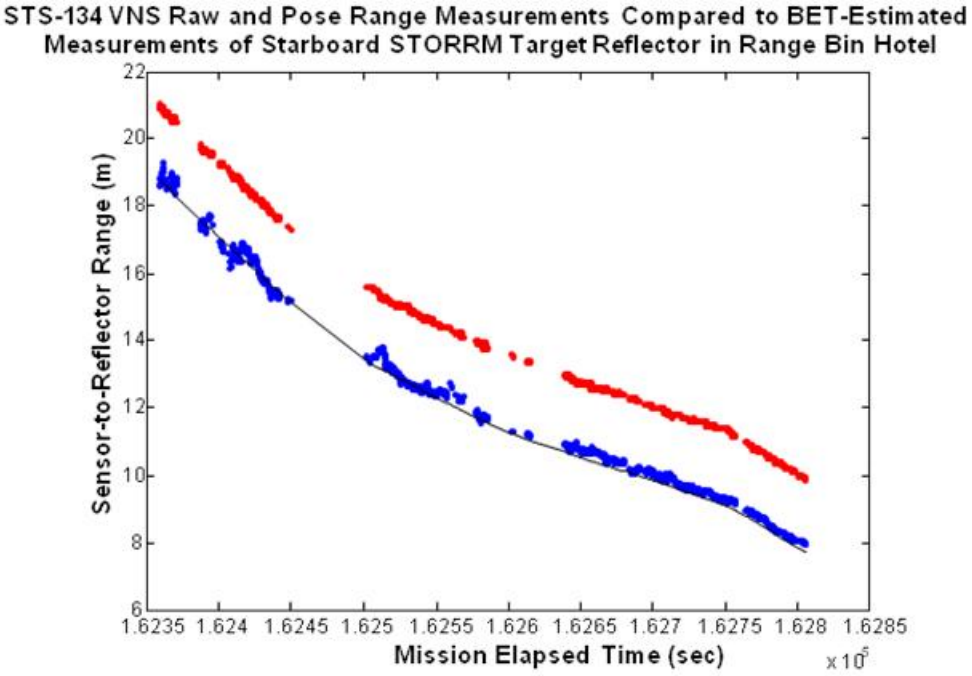

Figure 7.1-23. Overlay of TOF and Pose Range Estimates for Standoff Reflector

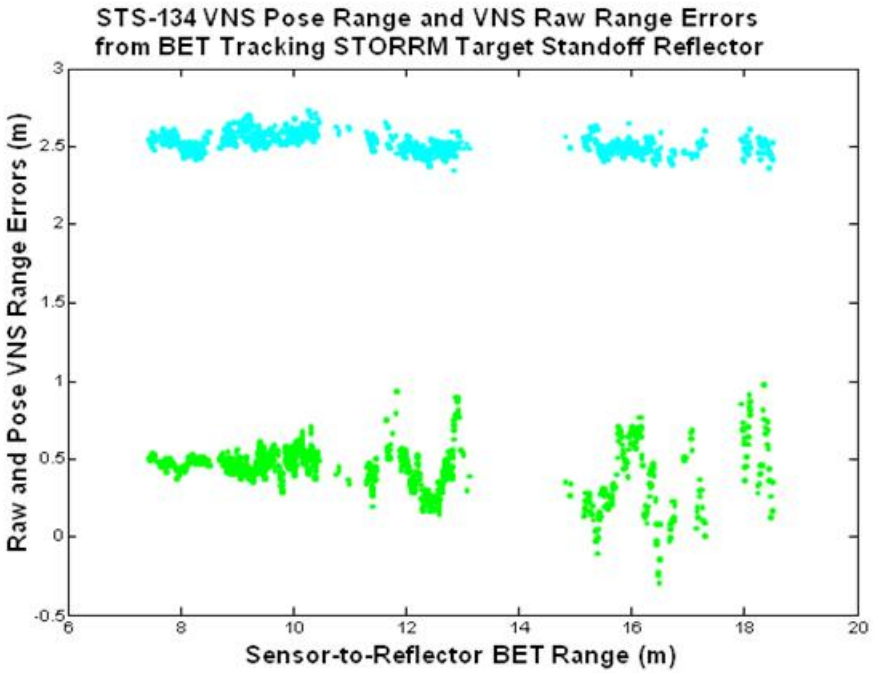

Figure 7.1-24. Estimated Range Errors of TOF and Pose Range Estimates for Standoff Reflector

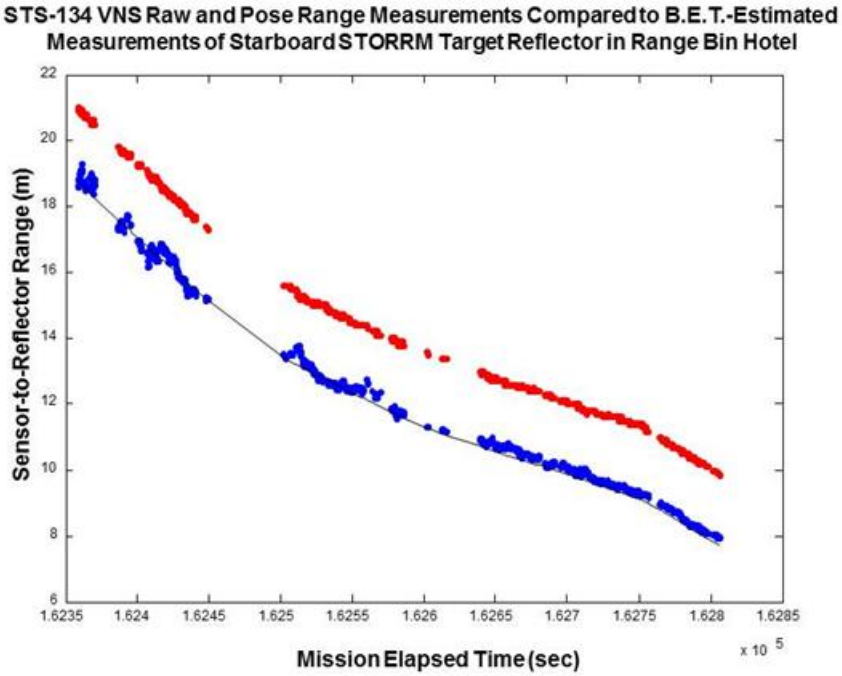

Figure 7.1-25. Overlay of TOF and Pose Range Estimates for Starboard Reflector

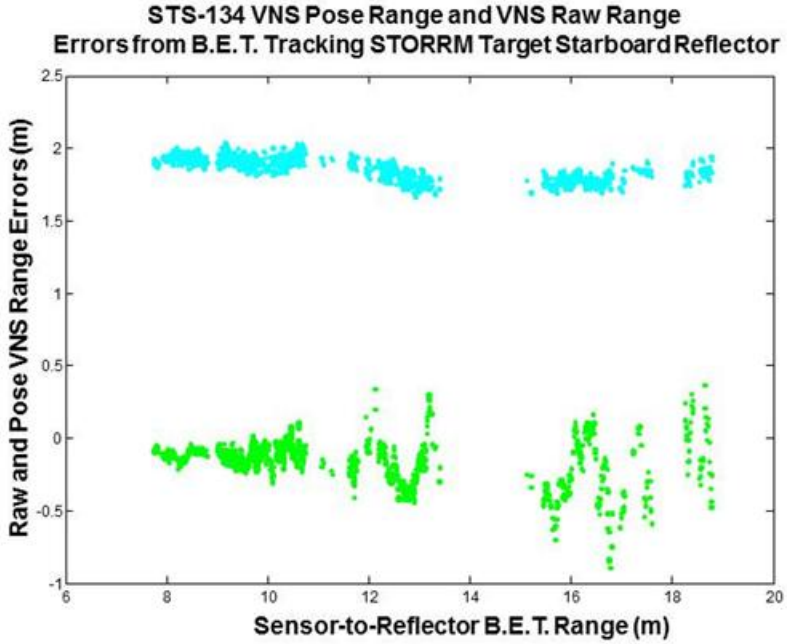

Figure 7.1-26. Estimated Range Errors of TOF and Pose Range Estimates for Starboard Reflector

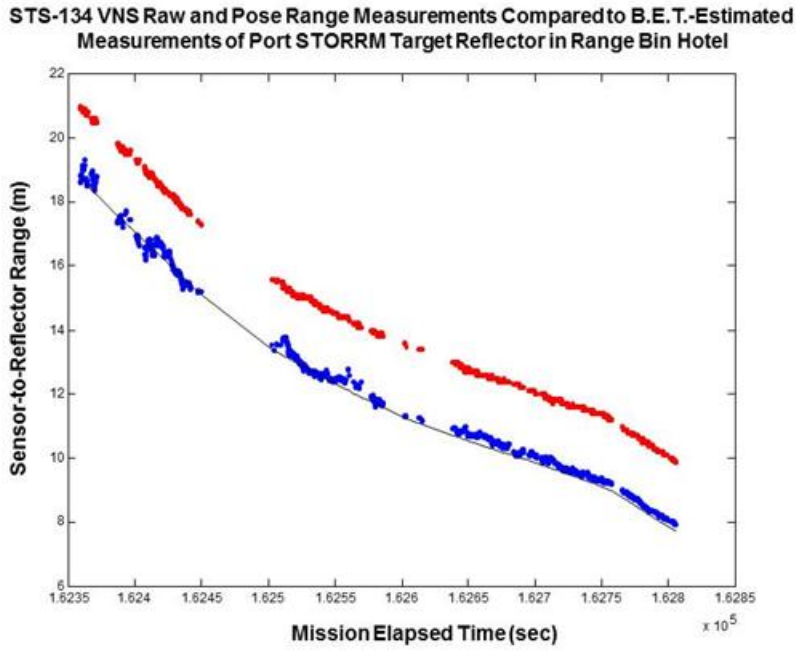

Figure 7.1-27. Overlay of TOF and Pose Range Estimates for Port Reflector

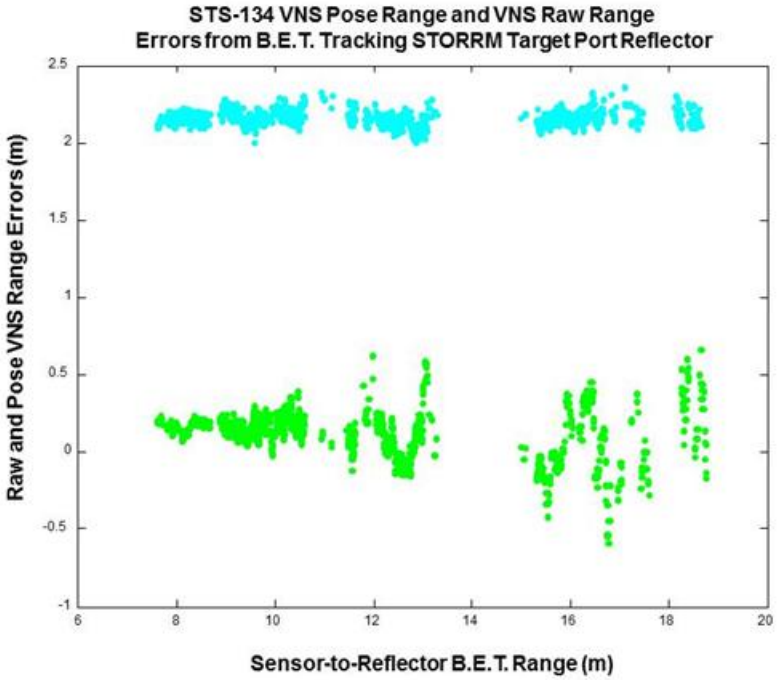

Figure 7.1-28. Estimated Range Errors of TOF and Pose Range Estimates for Port Reflector

The STORRM VNS pose estimate and the VNS raw data are within 45 cm of the BET for range bin Hotel, as shown in Figures 7.1-23 through 7.1-28. These plots show the relative errors between the BET and the VNS raw (not corrected for bias) TOF and pose range estimates. While the BET is an estimate, and cannot be treated as absolute truth, for the purposes of this assessment, the VNS is considered to meet its experiment requirement of 45 cm for range bin Hotel.

7.2 DragonEye

7.2.1 Overview of DragonEye DTO

The DragonEye DTO flew on STS-127 (July 2009) and STS-133 (February 2011). The STS-127 unit was a prototype TigerEye design based on a terrestrial unit, which featured a low-grade (i.e., lower quality) detector array. During STS-127, the laser failed during the undocking portion of the DTO. The STS-133 flight employed an off-the-shelf DragonEye (which was derived from the TigerEye line). The unit was modified to bring the laser transmit optics closer to the receiving optics. The DragonEye unit for STS-133 had several improvements over the unit flown on STS-127. For both DTO flights, the DragonEye operated in the simplest of manner: during the test window, the unit was powered on and all data was recorded to a data recorder. At the end of the test window, the unit and the data recorder were powered off. Listed in Table 7.2-1 is the range bin setting for the DragonEye. Note the unit only had one set of gains. This was due in part to the simple DTO approach whereby no commanding or telemetry occurred in real-time.

Table 7.2-1. DragonEye Range Bins

DragonEye Bin	Range Bounds
Standard Gain Setting	8 – 1000 m

There were three types of DragonEye data available to the assessment team. The first data set, delivered by SpaceX for the STS-127 flight, was a Matlab binary data file that contained the pixel location, intensity, and calculated range. The Matlab data was used in the NASA centroiding algorithm to generate centroids for this analysis. The STS-133 data consisted of SpaceX centroid data and DragonEye raw sequence data. The centroid data was generated by SpaceX's flight processing algorithms. The SpaceX centroid data was processed directly in the comparison to the BET. The raw sequence data was pre-processed so it could be fed into the centroiding algorithm. The DragonEye detector contains a 128 × 128 pixel array. Each "frame" contains 16384 pixels, and each pixel contains 20 intensity measurements (referred to as slices) and TOF index. The 20 slices and TOF index are processed to generate an intensity and range measurement for that pixel. This is performed for each pixel in the detector at every

measurement cycle (i.e., 688944 bytes for each frame). The processed raw sequence data was ready for the NASA centroiding algorithm. Reference 17 describes the process employed in converting the raw sequence data to usable format for the centroiding algorithm.

7.2.2 NASA Centroiding Algorithm for DragonEye Data

The centroiding algorithm used to process the DragonEye data is substantially different (and less sophisticated) than the STORRM VNS centroiding algorithm. These differences are largely due to the nature of the data and the amount of time available to build a customized processing algorithm. Specifically, the VNS has an angular resolution of 0.0787 degree/pixel, while the DragonEye has an angular resolution of 0.38 degree/pixel. Therefore, the angular resolution of the VNS is almost 5 times better than the DragonEye configuration flown on the STS-127 and STS-133. This, coupled with a different choice for the focus of the receive optics, means a reflector spans multiple pixels for the entire rendezvous in the VNS data, while spanning only a single pixel for much of the DragonEye rendezvous data. Because a typical reflector return only illuminates a single pixel in the DragonEye data, the size and shape criteria developed for processing the VNS data were not applicable. Finally, by selecting a centroiding algorithm for the DragonEye data, reliably detected centroids at close range could not be determined where spurious returns dominate the LIDAR imagery.

The DragonEye centroiding algorithm first applied a global threshold to the intensity image, keeping only pixels whose intensity is above a specified value. For the STS-127 and STS-133 data, a reasonable value was found to be 2800 (maximum intensity = 4095). Second, a check on the range of the remaining pixels was performed and pixels with incorrect ranges removed. This was done by removing pixels with a range less than a specified value (usually around 3 meters). At this point, it was observed removing the edges of the image eliminated much of the remaining noise. Finally, a connected components analysis was used to extract contiguous blobs of pixels in the intensity image that passed the identified checks. These blobs were centroided using the same center-of-mass approach as for the STORRM VNS data. Many reflectors only contained a single pixel, making the center-of-mass computation unnecessary for much of the data.

7.2.2.1 DragonEye Range Measurement Performance Analysis

Using the statistical methodology described in Section 6.5, this section presents the DragonEye performance in range and bearing sequentially. Figure 7.2-1 shows the DragonEye range measurements to TCS reflector 8 co-plotted with the corresponding sensor-to-reflector range computed from the BET.

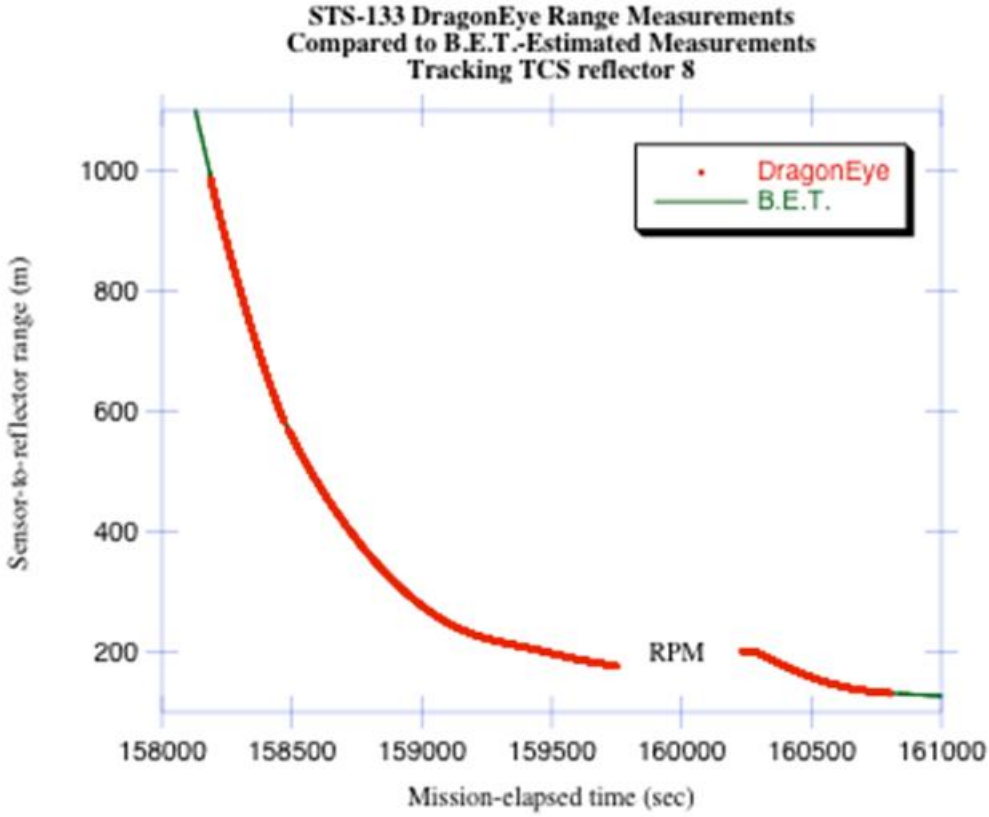

Figure 7.2-1. STS-133 DragonEye Range Measurements to Reflector 8 with BET-estimated Range

After examining several potential OLS polynomial regression models, computing the autocorrelation of the residuals, and refitting using generalized least squares, the team used a quartic model without a linear term, based on a combination of engineering judgment and statistical lack-of-fit tests. Figure 7.2-2 shows the estimated error in the DragonEye range measurements to TCS reflector 8 with the estimated bias and 90 percent confidence bands. The bias departs from zero (at level 0.10) at all but the closest ranges.

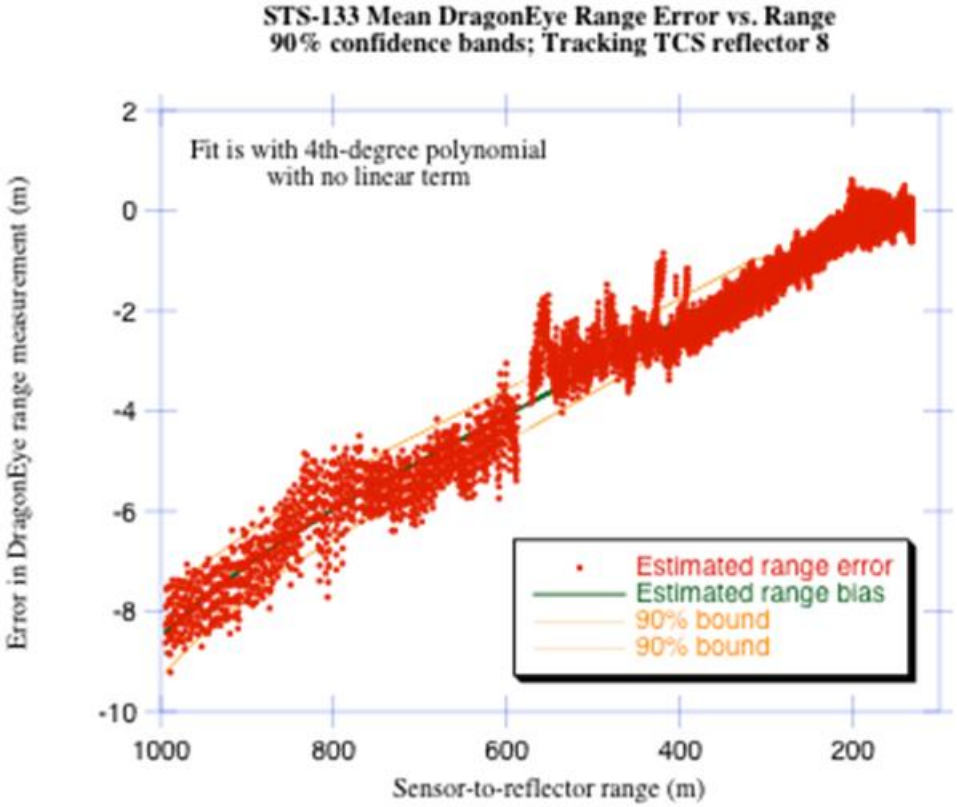

Figure 7.2-2. STS-133 DragonEye Bias with 90 Percent Confidence Bands

The noise was characterized by the standard deviation of the residuals. The estimates are shown in Table 7.2-2. The estimate from the second-difference method is a known underestimate because quantization error is a major contributor to the DragonEye range errors.

Table 7.2-2. Estimated Standard Deviations of DragonEye Range Measurement Noise; Tracking TCS Reflector 8; N = 10510

Method	Estimated standard deviation (m)
OLS regression of difference from BET, degree 1	0.357
GLS regression of difference from BET, degree 1	0.357
OLS regression of difference from BET, degree 4 ($\beta_1 = 0$)	0.347
GLS regression of difference from BET, degree 4 ($\beta_1 = 0$)	0.347
Second-difference method (known underestimate)	0.157

A two-sided 90 percent confidence intervals on the standard deviation of the noise, while DragonEye tracked reflector 8 is (0.338, 0.358) meter, was derived from the GLS residuals.

Figure 7.2-3 shows estimates of the standard deviations of the range noise for ten range bins, with an estimated standard deviation function that is linear with range. The standard deviation of the range noise varies linearly as a function of range. Details on computing the standard deviation as a function of range are given in Appendix B.

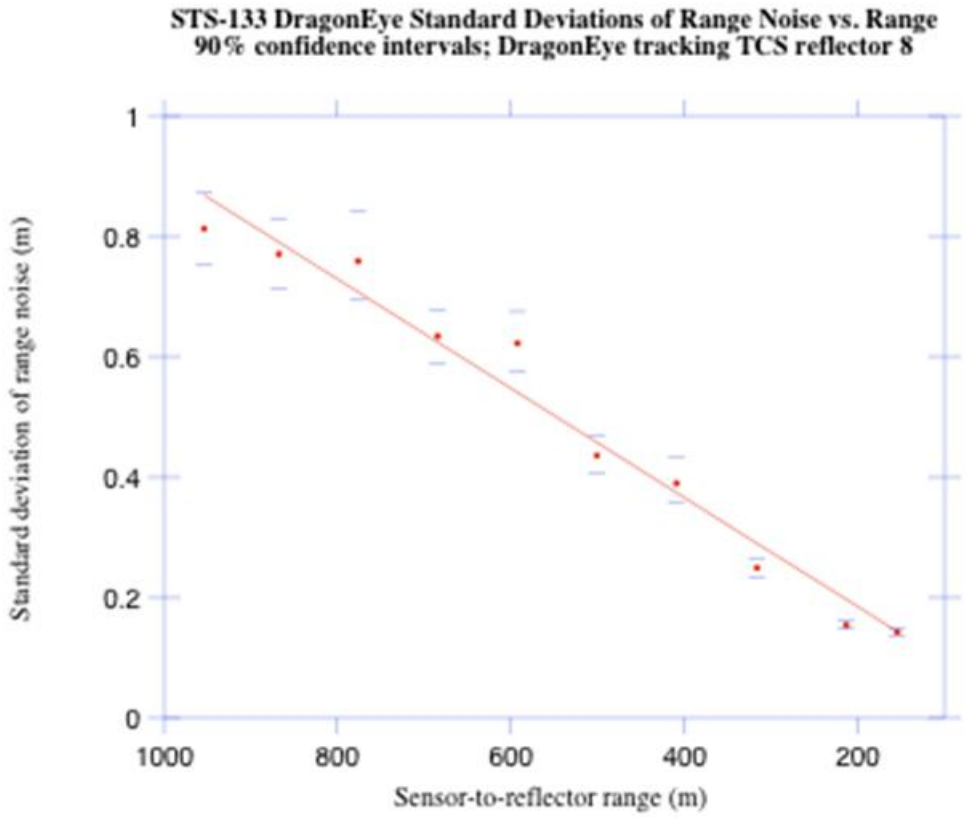

Figure 7.2-3. Estimated Standard Deviation of the Range Noise as a Function of the Range

DragonEye Range Measurement Performance while Tracking TCS Reflector 1 on STS-133

Figure 7.2-4 shows the range measurements to TCS reflector 1 co-plotted with the corresponding sensor-to-reflector range computed from the BET. Figure 7.2-5 shows estimated DragonEye range errors and range bias while tracking reflector 1 on STS-133 and are shown are 90 percent confidence bands on the estimated bias.

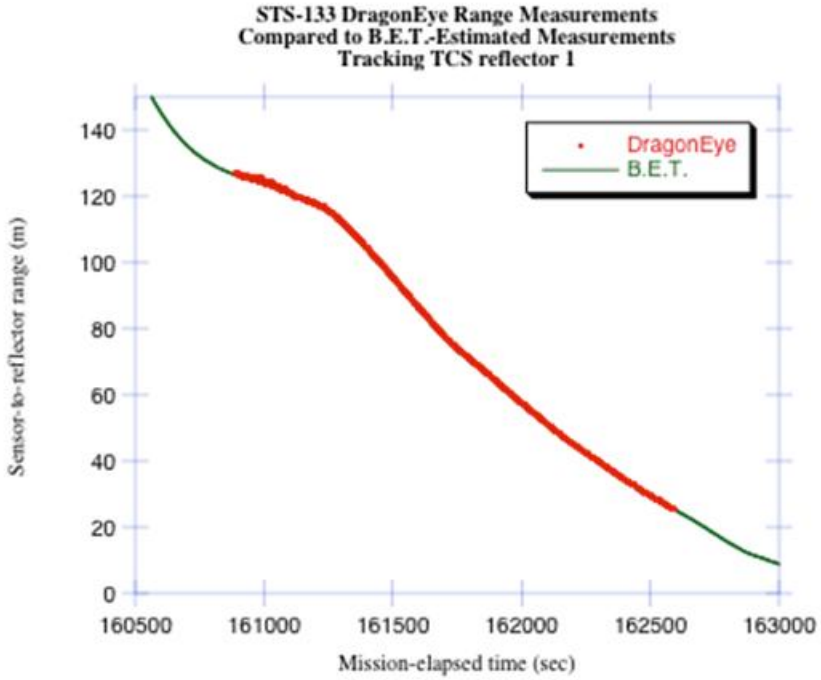

Figure 7.2-4. STS-133 DragonEye Range Measurements of Reflector 1 with BET-estimated Range

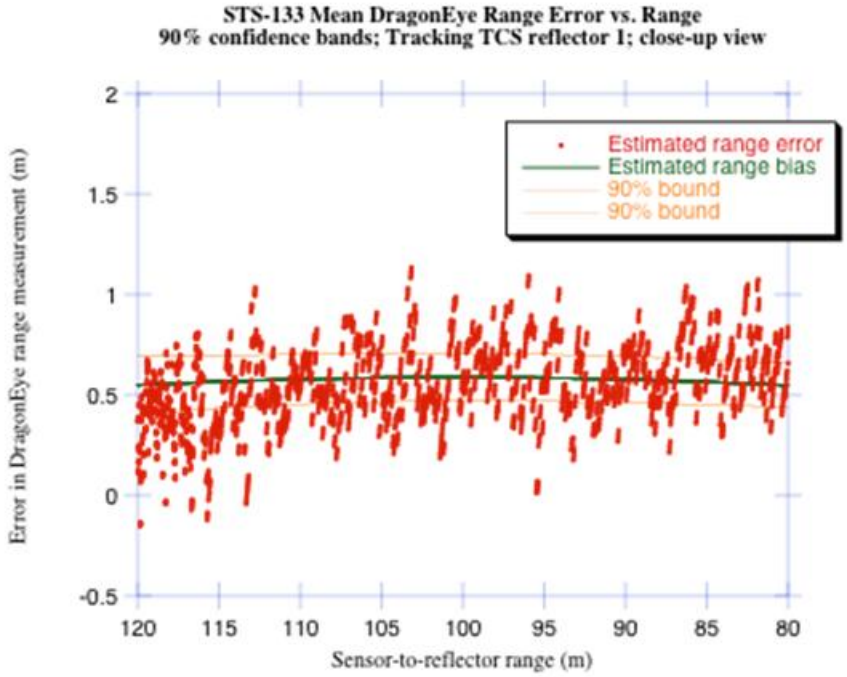

Figure 7.2-5. STS-133 DragonEye Bias with 95 percent Working-Hotelling and 90 percent Composite Bands

The DragonEye range errors are not normally distributed and have noticeable quantization error. Quantization is a result of the analog-to-digital resolution of the optical encoder. Of the 8471 residuals in the regression, 68 were larger than the others. The errors behave like a mixture of distributions. The 68 extreme residuals are approximately normally distributed with a mean of 1.028 meter and standard deviation of 0.200 meter. If these 68 extremes are removed, then the estimated standard deviation of the noise was 0.180 meter.

As was the case in tracking reflector 8, the estimated standard deviation by the second-difference method resulted in an underestimate because of the presence of the quantization error. Table 7.2-3 shows a comparison of the estimated standard deviation of the noise in the DragonEye range measurements while tracking reflector 1 using multiple methods. The greatest reliance was placed on the GLS regression method.

Table 7.2-3. Estimated Standard Deviations of DragonEye Range Measurement Noise; Tracking TCS Reflector 1; N = 8471

Method	Estimated standard deviation (m)
OLS regression of difference from BET	0.202
GLS regression of difference from BET	0.202
OLS regression of difference from BET; omit 68 extremes	0.180
Quadratic OLS regression of range measurement vs. time	2.996
Loess with smoothing parameter = .20	0.230
Quadratic OLS regression of range vs. time; omit first 1804 pts.	0.459
Quadratic OLS regression; last 3672 points	0.190
Second-difference method (known underestimate)	0.050

A 90 percent confidence interval on the standard deviation of the DragonEye range error while tracking TCS reflector 1 is (0.191, 0.216) meter, was derived from the GLS residuals. The noise decreases with range.

7.2.2.2 DragonEye Bearing Measurement Performance

DragonEye Bearing Measurement Performance while Tracking TCS Reflector 8 on STS-133

As mentioned in references 5 and 6, the TCS bearing and misalignment biases are unknown. They may be as large as 1 degree, though that is probably a worst case. A rotation was computed to attempt to align the BET and the DragonEye measurements [ref. 18]. It is not possible to separate the bias in the BET from the bias in the DragonEye bearing. The team reports the magnitude of the deviation between DragonEye and the BET, but did not ascribe it to the DragonEye bias. Estimates are reported with and without the alignment transformation, but plots are only shown for the aligned cases.

Figure 7.2-6 shows the horizontal angle measurements from DragonEye to TCS reflector 8, co-plotted with the corresponding estimates computed from the BET. The differences between the DragonEye horizontal measurements and the BET-estimated measurements are shown in Figure 7.2-7.

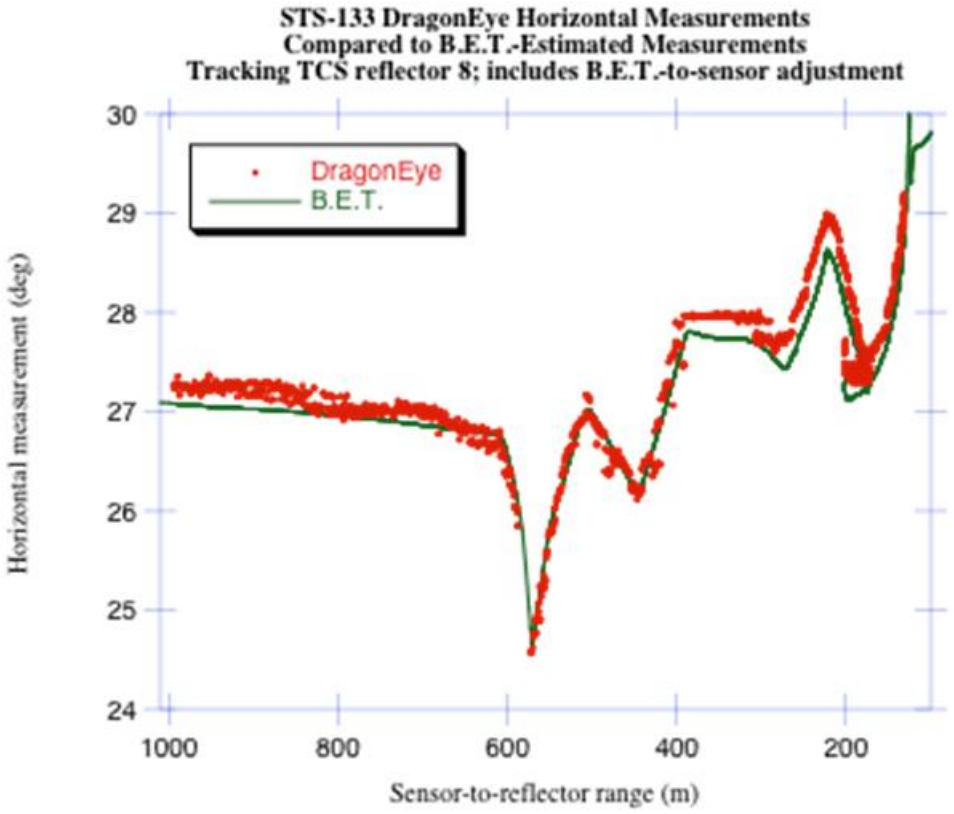

Figure 7.2-6. DragonEye Horizontal Measurements Compared to Altered BET Estimates

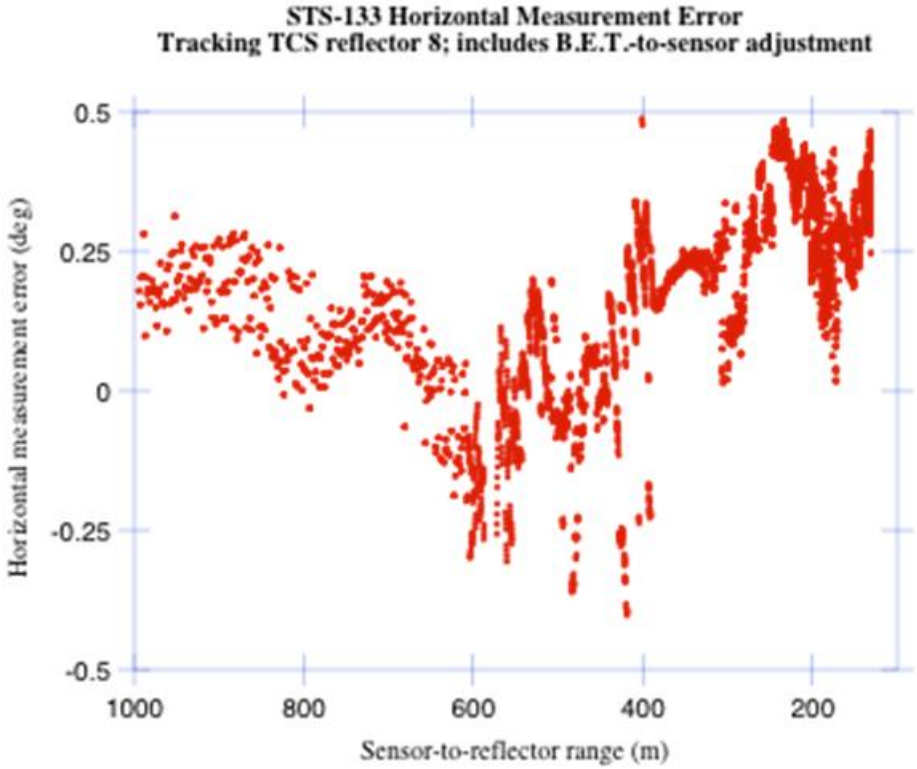

Figure 7.2-7. Estimated DragonEye Horizontal Measurement Error; Tracking TCS Reflector 8

Figure 7.2-8 shows the vertical angle measurements from DragonEye to TCS reflector 8, co-plotted with the corresponding estimates computed from the BET. The differences between the DragonEye vertical measurements and the BET-estimated measurements are shown in Figure 7.2-9.

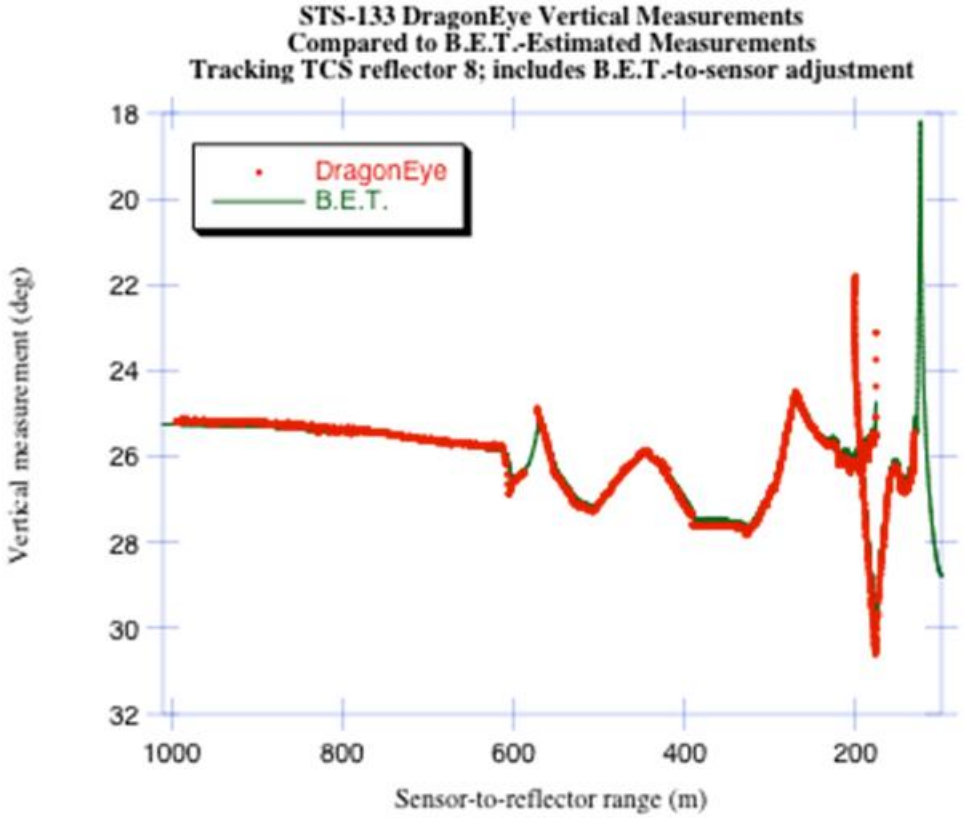

Figure 7.2-8. DragonEye Vertical Measurements Compared to Altered BET Estimates

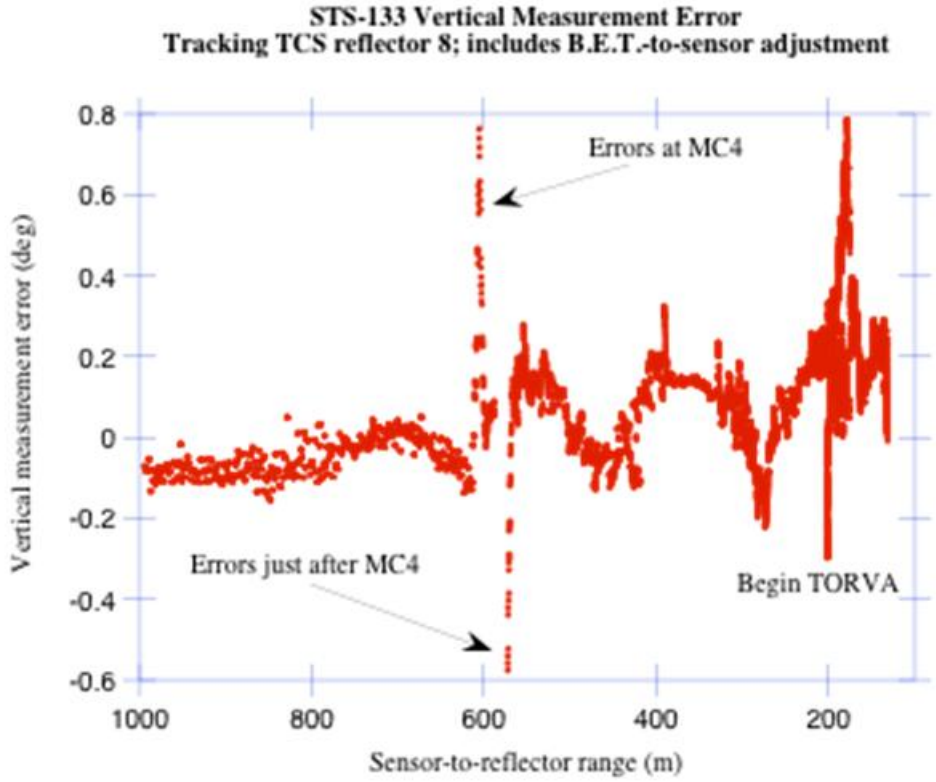

Figure 7.2-9. Estimated DragonEye Vertical Measurement Error; Tracking TCS Reflector 8

Figure 7.2-9 shows during and following the orbiter's MC4 the errors in the vertical angle measurement were larger than before MC4. The effects of the acceleration caused the increase in measurement error. RPOP records ΔV sensed by the orbiter's IMU. On two consecutive 4-second RPOP navigation cycles, the ΔV were 0.272 and 0.267 meter/sec. DragonEye lost track of reflector 8 for about 20 second. After reacquisition of reflector 8, three consecutive ΔV of 0.055, 0.055, and 0.038 meter/sec were recorded, and the vertical angle errors were unusually large at this time. The orbiter's attitude and attitude rate changed during the maneuver, but its knowledge of the attitude was not degraded. During the same time DragonEye experienced vertical angle errors as large as 2 degrees, the TCS residuals in the RPOP Kalman filter were about 0.1 degree. It can be concluded the DragonEye and TCS do not tolerate translational acceleration.

In moving from the R-bar to the V-bar, the orbiter rotates with respect to the inertial frame at twice the orbital angular velocity. This rotation is designed to facilitate the commander keeping the target within the TCS field of view. The series of maneuvers from the R-bar to the V-bar is known as the Twice Orbital Rate V-bar Approach (TORVA). At the conclusion of the TORVA,

the rotation is nulled with respect to LVLH. Figure 7.2-9 shows the accuracy of vertical measurement estimation is impacted at the initiation of the TORVA.

Figure 7.2-10 shows the magnitude of the ΔV while the translational maneuvers associated with the initiation of the TORVA occurred. The consequent increase in error in the vertical angle is seen in Figure 7.2-11. This was apparent by focusing solely on the period of time covered in Figure 7.2-10 and plotting the vertical error as a function of time. As can be seen in Figure 7.2-11, the vertical error grows approximately linearly with time. Note during this time, the twice-orbital rate rotation with respect to the inertial frame had not been initiated. Thus, the error is attributable to the translational ΔV, rather than the effect caused by rotation with respect to LVLH.

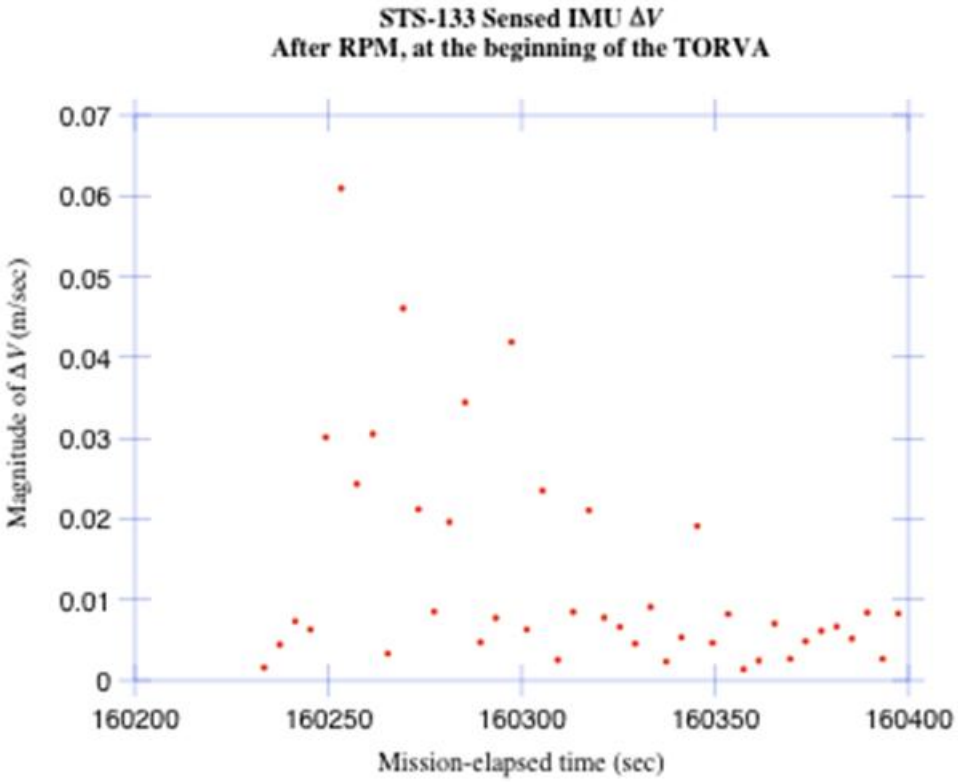

Figure 7.2-10. STS-133 Sensed IMU ΔV at the Beginning of the TORVA

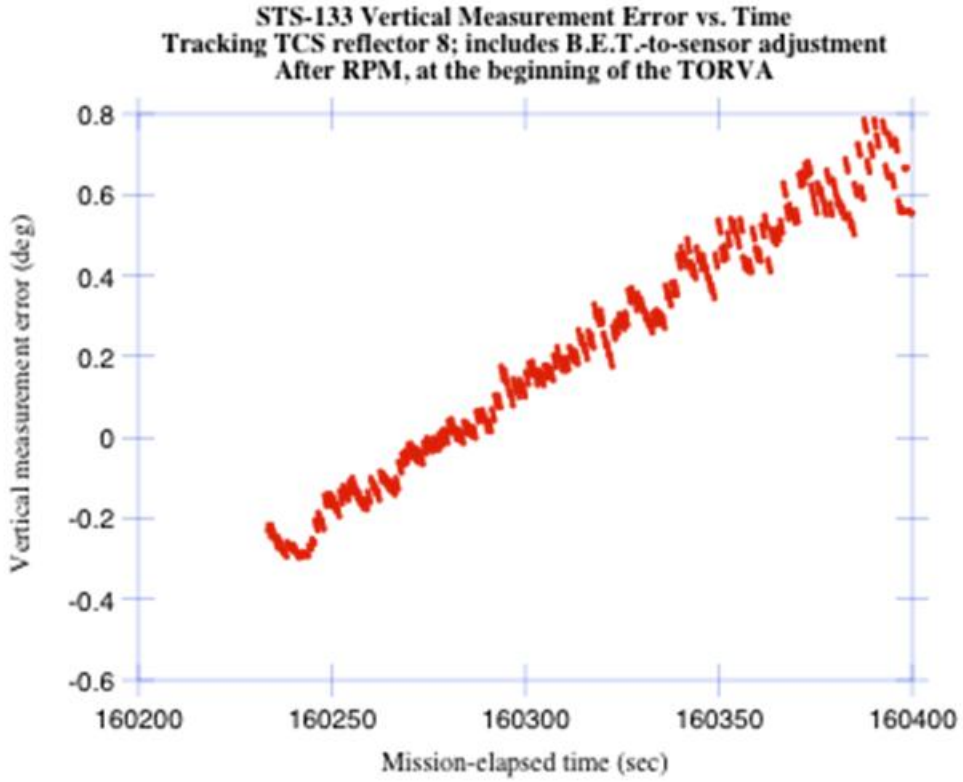

Figure 7.2-11. STS-133 Vertical Measurement Error versus Time at the Beginning of the TORVA

Table 7.2-4 gives estimates of the mean differences and standard deviations of the bearing errors with and without the alignment of the BET to the data. Recall each pixel represents 0.38 degree of angular measure. The statistics are given in pixels and degrees.

Table 7.2-4. Mean Differences and Standard Deviations of Bearing Errors; DragonEye Tracking TCS Reflector 8; N = 10491

	Mean diff. (pix)	Std. Dev. (pix)	Mean diff. (deg)	Std. Dev. (deg)
Horizontal, not aligned	4.143	0.411	1.574	0.156
Horizontal, aligned	0.614	0.390	0.233	0.148
Vertical, not aligned	0.450	1.007	0.171	0.383
Vertical, aligned	0.306	0.380	0.116	0.144

Ninety-percent bootstrap confidence intervals on the standard deviations computed from the aligned values are (0.146, 0.150) and (0.142, 0.147) degrees for the horizontal and vertical measurements, respectively. The sampling error in the estimates of the standard deviations was

small, because the sample size is $n = 10491$. The sample autocorrelation coefficients at lag 1 for the estimated horizontal and vertical measurement errors are 0.9816 and 0.9864, respectively.

DragonEye Bearing Measurement Performance while Tracking TCS Reflector 1 on STS-133

This section evaluates the DragonEye performance in measuring the bearing to reflector 1. Figure 7.2-12 shows the horizontal angle measurements from DragonEye co-plotted with the corresponding estimates computed from the BET.

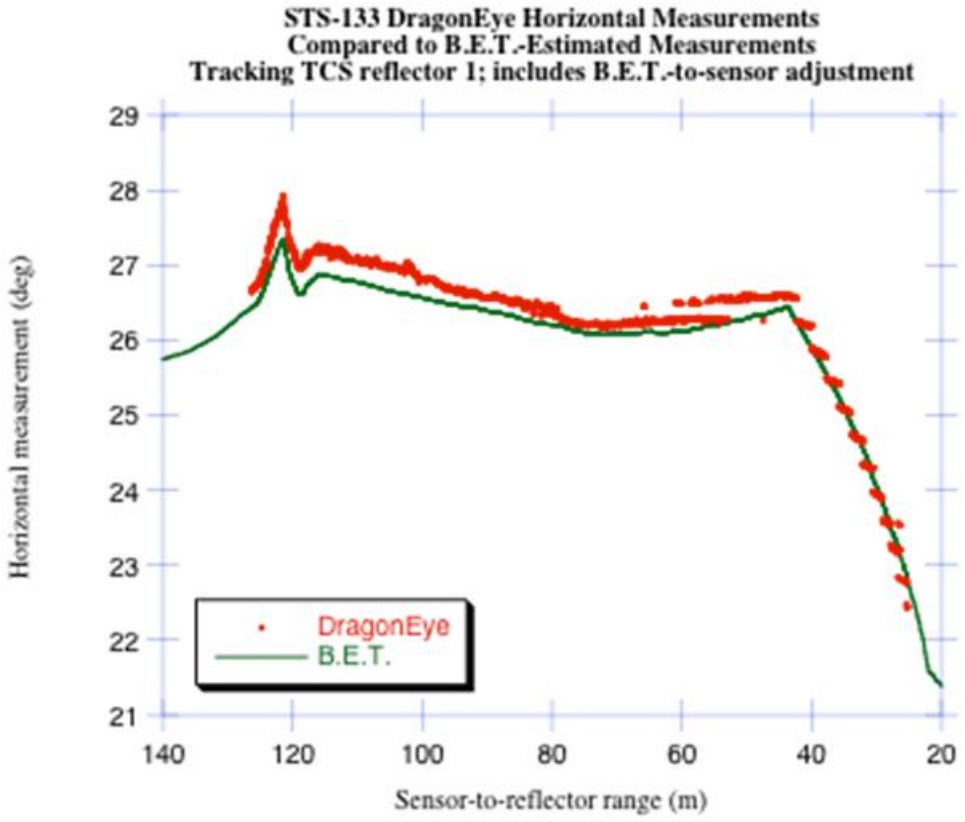

Figure 7.2-12. DragonEye Horizontal Measurements Compared to Altered BET Estimates

The quantization error evident in the range measurement data is even more obvious in the bearing data, because the DragonEye bearing measurements are quantized to a whole number of pixels. The focal plane array (FPA) resolution, FOV size, and focusing drives the system's ability to do subpixel resolution, which creates quantized bearing measurements. The differences between the DragonEye horizontal measurements and the BET-estimated measurements are shown in Figure 7.2-13.

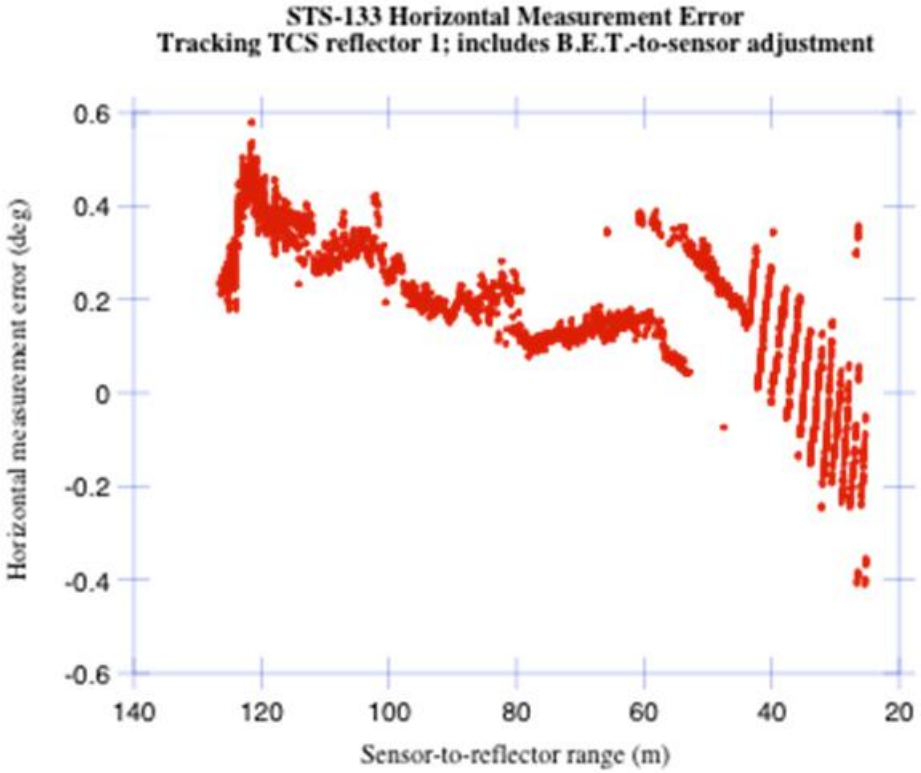

Figure 7.2-13. Estimated DragonEye Horizontal Measurement Error; Tracking TCS Reflector 1

Figure 7.2-14 shows the vertical angle measurements from DragonEye co-plotted with the corresponding estimates computed from the BET.

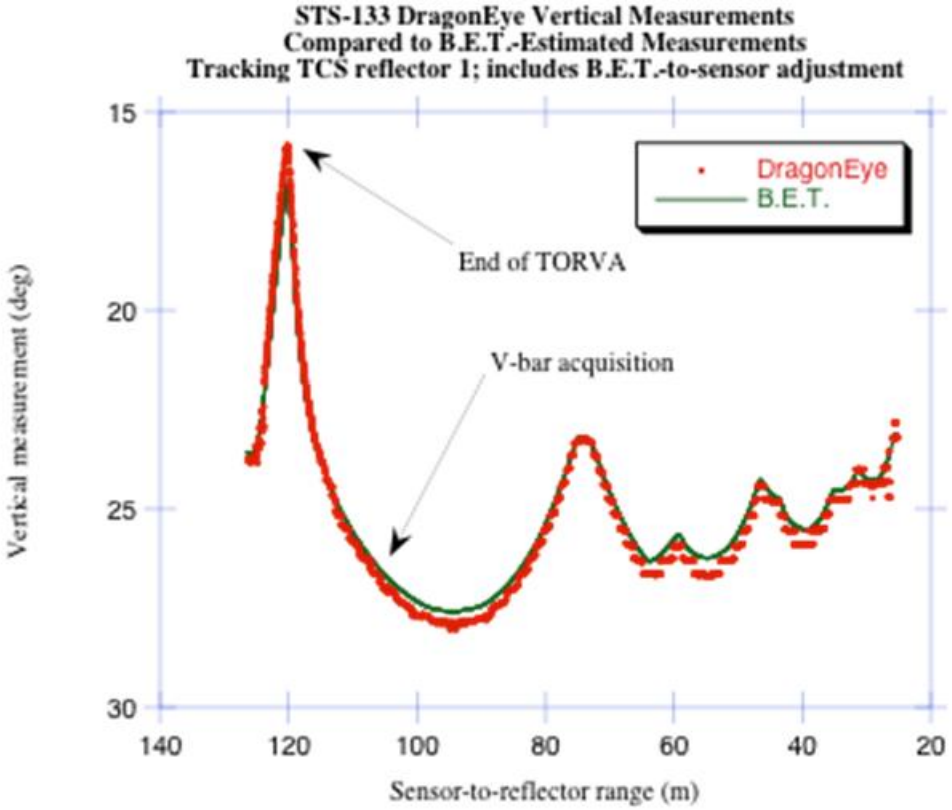

Figure 7.2-14. DragonEye Vertical Measurements Compared to Altered BET Estimates

The differences between the DragonEye vertical measurements and the BET-estimated measurements are shown in Figure 7.2-15.

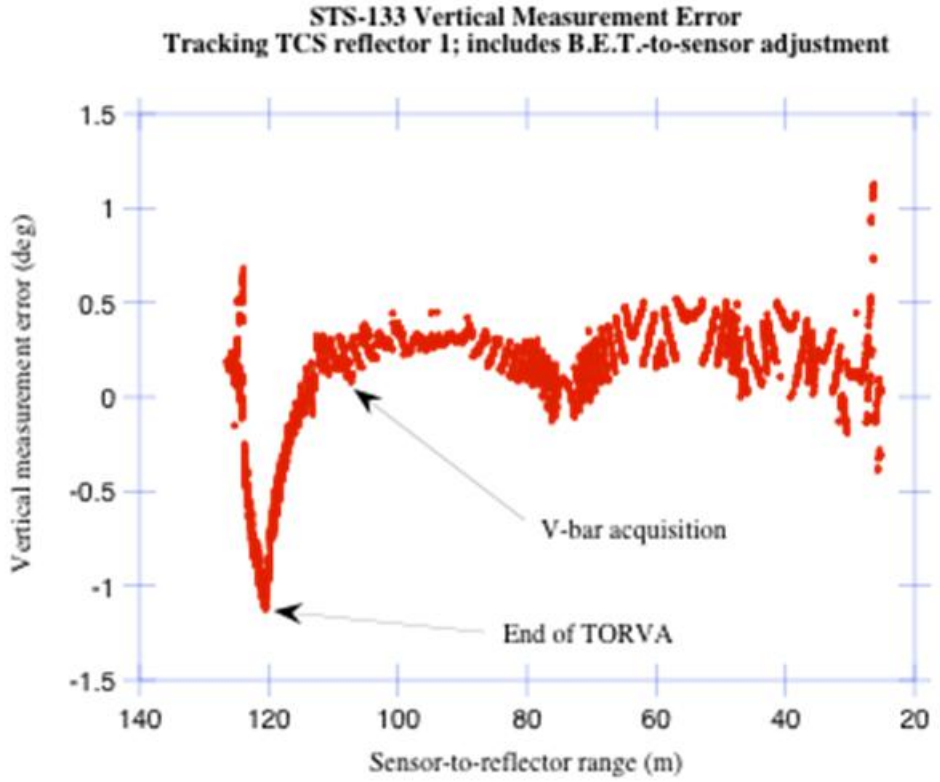

Figure 7.2-15. Estimated DragonEye Vertical Measurement Error; Tracking TCS Reflector 1

Figure 7.2-15 shows the error in the vertical angle grows in magnitude from acquisition of reflector 1 by DragonEye until the TORVA is completed. Completion of the TORVA is defined as the point the rotation of the orbiter with respect to LVLH as nulled. Figure 7.2-16 shows the in-plane relative motion during the time DragonEye tracked TCS reflector 1. Figure 7.2-17 shows the vertical angle rate computed from the difference of consecutive BET-estimated angles divided by the delta-time.

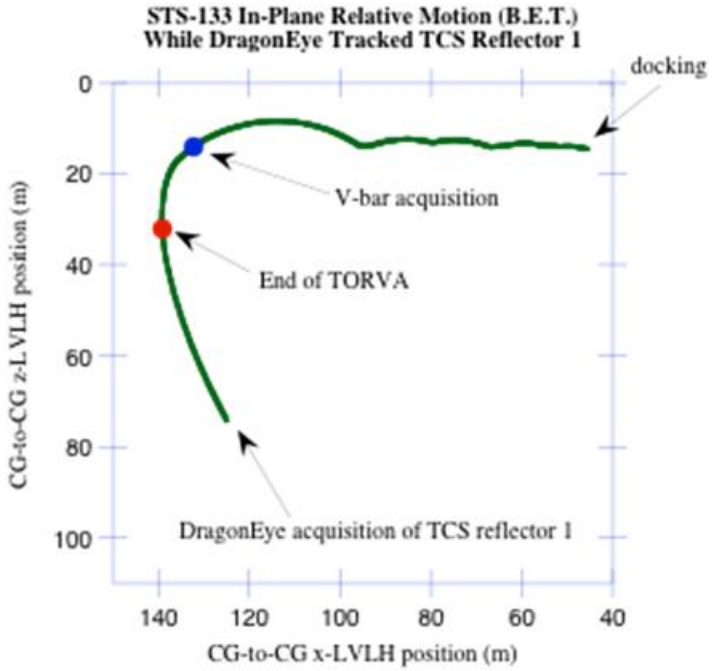

Figure 7.2-16. STS-133 In-plane Relative Motion while DragonEye Tracked TCS Reflector 1

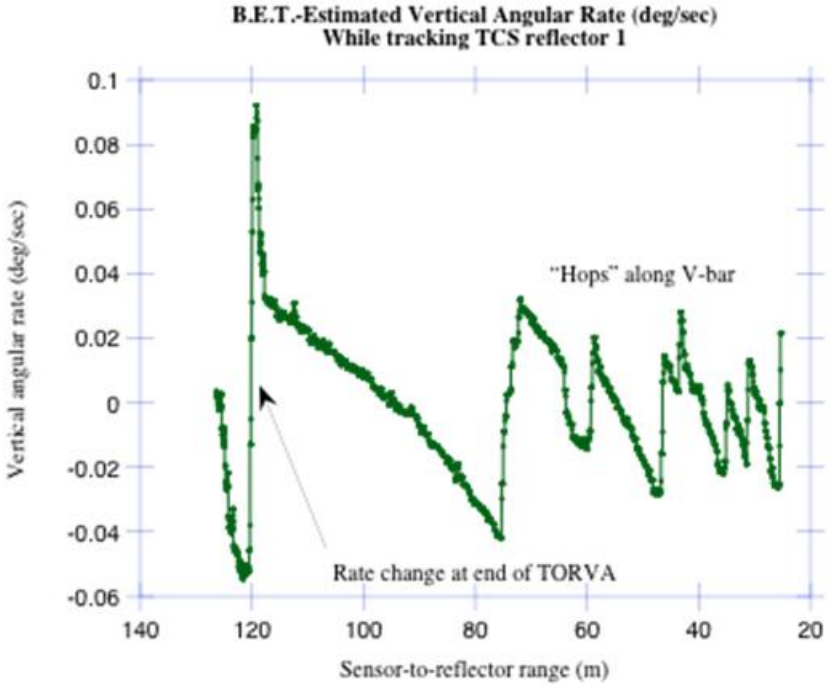

Figure 7.2-17. Estimated Vertical Angular Rate Computed from the BET

DragonEye does not tolerate rotation with respect to LVLH and performance was degraded by translational maneuvers, which was seen in tracking reflector 8.

Table 7.2-5 gives estimates of the mean differences and standard deviations of the bearing errors with and without the alignment of the BET to the data. Each pixel represents 0.38 degree of angular measure. The statistics are given in pixels and degrees.

Table 7.2-5. Mean Differences and Standard Deviations of Bearing Errors; DragonEye Tracking TCS Reflector 1 (N = 8471)

	Mean diff. (pix)	Std. Dev. (pix)	Mean diff. (deg)	Std. Dev. (deg)
Horizontal, not aligned	3.978	0.381	1.512	0.145
Horizontal, aligned	0.524	0.401	0.199	0.152
Vertical, not aligned	0.484	0.900	0.184	0.342
Vertical, aligned	0.289	0.885	0.110	0.336

Ninety-percent bootstrap confidence intervals on the standard deviations computed from the aligned values were (0.150, 0.155) degree and (0.330, 0.343) degree for the horizontal and vertical measurements, respectively.

The autocorrelation coefficients at lag 1 for the horizontal and vertical measurement residuals are 0.9825 and 0.9902, respectively.

7.2.3 DragonEye Performance Summary

Table 7.2-6 summarizes the DragonEye performance analysis performed by the NESC team.

Table 7.2-6. DragonEye Performance Analysis

DragonEye Bin	Range Bounds (m)	Est. Range Bias (m)	Stdev of Range Error (m)	Stdev of Horiz. Bearing Error (deg)	Stdev of Vert. Bearing Error (deg)
Standard Gain Setting	25 - 126 (refl 1)	0.03 - 3.64	0.202	0.152	0.336
Standard Gain Setting	196 - 585 (refl 2)	-1.11 - 0.90	0.242	0.102	0.223
Standard Gain Setting	196 - 259 (refl 3)	-0.77 - -0.09	0.291	0.135	0.097
Standard Gain Setting	132 - 995 (refl 8)	-8.42 - 0.11	0.347	0.148	0.144

Since there quantitative specifications were not provided for the DTO, the team extracted the following DragonEye specifications from the Dragon vehicle requirements as a point of reference. Note these specifications were not applicable to the DTO, however, they do provide a quantitative reference to assess performance.

- Range noise: ±15 cm (7 m < R < 50 m), ±100 cm (50 m < R 500 m), ±300 cm (500m < R < 1500 m)
- Range bias: 10 cm + R*1% (7 m < R < 50 m), R*1% (50 m < R < 500 m), R*1.5 percent (500 m < R < 1500 m)
- Bearing accuracy of ±0.176 degrees

All performance estimates were within the DragonEye vehicle specifications, with the exception of the vertical bearing specification that exceeded the specification during the tracking of reflector 1.

From analysis of the raw data, the team found that pixel saturation, which degrades peak determination (a flat peak), impacts range computation. Identifying the peak intensity

determines the TOF, effectively the range estimate. Selecting the maximum intensity can lead to range errors starting at 34 cm. Applying a curve-fit or matching filter to the intensity trace may allow finer range resolution to select a proper peak (subslice precision).

7.3 TriDAR Performance Analysis

Neptec's TriDAR flew on the Discovery on STS-135 in July of 2011. During the approach, a laptop on the orbiter was used to display TriDAR telemetry pages for the crew and to record data. The data used in this assessment was provided after NASA formally requested the data through the CSA. According to the conditions of the agreement with CSA, TriDAR raw data are not presented in this report, only differences from the BET.

TriDAR is a scanning LIDAR and does not use retro-reflectors. It uses a structure model to compare the scanned laser returns to compute its relative state. This means the TriDAR can be used for relative navigation with an uncooperative target, provided there exists a model of the structure. In addition, in this section, performance is not based on individual retro-reflective targets, rather it is based on orbiter to ISS CG-to-CG relative location.

The qualitative objectives of this TriDAR DTO were to fly the sensor, exercise the user interfaces, perform real-time pose estimation, and to demonstrate advancement of the TriDAR technology which was flown on two previous DTOs (STS-128 and STS-131). The only quantitative objective was to acquire the ISS at a range greater than 1 km, which was significantly farther than had been demonstrated on previous DTOs. There were some general expectations of performance based on the ISS Relative Navigation System (RNS) specifications [ref. 19] for 3 sigma accuracy for range noise around 25 millimeters (mm) and bias of 50 mm, and bearing noise around 1.0 degrees. However, these specifications were not applied to this DTO. Table 7.3-1 shows the TriDAR range bins.

Table 7.3-1. TriDAR Range Bins

TriDAR Bin	Range Bounds (m)
6T VBAR	1 – 21
5T VBAR	21 – 27
4T VBAR	27 – 52
3T VBAR	52 – 107
2T R2V	107 – 152
1T RBAR	152 – 228
Acq	228 – 1600

TriDAR operated in blob mode and 6-DOF pose. The blob mode calculates the range and bearing (azimuth and elevation) to the center of mass of the LIDAR scan returned point cloud. The 6-DOF pose mode processes the point cloud data and calculates the relative position and attitude of the SSACS frame with respect to the TriDAR frame, utilizing pre-loaded target CAD models.

During approach and docking on STS-135, the TriDAR acquired the ISS at a range of 2 km in blob mode. TriDAR entered pose mode before the RPM and then re-entered pose mode after the station was required post-RPM. In this analysis, the TriDAR data was analyzed in the blob mode pre-RPM and the 6-DOF pose mode post-RPM, omitting the data during the RPM and the pose data prior to the start of the maneuver.

7.3.1 TriDAR – Performance Analysis

Upon receipt of the data from Neptec, an initial review of the data was performed (detailed in Section 7.3.2). A BET for approach and docking to the ISS was generated for STS-135 and was used as a benchmark to evaluate the TriDAR performance. The BET pose is presented in orbiter to ISS CG. The TriDAR pose solution gives the SSACS location and attitude with respect to TriDAR frame. Therefore, accurate knowledge of the location of the TriDAR frame with respect to the orbiter to the ISS CG locations was needed to perform the coordinate translations. A diagram of the coordinate transformation process is shown in Figure 7.3-1. The orbiter attitude from the BET was needed to perform the comparison. The TriDAR data was corrected to account for the ODS pressurization error (described in the BET) and possible TriDAR mounting misalignments, which were derived empirically from the 6-DOF pose data.

The following are steps used to perform the transformation:

1. Rotate TriDAR coordinate frame to the OBF.
2. Adjust this rotation to account for ODS pressurization.
3. Correct for TriDAR misalignment.
4. Translate BET from ISS CG to SSACS origin.
5. Use the orbiter attitude with respect to LVLH to rotate BET to OBF.
6. Translate BET from orbiter CG to TriDAR focal point.

Because the TriDAR system time was set once from a control laptop on-board the orbiter (it drifted over the course of the mission), it was necessary to find the time offset to align the TriDAR data to the BET. Finally, because the BET data points occurs every 4 seconds, interpolation was necessary to match the TriDAR telemetry data frequency of 5 Hz.

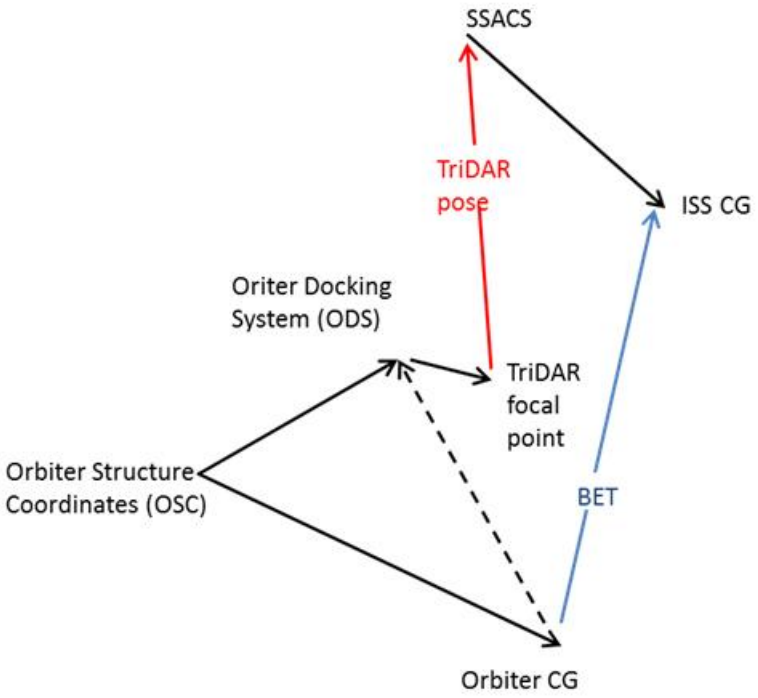

Figure 7.3-1. Coordinate Frame Translations from BET to TriDAR Pose

7.3.2 Data Review and Anomalies

The data delivered by Neptec contained TriDAR 3-DOF range and bearing (blob) and 6-DOF relative position and relative attitude (pose) states, which were computed on-board during approach and docking with the ISS. The data included time tags in coordinated universal time as recorded by a laptop, tracking state information, and data validity flags. Data with stale time-tags and invalid flag indicators were removed. Figure 7.3-2 shows the frequency of the stale and invalid data points. Most of the stale data occurred during blob mode at long range when the TriDAR was not updating the state as often as telemetry was being reported.

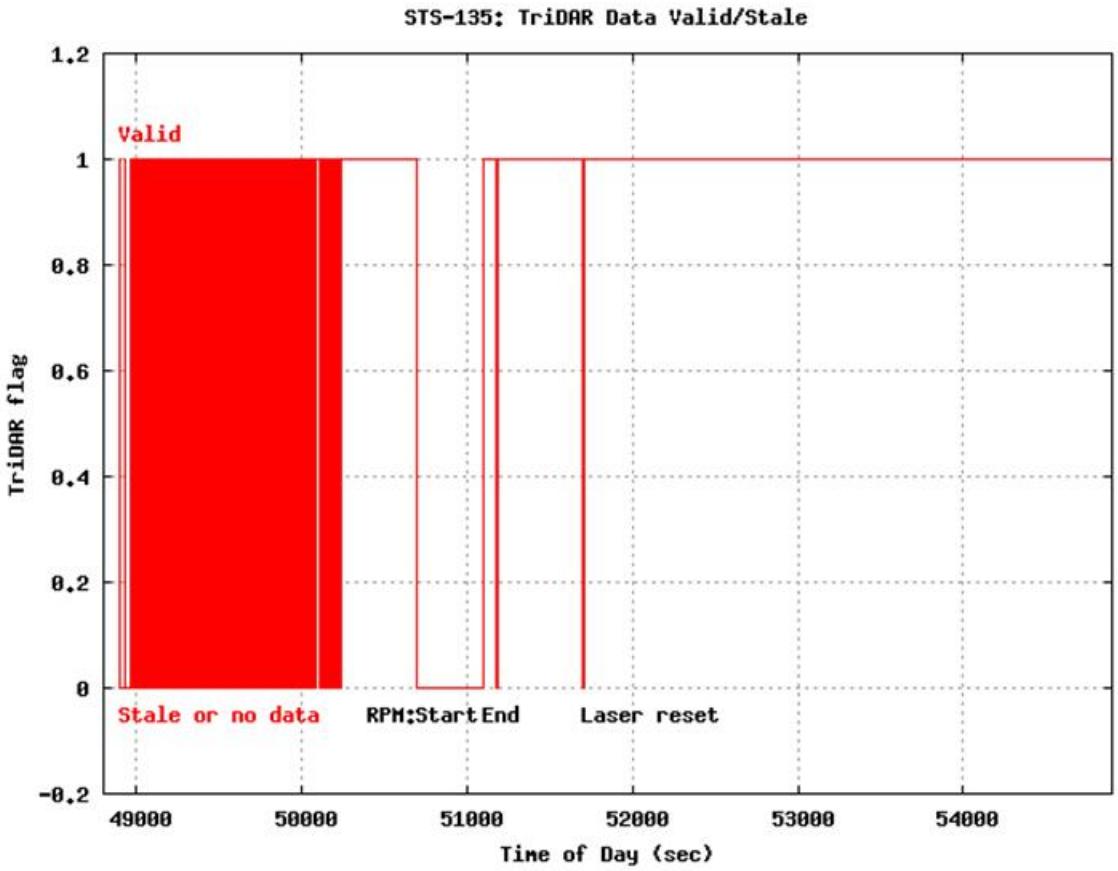

Figure 7.3-2. Frequency of Stale or Invalid Data in Early Phases of Trajectory (48893 to 50233 seconds) (Impact of RPM and laser reset is visible)

During the ISS approach, there were planned periodic resets of the TriDAR to test the reacquisition process. These resets occurred roughly every 10 minutes. The unit successfully demonstrated reacquisition after each reset. Periodic "reset" required stabilization time without user inputs (i.e., 30 seconds after reset command was issued to achieve "lock"). Figure 7.3-3 shows these resets and how they correspond to the TriDAR tracking states. There was an unexpected laser reset that occurred during pose tracking mode 2T annotated in Figures 7.3-2 and 7.3-3. The annotations in Figures 7.3-2 and 7.3-3 are left aligned with the event described.

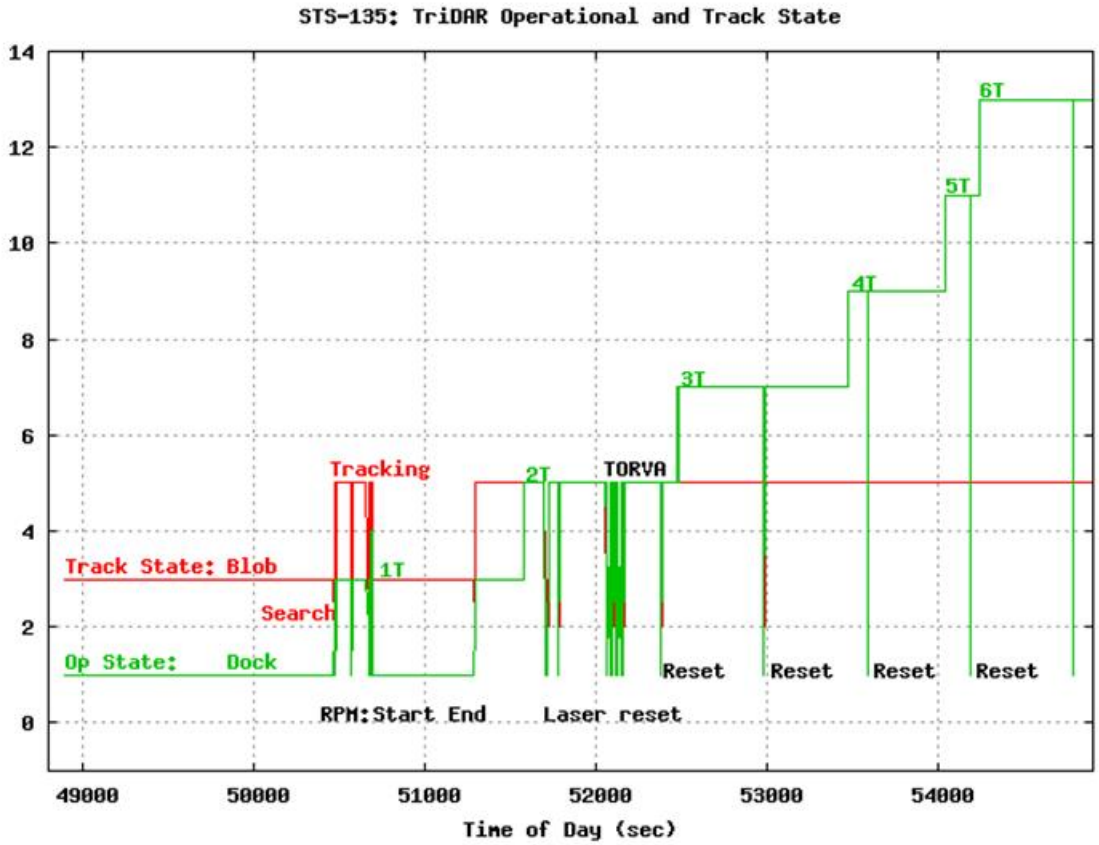

Figure 7.3-3. Tracking State and Operational State (Note that the periodic resets (annotated) are clearly defined; tracking state during transition from RBAR to VBAR seen after 52000 seconds, OpState cycling 1-3-5)

7.3.3 TriDAR – Blob Mode

7.3.3.1 Range

Range data acquisition occurred at a longer range (> 2 km) compared to the previous TriDAR DTOs due to laser hardware improvements. The blob range was compared against the BET (which starts at a range of 1600 meters) and the TriDAR estimated range error was plotted versus BET range (shown in Figure 7.3-4). Before blob-tracking lock started around 850 meters, sparse measurements of range and bearing were observed. The mean estimated range error was 2.5 meters and the estimated range noise was 3.44 meters. After blob mode lock and until RPM, the TriDAR locked to one solar array instead of a whole ISS structure, leading to a bias in the range and bearing.

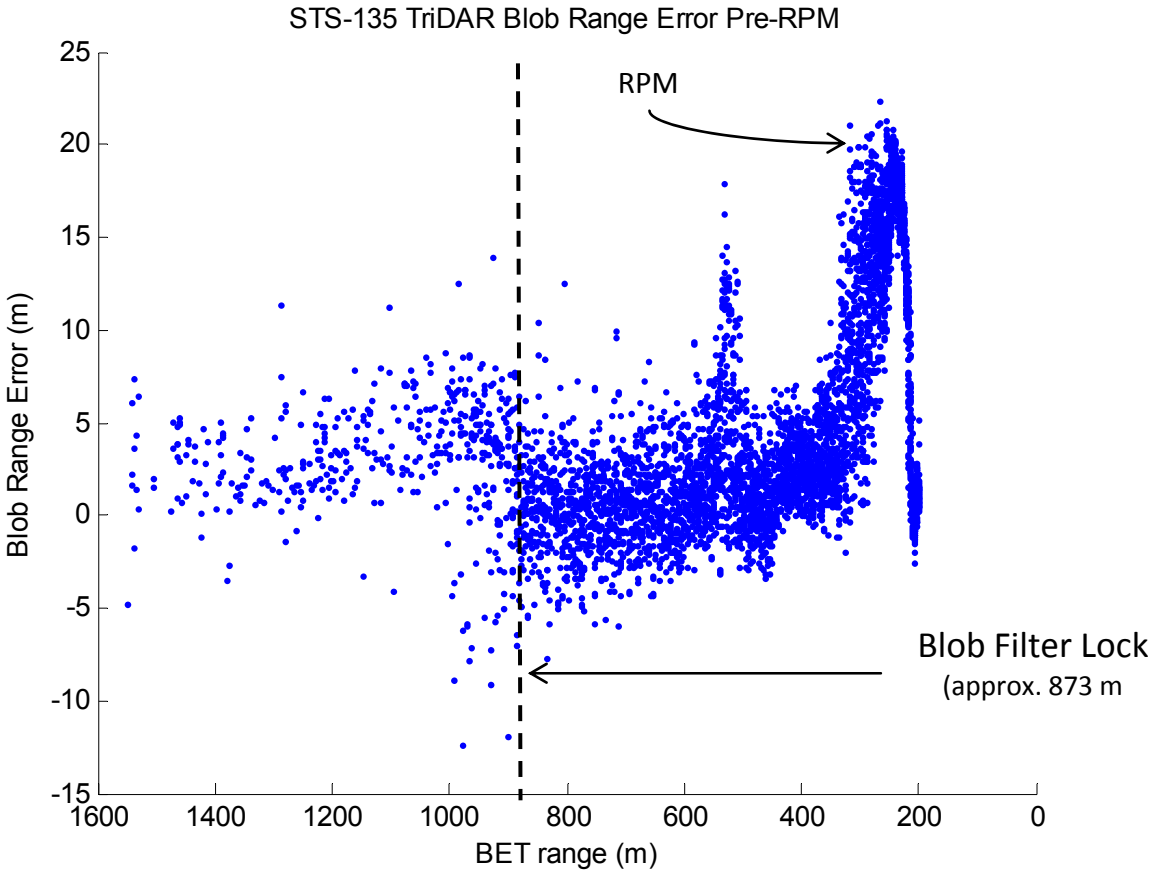

Figure 7.3-4. TriDAR Blob Mode Estimated Range Error

7.3.3.2 Bearing

The estimated bearing error in azimuth and elevation is shown in Figure 7.3-5. Note the majority of the bearing error is in the azimuth, consistent with the TriDAR tracking to one ISS solar array, rather than the entire station. At a range of 200 meters, the azimuthal bearing error is around 15 degrees, which translates to approximately 50 meters (i.e., roughly the distance to the center of the solar arrays with respect to the center of the ISS). Before the blob mode filter lock, the standard deviation of the azimuth error was 1.09 degrees and the standard deviation of the elevation error was 0.26 degrees.

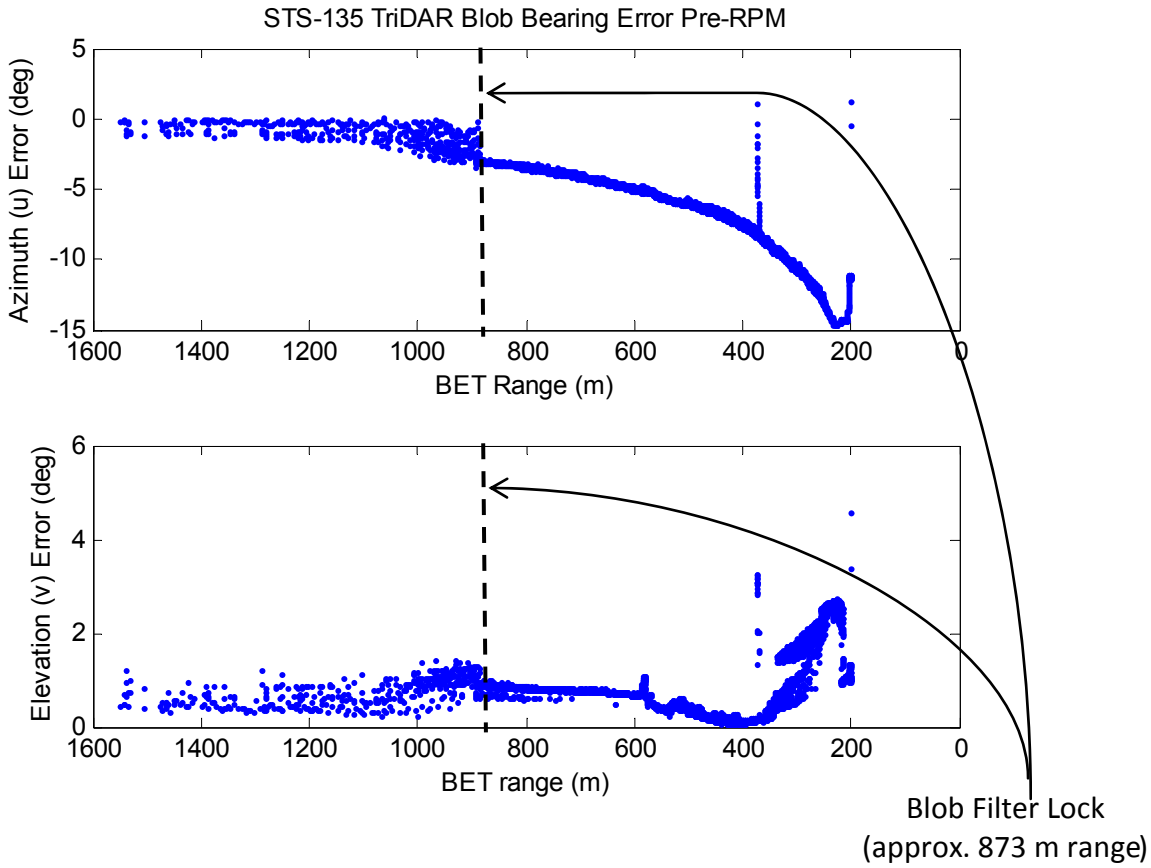

Figure 7.3-5. TriDAR Blob Mode Estimated Bearing Error

7.3.3.3 Summary of Statistics in Range and Bearing

A summary of the estimated bias and noise for range and bearing is provided in Table 7.3-2. Because the estimates for range and bearing biases were calculated using a simple mean, the estimate of the noise is not a true measure of the residual error (as from a curve-fit), but the standard deviation from the mean.

Table 7.3-2. Summary of TriDAR Blob Mode Statistics

	Before Blob Lock		After Blob Lock	
	Estimated Bias	Noise	Estimated Bias	Noise
Range (m)	2.50	3.44	4.96	6.23
Azimuth (deg)	-1.56	1.09	-7.99	3.66
Elevation (deg)	0.80	0.26	0.93	0.75

7.3.4 TriDAR – Pose Mode

Once transitioning to the pose mode after RPM, the TriDAR used six different tracking strategies (Table 7.3-1) based on the relative range of the orbiter to the ISS. There was one tracking mode for the RBAR approach (1T), one tracking mode for the TORVA (2T), and four tracking modes for the final VBAR approach (3T through 6T). These tracking strategies modify the scanned area of the ISS. Therefore, the geometry of the structure model used for the pose estimation is based on the relative position of the orbiter with respect to the ISS.

7.3.4.1 Pose Range

The estimated pose range error as compared to the BET was used to assess the performance of TriDAR for the final approach and docking. Figure 7.3-6 shows the estimated range error for all the pose data post-RPM and demarks the six different tracking strategies. The average estimated range bias over the final approach was -0.92 meters and the range noise was 0.145 meters.

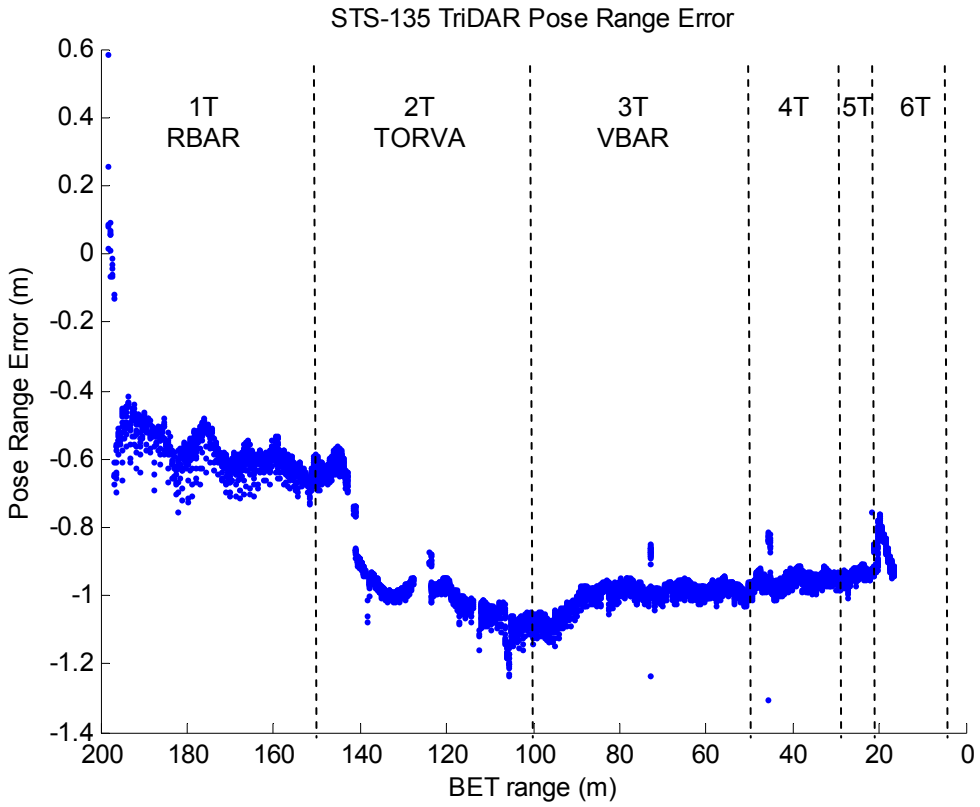

Figure 7.3-6. TriDAR Pose Mode Estimated Range Error

It was observed a larger bias was introduced during tracking mode 2T (TORVA). This occurred when the TriDAR algorithm entered a local minima [ref. 20], possibly due to an unexpected a laser reset and power cycling. The average estimated range bias for tracking mode 2T was -0.92 meters with a range noise of 0.14 meters. This phenomenon can be seen in Figure 7.3-3, where the TriDAR switches rapidly between tracking modes 1T and 2T just after 52000 seconds (labeled TORVA on the figure). Figure 7.3-7 shows the estimated range error versus BET range separated into the z component of relative positions (which is in the range direction) and the root-sum-squared vertical and horizontal components of relative position (X-Y RSS) during the TORVA maneuver. Figure 7.3-7 indicates the bias is introduced in the z-direction and the X-Y components contribute to the noise.

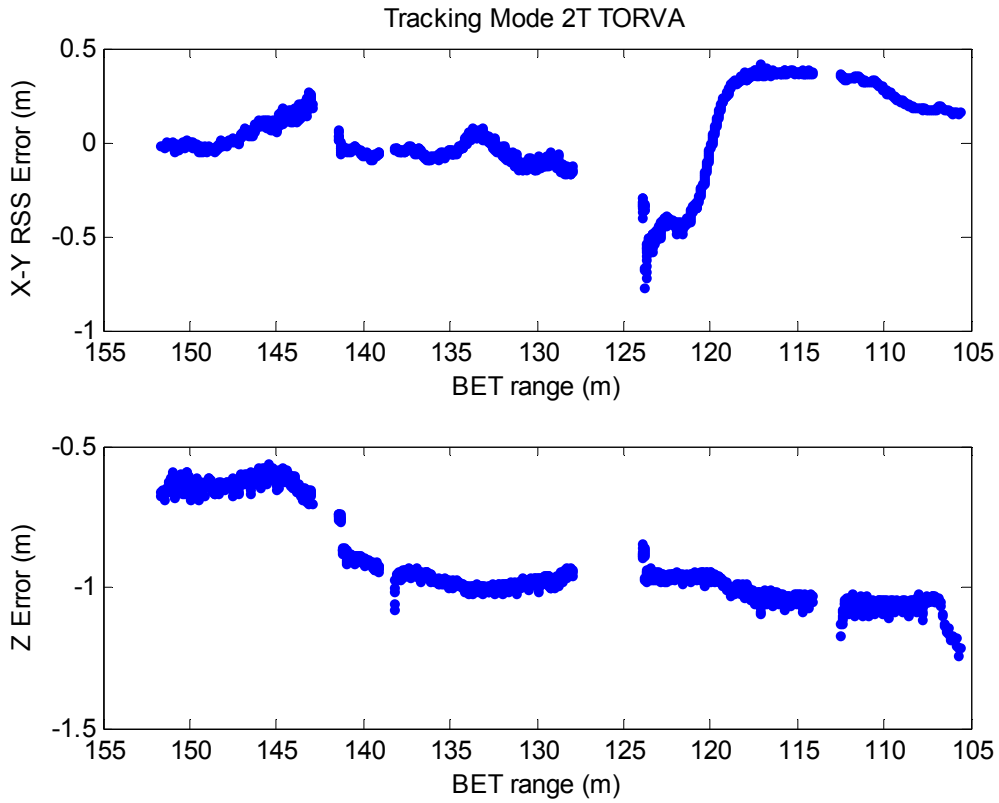

Figure 7.3-7. 2T TORVA Estimated Relative Position Error

There was a periodic variation in the range error found that can been seen in all of the range error plots and seen in Figures 7.3-8 and 7.3-9, tracking modes 1T and 6T, respectively. It was determined this "ripple" effect was caused by periodic hardware health data gathering routines, which were "starving" the CPU every 5 seconds. Neptec is addressing this issue in their new TriDAR hardware. Since time-stamps are applied after the pose algorithm processing is

complete, if algorithm is running slow, the pose solutions can correspond to an earlier moment in time than reported. When the pose solution is fed to the filter with an incorrect time-stamp, the measurement is improperly incorporated into the filter algorithm and causes the "ripple" in the data.

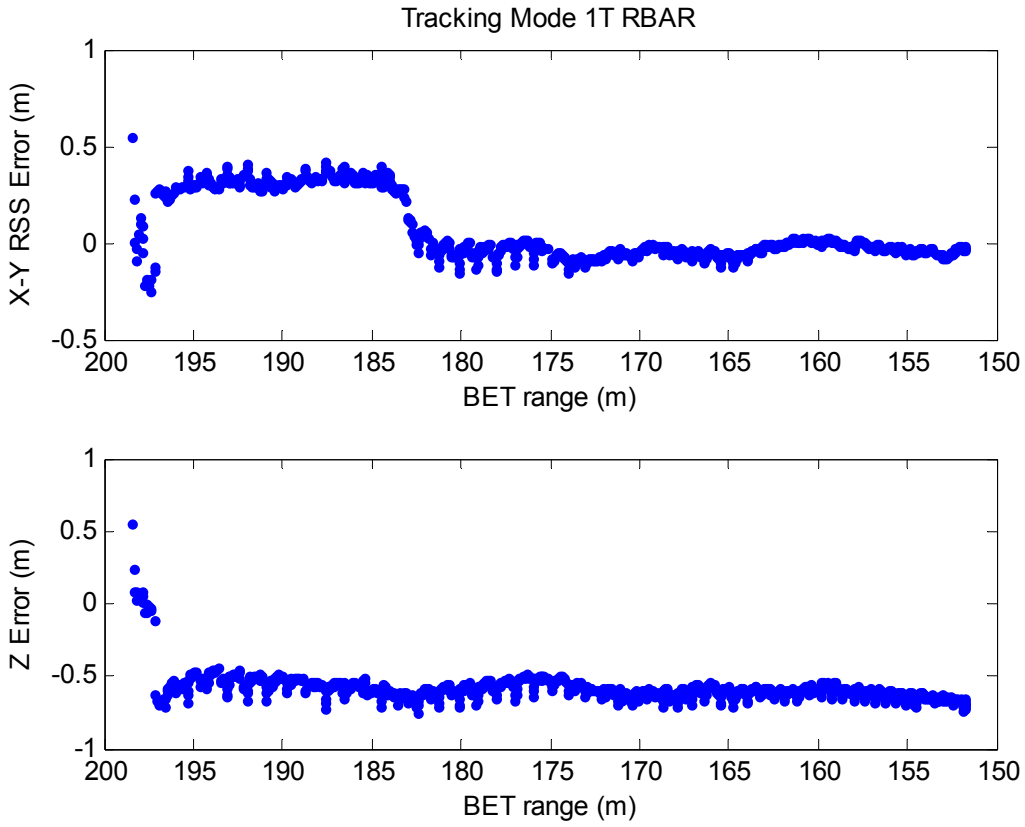

Figure 7.3-8. 1T RBAR Estimated Relative Position Error

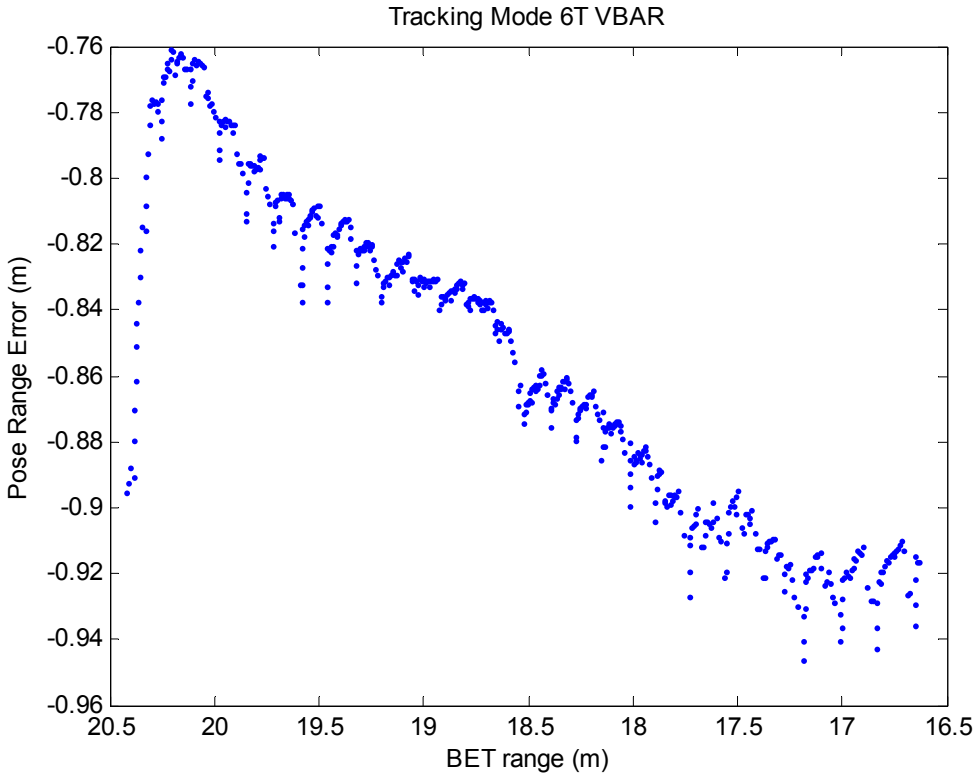

Figure 7.3-9. 6T VBAR Estimated Range Error

During VBAR acquisition, the estimated range noise improved to 0.042 meters as the TriDAR algorithms tightened in solution post TORVA (estimated range error is shown in Figure 7.3-10). In tracking mode 4T, the TriDAR performance was at its best with the estimated range noise at 0.021 meters. The contributions to the estimated range error and noise from the X-Y and Z components are shown in Figure 7.3-11. Note that a planned laser reset occurred at around the 46-meter range and the pose algorithm recovered. However, there are outliers that can been found in Figure 7.3-11, which did not have a "data invalid" flag associated to them in the TriDAR telemetry and were used by the TriDAR pose algorithms and filter.

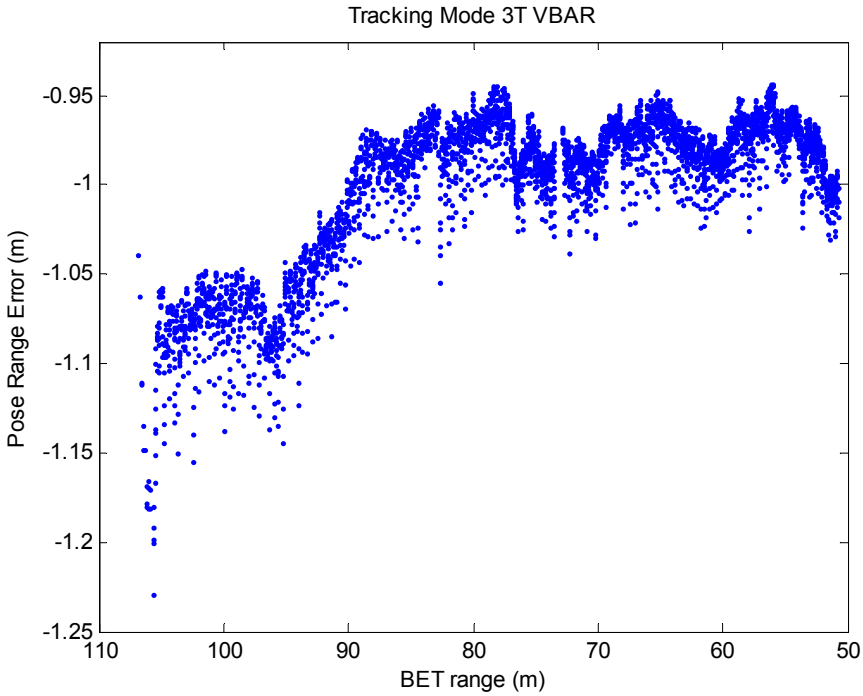

Figure 7.3-10. 3T VBAR Estimated Range Error

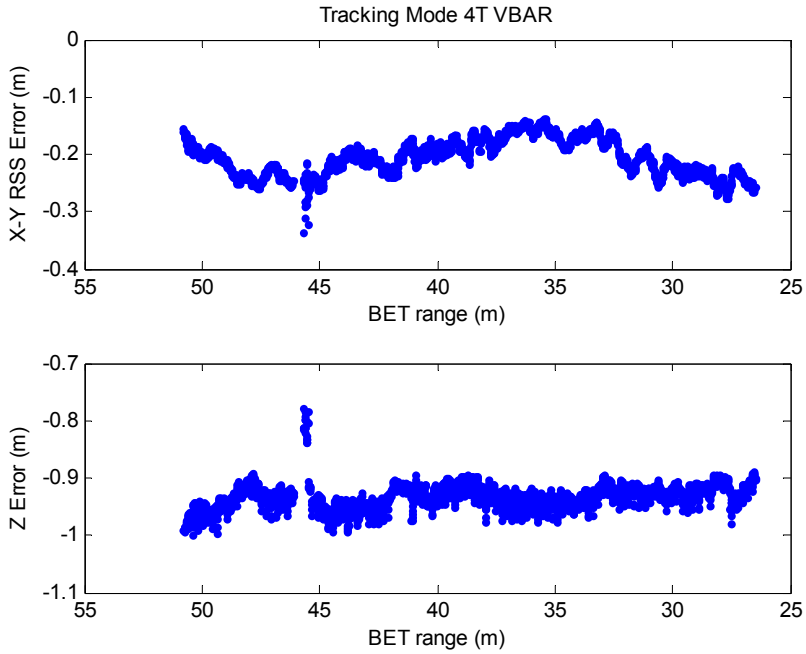

Figure 7.3-11. 4T VBAR Estimated Relative Position Error

A summary of the estimated range bias and noise for all six tracking strategies is given in Table 7.3-3.

Table 7.3-3. Summary of TriDAR 6-DOF Pose Statistics (range)

	Range Bin	Estimated Bias (m)	Noise (m)
X Position	1T	0.037	0.207
	2T	0.129	0.224
	3T	0.125	0.052
	4T	0.212	0.030
	5T	0.241	0.040
	6T	0.215	0.093
Y Position	1T	-0.006	0.074
	2T	0.091	0.085
	3T	0.144	0.033
	4T	0.153	0.017
	5T	0.108	0.032
	6T	0.222	0.093
XY RSS Position	1T	0.049	0.154
	2T	-0.001	0.227
	3T	-0.101	0.084
	4T	-0.205	0.032
	5T	-0.238	0.040
	6T	-0.207	0.093
Z Position	1T	-0.583	0.097
	2T	-0.919	0.143
	3T	-0.992	0.046
	4T	-0.931	0.022
	5T	-0.893	0.021
	6T	-0.826	0.044
RSS Range	1T	-0.577	0.100
	2T	-0.919	0.143
	3T	-0.998	0.042

	Range Bin	Estimated Bias (m)	Noise (m)
	4T	-0.951	0.021
	5T	-0.923	0.015
	6T	-0.852	0.048

7.3.4.2 Pose Relative Attitude

A similar analysis was performed for the relative attitude as for the range, separating the estimated relative attitude bias and noise for each tracking strategy. Table 7.3-4 summarizes the statistics for pose mode relative attitude. For brevity in this report, a plot of the relative attitude in pitch, yaw, and roll is shown in Figure 7.3-12 for the post-RPM approach and docking. The estimated relative attitude noise over the entire approach was 0.36 degrees in pitch, 0.51 degrees in yaw, and 0.63 in roll.

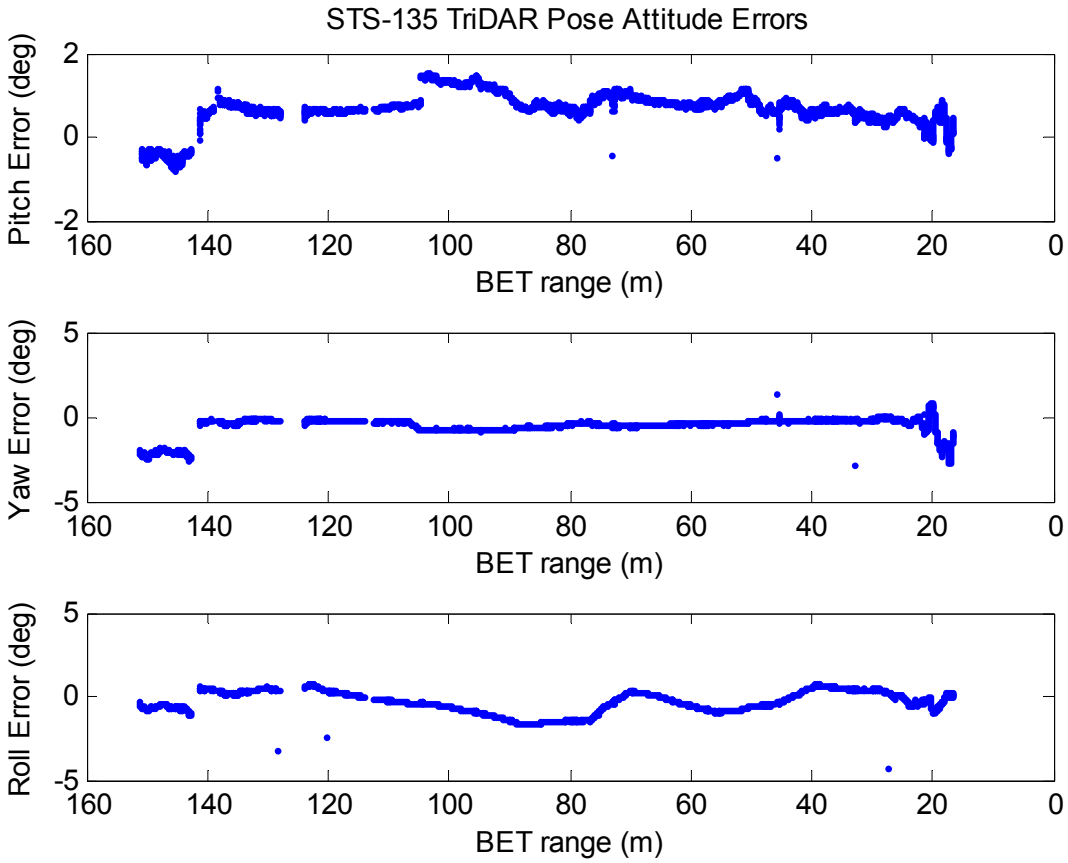

Figure 7.3-12. TriDAR Pose Mode Estimated Relative Attitude Error

Table 7.3-4. Summary of TriDAR 6-DOF Pose Statistics (Relative Attitude)

	Range Bin	Estimated Bias (deg.)	Noise (deg.)
Pitch	1T	-1.354	1.622
	2T	0.482	0.438
	3T	0.940	0.221
	4T	0.635	0.145
	5T	0.438	0.178
	6T	0.334	0.322
Yaw	1T	3.321	19.849
	2T	-0.534	0.719
	3T	-0.485	0.138
	4T	-0.164	0.087
	5T	-0.218	0.334
	6T	-1.199	0.929
Roll	1T	-48.425	65.939
	2T	0.153	0.437
	3T	-0.729	0.551
	4T	0.204	0.437
	5T	-0.221	0.198
	6T	-0.301	0.388
	6T	-0.852	0.048

7.4 General Discussion of TriDAR, STORRM VNS, and DragonEye

The range/bearing error plots for the TriDAR should not be directly compared to the STORRM VNS or DragonEye results. There are important nuances that make such a comparison difficult and likely lead to incorrect conclusions.

The fundamental issue is the STORRM VNS and DragonEye DTOs focused on using the LIDARs for rendezvous with a "cooperative" target, while the TriDAR focused on rendezvous with a "non-cooperative" target. In the present context, the term "cooperative target" refers to a vehicle equipped with reflectors at known locations to aid the LIDAR in tracking specific points on the target vehicle. All of the range residual plots for the VNS and DragonEye were computed for specific reflector observations and the reflector identification was performed as part of the post-flight analysis (although this must be done on-board in real-time in an actual mission). In

contrast, during the "blob mode" used at long ranges, the TriDAR computes range/bearing to the center-of-mass of the observed 3-dimensional point cloud. Because the sensor is not tracking any known point on the vehicle, the best that can be done was to compare the result to the target CG. It should not be surprising to see a larger bias in the range error plots for the TriDAR because a specific point on the ISS for the sensor tracking is not being specified.

For a significant portion of the STS-135 approach, the TriDAR was only obtaining returns from one of the solar arrays, and was therefore computing the range/bearing to the center-of-mass of just this portion of the ISS (resulting in a bias relative to the ISS CG). Further, from measurement-to-measurement a different amount of the structure provided a sufficiently strong return to be included in this 3-D point cloud, leading to larger range noise than if one was viewing either the whole ISS or a specific point on the ISS.

In contrast, the STORRM VNS and DragonEye DTOs were used to detect small reflectors (1-5 pixels in diameter, depending on range) over the entire rendezvous, thus avoiding the difficulties seen by the TriDAR in "blob mode." STORRM VNS and DragonEye were tracking small objects (rather than observing only a portion of the object) mounted at known locations relative to the ISS CG. It should be stressed, however, that either the VNS or the DragonEye could be used in a "non-cooperative" mode rather than a "cooperative" mode. In addition, Soyuz solar arrays and windows produce strong returns on both flash LIDARS (STORRM and DragonEye). By adjusting the LIDAR sensor settings, the returns can be observed from the target (sometimes called "skin tracking") as was done with the TriDAR. The primary difference now lies in how the data points are obtained – the TriDAR is a type of scanning LIDAR, while the VNS/DragonEye are flash LIDARs.

8.0 Findings, Observations, and NESC Recommendations

8.1 STORRM VNS Findings, Observations, and NESC Recommendations

F-1. The STORRM DTO met its objectives providing operational and performance data to continue system maturity.

F-2. The STORRM calibration/correction and centroiding was performed post-flight.

F-3. The performance of bin Echo (162 – 324 meters) exceeded the range specification.

F-4. Biases were discovered in ground testing and from comparison to the BET.

F-5. Discontinuities in range bin transitions (e.g., Alpha to Bravo were 90-meter jumps) and pose-based processing were discovered. This discontinuity was also observed in the pose-based processing.

F-6. The use of second-differencing noise analysis led to underestimates of noise performance in some cases when time-based autocorrelation was present in the data.

O-1. Marginal performance was observed in range bin Delta (324 – 648 meter) that may have been a precursor to the degradation that occurred in range bin Echo (162 – 324 meter).

The following NESC recommendations are directed to the AR&D CoP.

R-1. Conduct VNS processing development to mature the algorithms implemented within the sensor and navigation system to provide in-flight, on-board range, and bearing. ***(F-1, F-2)***

R-2. Determine the root cause of the performance issue of range bin Echo. ***(F-3, O-1)***

R-3. Perform additional VNS preflight ground testing across all range bins to characterize system range performance. ***(F-3, F-4, F-5)***

R-4. Investigate the autocorrelation structure of time-series data before applying the second-difference method using polynomial or local regression methods. ***(F-6)***

- If the data appear uncorrelated, then the second-difference method may be appropriate.
- If the data can be modeled as first-order autoregressive, then the second-difference method should be modified (see Appendix H).

8.2 DragonEye Findings, Observations, and NESC Recommendations

F-7. The DragonEye DTO met its qualitative objectives as performance specifications for the DTO unit were not established.

F-8. The DragonEye bearing measurements did not meet the Dragon vehicle specifications during tracking of reflector 1 planar.

F-9. The intensity peak determination impacts range measurement for every pixel (i.e., as much as 34 cm error due to peak determination). Pixel saturation impacts ability to determine actual peak, and centroiding and feature identification.

F-10. The DragonEye performance is adversely affected by host vehicle rotation with respect to the LVLH reference frame and when the host vehicle undergoes translational maneuvers.

O-2. The FPA resolution, FOV size, and focusing drives the system's ability to do subpixel resolution, which create quantized bearing measurements.

O-3. There were significant design differences and maturity levels of the systems flown on STS-127 and STS-133. These include laser failure due to contamination and detector gain settings and performance (noisy pixels).

The following NESC recommendations are directed to the AR&D CoP.

R-5. Consider adjusting the camera design (e.g., the FOV and/or the focus) to achieve the identified specifications, or change. The specifications should reflect actual flight requirements. ***(F-8, O-2)***

R-6. Apply a robust processing algorithm (e.g., curve-fitting) to find the peak intensity, which will drive the range measurement. ***(F-9)***

R-7. Notify users that DragonEye performance is adversely affected by host vehicle rotation with respect to the LVLH reference frame and when the host vehicle undergoes translational maneuvers. ***(F-10)***

8.3 TriDAR Findings, Observations, and NESC Recommendations

F-11. The TriDAR DTO met its qualitative objectives as performance specifications for the DTO unit were not established.

F-12. There was a 1-meter range bias that was unable to be reconciled over range from 200 meters to ISS dock.

F-13. In long-range blob mode, TriDAR identified a single ISS solar array rather than the entire ISS, which resulted in range errors of 20 meters and bearing errors of up to 50 meters in the y-axis.

F-14. The data time tag was performed at the end of the processing resulting in asynchronous output of pose parameters due to CPU workload (e.g., health and status checking, infrared camera processing, etc.).

F-15. Data quality issues included: stale measurement data that were flagged as valid, duplicated time-stamp data, and a lack of data quality flags to indicate validity.

O-4. Periodic "reset" required stabilization time without user inputs (i.e., roughly 30 seconds after reset command was issued to achieve "lock").

O-5. Unplanned laser reboot during 2T TORVA tracking due to laser power safety monitoring system trip resulted in a lower power setting (safe mode). Using high-power laser mode would be better or consider using eye-safe laser for manned operations.

The following NESC recommendations are directed to the AR&D CoP.

R-8. Determine the root cause of the 1-meter range bias, which may involve reconciliation of CAD geometry, reference coordinate systems, and/or more extensive ground testing. ***(F-12)***

R-9. Direct TriDAR to output its scan window size for target returns in real-time as inputs to a navigation filter that can determine whether the scan is incomplete based on *a priori* target vehicle knowledge. ***(F-13)***

R-10. Apply time stamps real-time and add data quality flags to the TriDAR output. ***(F-14, F-15)***

8.4 Overall Findings, Observations, and NESC Recommendations

F-16. When processing raw sequence or intensity and range data from Flash LIDAR sensors, data exclusion of erroneous range data based on the knowledge of FOV, range, and/or known bad/poor pixels is critical to measurement performance.

O-6. Soyuz solar arrays and windows produce strong returns on both flash LIDARS (STORRM and DragonEye).

O-7. Flash LIDAR processing could encompass non-cooperative targets (i.e., non-centroid output processing).

O-8. Numerous spurious reflections that were not LIDAR reflectors occurred for the DragonEye and STORRM VNS DTOs. By contrast, the TCS, which was a scanning LIDAR used during the SSP for proximity operations and docking, provided few spurious reflections throughout its lifetime. Spurious reflections make reflector identification and navigation difficult.

The following NESC recommendations are directed to the AR&D CoP.

R-11. Perform algorithm development and testing to enable robust and reliable preprocessing of flash LIDAR imagery data. ***(F-16)***

R-12. Continue investments in STORRM VNS and DragonEye algorithm maturity for real-time flight applications (e.g., range calibration/correction and centroiding). ***(F-16)***

9.0 Alternate Viewpoint

There were no alternate viewpoints identified during the course of this assessment by the NESC team or the NRB quorum.

10.0 Other Deliverables

No unique hardware, software, or data packages, outside those contained in this report, were disseminated to other parties outside this assessment.

11.0 Lessons Learned

LL-1. For future LIDAR assessments, consideration should be given to resources required to obtain and archive the data sets. The DTO data required significant effort and resources. When conducting joint experiments, NASA should establish data-sharing requirements and agreements.

12.0 Recommendations for NASA Standards and Specifications

No recommendations for NASA standards and specifications were identified as a result of this assessment.

13.0 Definition of Terms

Corrective Actions	Changes to design processes, work instructions, workmanship practices, training, inspections, tests, procedures, specifications, drawings, tools, equipment, facilities, resources, or material that result in preventing, minimizing, or limiting the potential for recurrence of a problem.
Finding	A relevant factual conclusion and/or issue that is within the assessment scope and that the team has rigorously based on data from their independent analyses, tests, inspections, and/or reviews of technical documentation.
Lessons Learned	Knowledge, understanding, or conclusive insight gained by experience that may benefit other current or future NASA programs and projects. The experience may be positive, as in a successful test or mission, or negative, as in a mishap or failure.
Observation	A noteworthy fact, issue, and/or risk, which may not be directly within the assessment scope, but could generate a separate issue or concern if not addressed. Alternatively, an observation can be a positive acknowledgement of a Center/Program/Project/Organization's operational structure, tools, and/or support provided

Problem	The subject of the independent technical assessment.
Proximate Cause	The event(s) that occurred, including any condition(s) that existed immediately before the undesired outcome, directly resulted in its occurrence and, if eliminated or modified, would have prevented the undesired outcome.
Recommendation	A proposed measurable stakeholder action directly supported by specific Finding(s) and/or Observation(s) that will correct or mitigate an identified issue or risk.
Root Cause	One of multiple factors (events, conditions, or organizational factors) that contributed to or created the proximate cause and subsequent undesired outcome and, if eliminated or modified, would have prevented the undesired outcome. Typically, multiple root causes contribute to an undesired outcome.
Supporting Narrative	A paragraph, or section, in an NESC final report that provides the detailed explanation of a succinctly worded finding or observation. For example, the logical deduction that led to a finding or observation; descriptions of assumptions, exceptions, clarifications, and boundary conditions. Avoid squeezing all of this information into a finding or observation

14.0 Acronyms List

AA	Associate Administrator
AFT	Aft pointing
AR	Auto-regressive
AR&D	Autonomous Rendezvous and Docking
BAH	Booz Allen Hamilton
BET	Best Estimated Trajectory
CG	Center of Gravity
cm	centimeters
CoP	Community of Practice
CSA	Canadian Space Agency
DC	Docking Camera
deg/sec	degree/second
DoF	Degree-of-Freedom
DRU	Data Recording Unit
DTO	Development Test Objective
FD	Flight Day
FGB	Functional Cargo Block (RSA module)
FOR	Field of Regard

FOV	Field-of-View
FPA	Focal Plane Array
FWD	Forward pointing
GLS	Generalized Least Squares
GN&C	Guidance, Navigation, and Control
GSFC	Goddard Space Flight Center
GUI	Graphical User Interface
HEOMD	Human Exploration and Operations Mission Directorate
Hz	Hertz Cycles per Second
IMU	Inertial Measurement Unit
IR	Infrared
JEM	JAXA Experiment Module
JSC	Johnson Space Center
km	kilometers
LaRC	Langley Research Center
LIDAR	Light Detection and Ranging
LVLH	local vertical, local horizontal
m	meter
mm	millimeters
MPCV	Multi-Purpose Crew Vehicle
NESC	NASA Engineering and Safety Center
NRB	NESC Review Board
OBF	Orbiter Body Frame
ODRC	Orbiter data reduction complex
ODS	Orbiter Docking Station
OLS	Ordinary Least Squares
OSC	Orbiter Structure Coordinate
PI	Principal Investigator
PMA	Pressurized Mating Adaptor
RelNav	Relative Navigation
RNS	Relative Navigation System
RPOP	Rendezvous and Proximity Operations Program
SEA	Sensor Enclosure Assembly
SM	Service Module (RSA Module)
SME	Subject Matter Expert
SSACS	Space Station Analysis Coordinate System
SSP	Space Shuttle Program
STS	Space Transportation System
TCS	Trajectory Control Sensor
TOF	Time of Flight
TORVA	Twice Orbital Rate V-bar Approach

TriDAR	Triangulation and LIDAR
TRL	Technology Readiness Level
VNS	Vision Navigation Sensor

15.0 References

1. Gelb, A., *Applied Optimal Estimation,* M.I.T. Press, 1974.
2. Clark, F. D., "TCS Performance Analysis: STS-97 Through STS-135," SSV-11-013, GCD-11-495, 20 Jul 2011.
3. Onboard Navigation System Characteristics," Engineering Directorate, Aeroscience and Flight Mechanics Division, JSC-26289, Rev. 3, August 2004.
4. "Space Shuttle Operational Level C Functional Subsystem Software Requirements document; Guidance Navigation, and Control; Part B, On-Orbit Navigation," STS-83-0006F, 26 June 1991.
5. Clark, F. D., "STS-133 Best-Estimated Trajectory during Approach to the ISS," GCD-12-432, 10 Jul 2012.
6. Clark, F. D., "STS-134 Best-Estimated Trajectory during Approach to the ISS," GCD-12-432, 10 Jul 2012.
7. Stapleton, J. H., *Linear Statistical Models*, John Wiley & Sons, Inc., 1995.
8. Neter, J., and Wasserman, W., *Applied Linear Statistical Models*, Richard D. Irwin, Inc., 1974.
9. JSC Engineering Directorate, Aeroscience and Flight Mechanics Division, "Data Analysis Results for the Sensor Test for Orion RelNav Risk Mitigation (STORRM), draft, May 2012.
10. Christian, J., Robinson, S., D'Souza., and Ruiz., "Cooperative Relative Navigation of Spacecraft at Close Range using Flash LIDARs, October 2012.
11. Efron, B., and Tibshirani, R. J., *An Introduction to the Bootstrap*, Chapman & Hall, Inc., 1993.
12. Efron, B. and Gong, G., "A Leisurely Look at the Bootstrap, the Jackknife, and Cross-Validation," *The American Statistician*, Vol. 37, No. 1, Feb. 1983, pp. 36–48.
13. D'Agostino, R. B., and Stephens, M. A., *Goodness-of-Fit Techniques*, Marcel Dekker, Inc., 1986.
14. Patangan, M., "STS-134 TCS Expected Reflector Locations," ESCG-4375-12-OGNC-MEMO-0016, 31 July 2012.

15. Clark, F. D., "Estimation of Autocorrelation and Variance from Second Differences When Data Are Correlated," GCD-12-461, 14 Nov. 2012.
16. Cleveland, W. S., *Visualizing Data*, Hobart Press, 1993.
17. STS-133 DragonEye Processed Data, S. P. Cryan/NASA-JSC (EG2), 31 August 2012.
18. Patangan, M., "STS-133 DragonEye Expected Reflector Locations," ESCG-4375-12-OGNC-MEMO-0016, 31 July 2012.
19. S684-14919, Initial Release Specification for the ISS – Based Relative Navigation System, 03 April 2012.
20. (Neptec Report)_STS-135 TriDAR DTO Post Flight Report, August 2011
21. Christian, J. A., "Reference Frames Definitions, Pixel Readout Order, and Image Display Conventions for Processing STORRM Vision Navigation Sensor (VNS) and Docking Camera Data," NASA Johnson Space Center, FltDyn-CEV-10-139, November 23, 2010.
22. Configuration Analysis Modeling and Mass Properties (CAMMP) Team, "On-Orbit Assembly, Modeling, and Mass Properties Data Book", JSC 26557 Rev. AD Vol. 1, International Space Station Program, NASA Johnson Space Center, Houston, TX, July 2009.

16.0 Appendices (Stand Alone Volume)

Appendix A.	STS-134 VNS Performance Analysis
Appendix B.	STS-133 DragonEye Performance Analysis
Appendix C.	STS-127 DragonEye Performance Analysis
Appendix D.	STS-134 Best-Estimated Trajectory
Appendix E.	STS-135 Best-Estimated Trajectory during Approach to the ISS
Appendix F.	STS-133 Best-Estimated Trajectory for DragonEye
Appendix G.	STS-127 Best-Estimated Trajectory during approach to the ISS
Appendix H.	Estimation of Autocorrelation and Variance from Second Differences When Data Are Correlated
Appendix I.	Attitude Misalignment between the STORRM VNS and the STS-134 Best Estimated Trajectory
Appendix J.	VNS and ISS Configuration Definitions
Appendix K.	STORRM Retro Visibility Tool Overview

REPORT DOCUMENTATION PAGE

Form Approved
OMB No. 0704-0188

1. REPORT DATE *(DD-MM-YYYY)*	2. REPORT TYPE	3. DATES COVERED *(From - To)*
01- 05 - 2013	Technical Memorandum	March 2012 - April 2013

4. TITLE AND SUBTITLE
Relative Navigation Light Detection and Ranging (LIDAR) Sensor Development Test Objective (DTO) Performance Verification

5a. CONTRACT NUMBER

5b. GRANT NUMBER

5c. PROGRAM ELEMENT NUMBER

6. AUTHOR(S)
Dennehy, Cornelius J.

5d. PROJECT NUMBER

5e. TASK NUMBER

5f. WORK UNIT NUMBER
869021.05.07.09.03

7. PERFORMING ORGANIZATION NAME(S) AND ADDRESS(ES)
NASA Langley Research Center
Hampton, VA 23681-2199

8. PERFORMING ORGANIZATION REPORT NUMBER
L-20263 NESC-RP-11-00753

9. SPONSORING/MONITORING AGENCY NAME(S) AND ADDRESS(ES)
National Aeronautics and Space Administration
Washington, DC 20546-0001

10. SPONSOR/MONITOR'S ACRONYM(S)
NASA

11. SPONSOR/MONITOR'S REPORT NUMBER(S)
NASA/TM-2013-217992

12. DISTRIBUTION/AVAILABILITY STATEMENT
Unclassified - Unlimited
Subject Category 16 Space Transportation and Safety
Availability: NASA CASI (443) 757-5802

13. SUPPLEMENTARY NOTES

14. ABSTRACT

The NASA Engineering and Safety Center (NESC) received a request from the NASA Associate Administrator (AA) for Human Exploration and Operations Mission Directorate (HEOMD), to quantitatively evaluate the individual performance of three light detection and ranging (LIDAR) rendezvous sensors flown as orbiter's development test objective on Space Transportation System (STS)-127, STS-133, STS-134, and STS-135. This document contains the outcome of the NESC assessment.

15. SUBJECT TERMS
NASA Engineering and Safety Center; Space Transportation System; Light detection and ranging; Sensor Test for Orion RelNav Risk Mitigation; Triangulation and LIDAR; DragonEye

16. SECURITY CLASSIFICATION OF:			17. LIMITATION OF ABSTRACT	18. NUMBER OF PAGES	19a. NAME OF RESPONSIBLE PERSON
a. REPORT	b. ABSTRACT	c. THIS PAGE			STI Help Desk (email: help@sti.nasa.gov)
					19b. TELEPHONE NUMBER *(Include area code)*
U	U	U	UU	108	(443) 757-5802